Available online at www.sciencedirect.com

ScienceDirect

Physics of Life Reviews ••• (••••) •••–•••

PHYSICS of LIFE reviews

www.elsevier.com/locate/plrev

Review

Multiscale approach to pest insect monitoring: Random walks, pattern formation, synchronization, and networks

Sergei Petrovskii [a,*], Natalia Petrovskaya [b], Daniel Bearup [a]

[a] *Department of Mathematics, University of Leicester, University Road, Leicester LE1 7RH, UK*
[b] *School of Mathematics, University of Birmingham, Birmingham B15 2TT, UK*

Received 18 July 2013; accepted 4 February 2014

Communicated by J. Fontanari

Abstract

Pest insects pose a significant threat to food production worldwide resulting in annual losses worth hundreds of billions of dollars. Pest control attempts to prevent pest outbreaks that could otherwise destroy a sward. It is good practice in integrated pest management to recommend control actions (usually pesticides application) only when the pest density exceeds a certain threshold. Accurate estimation of pest population density in ecosystems, especially in agro-ecosystems, is therefore very important, and this is the overall goal of the pest insect monitoring. However, this is a complex and challenging task; providing accurate information about pest abundance is hardly possible without taking into account the complexity of ecosystems' dynamics, in particular, the existence of multiple scales. In the case of pest insects, monitoring has three different spatial scales, each of them having their own scale-specific goal and their own approaches to data collection and interpretation. In this paper, we review recent progress in mathematical models and methods applied at each of these scales and show how it helps to improve the accuracy and robustness of pest population density estimation.

Keywords: Insect monitoring; Trapping; Diffusion; Levy walk; Numerical integration; Dispersal

Contents

* Corresponding author.

http://dx.doi.org/10.1016/j.plrev.2014.02.001
1571-0645/

1. Introduction

The structure and functioning of ecosystems have long been paradigms of complexity [26,86]. In particular, it has been increasingly recognized that ecosystem properties arise as a result of coupling between processes going on different spatial scales [61,75,84,169]. The notion of multiple scales applies to virtually all aspects of ecosystem functioning and to ecosystem monitoring, in particular, to pest insect monitoring. Pest monitoring is an issue of huge practical importance, especially in agricultural ecosystems or 'agro-ecosystems'. Indeed, pests are a sustained and significant problem in the production of food across the globe. Crops are vulnerable to attack from pests both during the growing process and after they have been harvested. Estimates of the annual worldwide loss due to pests at the pre-harvest stage lie between 35 and 42% [106,133]. In particular, the pre-harvest loss of 14–15% of the world's crops has been attributed to harmful insects [136,134].

Effective and reliable ecological monitoring is required in order to provide detailed and timely information about pest species. In agro-ecosystems, monitoring is usually a part of the integrated pest management (IPM) [28,82]. The basic principle of the IPM is that a control action is only used if and when it is necessary. The decision of whether or not to implement a control action is made by comparing the abundance of pests against some threshold level, i.e. the limit at which intervening becomes worth the effort and expense. Such threshold values can be decided upon by taking a variety of factors into consideration. Economic thresholds are most commonly used [162] as the overriding concern is that the pest management program is financially viable (e.g. see [63]).

Once the pest abundance exceeds the threshold, the IPM decision is to intervene and implement a control action, usually application of chemical pesticides. However, use of chemical pesticides has many drawbacks. The first of these is the damage caused to the environment. It has been estimated that around $3 \cdot 10^9$ kg are used across the globe per year [134]. As a result, pesticides significantly contribute to air, soil and water pollution, and there is growing evidence linking their use to human illnesses [4,135]. Note that the per capita efficiency of chemical pesticides is estimated to be quite low as, on average, less than 0.1% of them reach their targeted pest [132].

Secondly, use of chemical pesticides results in significant additional costs added to the agricultural product. Indeed, it is estimated that around $40 billion per year is spent on pesticides [134]. Hence a reduction in the amount of pesticides used would be clearly desirable from the economic perspective.

Finally, indiscriminate or preemptive use of pesticides can make them less efficient. For instance, regular use of pesticides can result in the pest becoming resistant, thus making future management a more difficult task [8]. Another unwanted side effect is that the pesticide can have lethal or sub-lethal effects on natural enemies [157] which can cause a resurgence in the pest population or a secondary pest to emerge.

Thus, accurate monitoring is key to the decision process [28,92]. There is an urgent need for reliable methods to estimate the pest population size in order to avoid unjustified pesticides application and yet to prevent pest outbreaks. In this paper, we review some of the recent research in pest monitoring models and methods applied on different spatial scales.

Two essential components of monitoring are data collection and data processing and/or interpretation. These are not independent as a reliable estimate of the population density resulting from data processing can only be obtained if the collected data contain sufficient information. The latter can be achieved if the spatial arrangement of the data is made consistent with the spatial structure of the agro-ecosystem as given by the self-organized spatiotemporal patterns in the pest species distribution and by the environmental forcing through heterogeneous landscape and weather patterns.

Please cite this article in press as: Petrovskii S, et al. Multiscale approach to pest insect monitoring: Random walks, pattern formation, synchronization, and networks. Phys Life Rev (2014), http://dx.doi.org/10.1016/j.plrev.2014.02.001

A common method to collect field data regarding insect abundance is trapping. A number of traps are installed across the monitored area, e.g. in a field or grassland. They are emptied on a regular basis, their content is analyzed, different species identified and counted. The trap counts are then used to estimate the population density of harmful species at the positions of the traps. Correspondingly, there are three basic spatial scales in the pest monitoring problem. The research approaches depend on the spatial scale where the data are collected, and in this paper we discuss relevant physical/biological mechanisms and an adequate mathematical framework for each spatial scale involved.

The first and smallest spatial scale is related to a single trap. The relevant biological process is individual insect movement and the corresponding theoretical framework is a random walk [127]. The main challenge here is to separate the effects of population density from the effects of movement,[1] in particular, to reveal how the trap counts (and, consequently, the estimate of population density in the vicinity of the trap) may be affected by the type of stochastic process, i.e. whether it is Brownian motion or a Levy flight. The problem is made more difficult by the inherent stochastic variation of individual traits that sometimes can make it impossible to distinguish between Brownian motion and Levy flights [124]. Also, the presence of other movement modes (cf. "composite Brownian motion") or the discretization of continuous individual movement on an inadequate time-scale may result in "superficial Levy flights" [69,78].

The next spatial scale arises when the information about pest density obtained at several different locations (e.g. from several traps) has to be used in order to estimate the average pest density over a certain area, e.g. over a large agricultural field. A standard approach used in ecology is based on calculating the arithmetic average of local densities. This approach, although efficient in the case of an approximately uniform spatial population distribution, becomes ineffective and inaccurate if the distribution is heterogeneous, e.g. due to pattern formation. However, pattern formation in ecological populations is a phenomenon commonly seen in ecological data [47] and explained by well-developed theories [110,88]. To address this, a new approach to estimate the average population density from sparse discrete spatial data (e.g. trap counts collected in the nodes of a spatial grid) has recently been developed [116,117] and was shown to be effective even in case of very coarse spatial data and a very patchy population distribution [119]. In the case of 'extreme aggregation', i.e. where the population density forms a sharp narrow peak, it was shown that the system attains probabilistic properties: the average population density becomes a stochastic variable and the system is quantified by the probability that its value lies in a pre-defined range [44]. A general conclusion is that, at this spatial scale, a robust estimate of the population size can be possible even on a very coarse grid if some properties of the population distribution are known, thus linking this problem to the problem of pattern formation [118].

The largest spatial scale in the problem of pest monitoring is the landscape scale that may include many agricultural fields as well as non-farmed habitats and non-agricultural areas. The main problems here are to reveal long-distance cross-correlations between the pest abundance in different fields or habitats, the phenomenon known as synchronization, and to identify the mechanisms resulting in synchronization. Two main mechanisms that can synchronize the population dynamics in different fields are known to be coupling by inter-habitat dispersal and the effect of spatially correlated noise. Whilst synchronization by noise is usually isotropic, synchronization by dispersal can exhibit clear directional preference [15]. Having revisited some recent results, we show that dispersal between different habitats can occur through a certain self-organized network. Such a network can arise as a result of the interplay between landscape properties, weather conditions and the behavioral response of the dispersing insects. As a result, close fields can be virtually uncorrelated but some fields as far away from each other as a few hundred kilometers can be almost perfectly synchronized.

The paper is structured according to the three spatial scales outlined above; see Sections 2 to 4, respectively. After the scale-specific problems and research approaches are discussed, we then consider the coupling between these scales (Section 5). In particular, we discuss how the processes acting on these different spatial scales can be related, what are the mechanisms and the relevant modeling approaches, and how the information obtained on one scale can be translated to the other scales in order to increase the robustness and effectiveness of pest insect monitoring across spatial scales.

[1] This problem is also known as the "activity-density paradigm" [165]: clearly, a similar increase in the trap counts may result either from an increase in the pest population density or from an increase in the intensity of the individual movement.

Please cite this article in press as: Petrovskii S, et al. Multiscale approach to pest insect monitoring: Random walks, pattern formation, synchronization, and networks. Phys Life Rev (2014), http://dx.doi.org/10.1016/j.plrev.2014.02.001

2. Single trap problem

In pest insect monitoring, as well as in insect studies in general, information about the local abundance of a given species is usually obtained by installing traps and analyzing trap counts. Depending on the traits of the target species, the traps can be of different designs. In the case of walking or crawling insects, a trap is essentially just a hole in the ground, often with a cup or bowl inserted inside in order to make it easier to empty. They can be of different shape. Traps of a circular shape are most common, although a variety of other shapes and design are used as well [130,49]. The size of the trap is usually much larger (by the factor of $\sim 10^2$) than the typical body size of the monitored insects. Traps are escape-proof; once an insect gets inside, it is held captive and is eventually killed. Also, traps can be either baited, i.e. using a certain agent that attracts insects to the trap such as light or pheromone, or non-baited. Because baited traps alter the insect behavior, they are much more difficult to model and the corresponding theory is largely absent. Here we mostly consider non-baited traps.

In this section, we revisit two different (albeit related) approaches to trap counts modeling and interpretation: the individual-based approach, where the movement of each individual is followed explicitly, and the mean-field approach, where trap counts are described in term of the population density in the vicinity of the trap. We will show that, in order to achieve a good understanding of trap counts, the two approaches should be used together.

Interpretation of trap counts aiming to estimate the population abundance in the vicinity of a trap is not at all straightforward. The essence of the challenge is readily seen from the following example. Consider a trap of radius r that has caught C_1 insects after having been exposed for time T. This simple situation brings to the fore a number of questions concerning whether we can obtain the population density U_0 from this information. (i) If this information is sufficient, how do we actually calculate U_0? (ii) If this information is insufficient, then what else (e.g. how many more counts) do we need to know in order to get a reasonably accurate estimate of the population density? (iii) How the additional information can be used in order to improve the accuracy of the estimate? Further in the text, we will refer to it as the 'single trap problem'. Existing semi-empirical approaches suggest that $U_0 = \kappa C_1/(DT)$ where D is the diffusion coefficient and κ is a certain numerical coefficient, thus regarding DT as the effective 'catchment area' [30, 165]. However, this approach does not work in the case of repeated trap counts because it does not take into account the perturbation to the spatial distribution of the insects introduced by the trap. Moreover, a consistent theory and robust computational algorithms only exist in the case where insects perform Brownian motion. There is increasing evidence that animals may perform non-Brownian motion such as Levy flights, but a theory relating the corresponding trap counts to population density is lacking. Note that the problem of trapping has been studied extensively in physics (e.g. see [50]) including the case of anomalous diffusion [93], but most of the studies are concerned with large-time asymptotics while for insect monitoring short-time dynamics is of primary interest.

2.1. Individual-based approach

It is common knowledge that animals move in space. Such motion is regarded as an essential feature of animal life. Through their individual movement, animals make better use of the environment, e.g. by foraging, by searching for a mating partner, by avoiding predators, etc. Once a trap is installed, it introduces a perturbation into the movement; when an animal (e.g. insect) encounters the trap on its way, it will fall into it with a certain probability. This probability can depend on the trap design (e.g. it is larger for baited traps than for non-baited ones) and on the species traits. For well-designed traps, it is close to one, and this is what we are going to assume throughout the text without a loss of generality.

Before the animal will have a chance to fall into the trap, it has to get close to the trap boundary. Therefore, we first need to consider the movement in a more formal way. For the sake of clarity, here we focus on movement in two spatial dimensions, i.e. in the plane (x, y). Our analysis therefore immediately applies to trapping of walking or crawling insects in a field. Reduction of the approach to a simpler 1D case or its extension onto a slightly more general 3D case are relatively straightforward.

Generally, movement of an individual animal takes place along a certain curvilinear path or trajectory. In observations, the animal's position is usually recorded not continuously but at certain moments (say, $t_0, t_1, \ldots, t_i, \ldots$), for instance, by taking snapshots of the movement arena. Correspondingly, the curvilinear path is mapped into a broken line defined by the positions $\mathbf{r}_i = \mathbf{r}(t_i)$, $i = 0, 1, \ldots$, of the animal [168]; see Fig. 1. For the sake of simplicity, we assume that $t_{i+1} - t_i = \Delta t = const$ for all i. Over the interval Δt, the animal moves along the straight line from $\mathbf{r}_{i-1}$

Please cite this article in press as: Petrovskii S, et al. Multiscale approach to pest insect monitoring: Random walks, pattern formation, synchronization, and networks. Phys Life Rev (2014), http://dx.doi.org/10.1016/j.plrev.2014.02.001

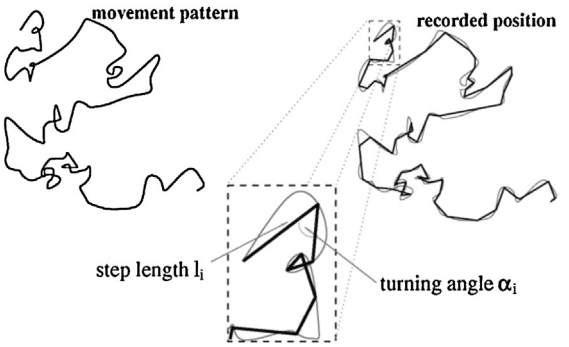

Fig. 1. A sketch of animal movement path and its discretization (from [70], with permissions).

to $\mathbf{r}_i$, thus covering the distance $l_{i-1} = |\mathbf{r}_i - \mathbf{r}_{i-1}|$ with the average velocity $\mathbf{v}_i = (\mathbf{r}_i - \mathbf{r}_{i-1})/\Delta t$. When it reaches its next position $\mathbf{r}_i$, it immediately turns by an angle α_i and moves to $\mathbf{r}_{i+1}$ covering distance l_i with the average velocity $\mathbf{v}_{i+1} = (\mathbf{r}_{i+1} - \mathbf{r}_i)/\Delta t$, then turns by the angle α_{i+1}, moves in the new direction, and so on. Clearly, this is a caricature of the actual movement and, unless the interval Δt is very small, some information about the animal movement is lost. (It is perhaps more appropriate to talk about the animal displacement from its initial position rather than about actual movement.) However, this approach still works well if the temporal scale of the particular phenomenon under study (which depends on the ecological context of animal movement) is much larger than the time-scale Δt of observations [34,43,70,143,168]. Indeed, for $\Delta t \to 0$, the broken line clearly converges to the original curvilinear path.

An uninterrupted movement along the broken line is completely described by two sequences, i.e., the sequence of step lengths $l_0, l_1, \ldots, l_i, \ldots$, and the sequence of turning angles $\alpha_1, \alpha_2, \ldots, \alpha_i, \ldots$. A major issue is the statistical properties of these sequences. To a certain extent, the answer depends on Δt. Assuming that the movement path is a smooth curve and Δt is sufficiently small, the $(i+1)$th step will be almost in the same direction as the ith one because in the limit $\Delta t \to 0$ both directions converge to the direction of the tangent line; therefore, $\alpha_i \approx 0$. Similarly, one can expect $l_{i+1} \approx l_i$; indeed, abrupt changes in the movement speed of a 'particle' of a finite mass are forbidden by Newton's Second Law as they would require infinitely large force. However, in the course of time small deviations accumulate. For a larger Δt, the piece of the animal path contained between $\mathbf{r}_i$ and $\mathbf{r}_{i+1}$ can take a complicated shape. Correspondingly, α_i is not necessarily small anymore, and l_{i+1} can be very different from l_i.

The next question is whether the variables l and α are deterministic or 'random', i.e. stochastic. For biological arguments, it seems improbable that at any given moment an animal moves randomly; a common assumption is that the speed and direction of its movement appear as a response to certain external stimuli [168]. However, the number of stimuli affecting the animal's movement can be large. As a result, even if the response to each stimulus is well defined and perfectly deterministic, the resultant response is likely to be complicated. This is exactly the context where Newtonian mechanics gives way to statistical mechanics [10]. Especially when the focus is on the path 'as a whole', as it often is in the dispersal studies [174], it is not instructive to look for a particular reason behind every animal's turn or move. On the contrary, a convenient description of individual movement is obtained by considering the step length l and the turning angle α as stochastic variables defined by their probability density functions (pdf), say, $\varphi(l)$ and $\psi(\alpha)$.

It is clear from the above argument that $\psi(\alpha) \to \delta(\alpha)$ for $\Delta t \to 0$, where $\delta(\alpha)$ is the Dirac function. For any Δt finite but small, $\psi(\alpha)$ is a dome-shaped function with the maximum at $\alpha = 0$. This means that the preferred direction of the next step coincides with the direction of the previous step and large turning angles are suppressed; the corresponding movement pattern is called a Correlated Random Walk (CRW) [76]. With an increase in Δt, the animal will eventually 'forget' the direction of its previous step as the part of the original curvilinear path between $\mathbf{r}_i$ and $\mathbf{r}_{i+1}$ will include more and more bends and curls; therefore, for a sufficiently large Δt the random walk becomes isotropic, i.e. $\psi(\alpha) \approx const = 1/(2\pi)$. This is sometimes referred to as the tangling impact of the turning angles [13] and is obtained from the CRW in the multi-step limit [76]. In the following, we will mostly focus on isotropic random walks where the pdf for the turning angle is uniform around the circle.

The procedure described above is a standard protocol used in field or laboratory studies on animal movement where the distribution of steps and/or turning angles can be obtained from the collected data [51,90]. It can also be used as a baseline for a theoretical insight into the dynamics of trap counts. Having the probability density functions available

Please cite this article in press as: Petrovskii S, et al. Multiscale approach to pest insect monitoring: Random walks, pattern formation, synchronization, and networks. Phys Life Rev (2014), http://dx.doi.org/10.1016/j.plrev.2014.02.001

(e.g. from a previous study on the given species), one can simulate the movement of each individual in the field [31,70] and calculate the trap counts straightforwardly [127,179].

Consider an individual that is situated at a position $\mathbf{r}_i = (x_i, y_i)$ at time t_i. Its position $\mathbf{r}_{i+1} = (x_i + \xi_i, y_i + \eta_i)$ at the next moment t_{i+1} can be written down as $\mathbf{r}_{i+1} = \mathbf{r}_i + (\Delta\mathbf{r})_i$ where $(\Delta\mathbf{r})_i$ is the ith step along the path. In the local polar coordinates, $\Delta\mathbf{r}_i = (l_i, \alpha_i)$ where l_i is the step length and α_i is the turning angle. Alternatively, in Cartesian coordinates $(\Delta\mathbf{r})_i = (\xi_i, \eta_i)$ and the path is defined by the pdfs for the random variables ξ_i and η_i, and can be simulated accordingly.

Consider the case of insects performing Brownian motion defined by the following pdfs:

$$\varrho(\xi) = \frac{1}{\delta\sqrt{2\pi}} \exp\left[-\frac{\xi^2}{2\delta^2}\right], \qquad \varrho(\eta) = \frac{1}{\delta\sqrt{2\pi}} \exp\left[-\frac{\eta^2}{2\delta^2}\right]. \tag{1}$$

Note that our choice of zero mean and the same variance δ^2 for $\varrho(\xi)$ and $\varrho(\eta)$ implicitly assumes that the movement does not have any directional bias and hence it occurs in an isotropic environment, e.g. it is not affected by the wind.

The distribution of steps and turning angles can be easily obtained from (1). Indeed, consider an animal positioned at the origin. The probability that it will move into an (infinitesimally) small vicinity of the point $(\xi, \eta) = (l, \alpha)$ over the next time step is:

$$dP = \varrho(\xi)\varrho(\eta)\, d\sigma, \tag{2}$$

where $d\sigma$ is the area of the vicinity. For an infinitesimally small vicinity, the details of its geometry do not matter and therefore $d\sigma = d\xi\, d\eta = l\, dl\, d\alpha$. Taking into account Eqs. (1) and recalling that $\xi^2 + \eta^2 = l^2$, from (2) we then obtain:

$$dP = \frac{1}{2\pi\delta^2} \exp\left(-\frac{l^2}{2\delta^2}\right) l\, dl\, d\alpha. \tag{3}$$

However, in polar coordinates, the probability dP is

$$dP = \varphi(l)\psi(\alpha)\, dl\, d\alpha \tag{4}$$

(assuming that l and α are mutually independent) where $\varphi(l)$ and $\psi(\alpha)$ are the probability density functions for l and α, respectively. Comparing the right-hand sides of (3) and (4), we obtain the expression for $\psi(\alpha)$:

$$\psi(\alpha) = \frac{1}{2\pi}. \tag{5}$$

Indeed, in the absence of a preferred direction, all directions are equivalent and therefore α must be distributed uniformly over the circle.

As for the distribution of step length, we obtain:

$$\varphi(l) = \frac{l}{\delta^2} \exp\left(-\frac{l^2}{2\delta^2}\right). \tag{6}$$

Obviously, the description of the movement path in terms of pdfs (5)–(6) for the step and turning angle is equivalent to the description with pdfs for ξ and η as given by Eqs. (1). Interestingly, in a more general case this is not necessarily true. Indeed, for any probability density function other than the normal distribution, ξ^2 and η^2 do not fold into l^2. In particular, in the case of a Levy flight, the increments in x and y are not independent [77]. Considering them as independent may result in an artificial movement path where all long jumps are aligned with either axis x or y, cf. Fig. 3 from [77]. Correspondingly, in order to simulate a sample path, one should either use another procedure of generating the increments that is considerably more complicated [77] or use the alternative description of the steps in the polar coordinates.

We also mention here that the properties of individual animal movement can be considerably different for different $\varphi(l)$, in particular depending on whether the rate of decay of φ at large l is fast enough to ensure the existence of the mean and the variance or not; the latter is often referred to as a "fat-tailed" distribution [174]. In Section 2.5, we will consider this issue in more detail.

A trap introduces a perturbation to the movement. Once the animal's path crosses the trap boundary, the animal is trapped and the path terminates. Consider a trap of circular shape with radius R and its center at $(\bar{x}, \bar{y})$. In mathematical terms, a given animal is caught at moment t_i if:

Please cite this article in press as: Petrovskii S, et al. Multiscale approach to pest insect monitoring: Random walks, pattern formation, synchronization, and networks. Phys Life Rev (2014), http://dx.doi.org/10.1016/j.plrev.2014.02.001

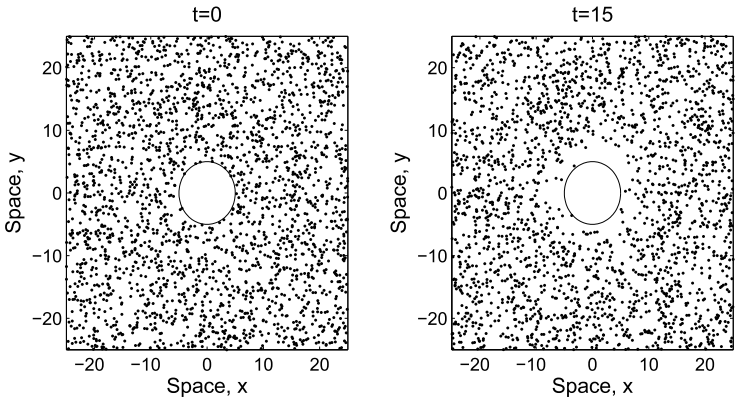

Fig. 2. Population of insects performing Brownian motion as defined by (1) with $\delta^2 = 0.02$; snapshots are shown at $t = 0$ (left) and $t = 15$ (right), i.e. after 1500 steps with a hypothetical value $\Delta t = 0.01$. Only a part of the computational domain is shown, the total size is 100×100. The initial population density is $U_0 = 1$ which corresponds to the total initial population size of $K = 10^4$.

$$(x_i - \bar{x})^2 + (y_i - \bar{y})^2 < R^2. \tag{7}$$

In ecological applications, there is not just one insect wandering in the field but many of them, say, K. Correspondingly, when the population dynamics are simulated using the individual-based approach, at each time step the new positions for all K animals are calculated using the same probability density functions.[2] At each time step, after the new position for each of the insects has been simulated, the condition (7) is applied. The trap counts are obtained accordingly: when the position of an animal is first observed to be inside the trap, the corresponding path is terminated and the trap count increases by one.

Fig. 2 shows snapshots of the population distribution simulated using the above procedure in a square arena or domain $L \times L$ (with $L = 100$, in abstract units) and a circular trap of radius $R = 5$ installed in the center of the domain. For the initial condition (Fig. 2, left), we first took K insects and distributed them randomly across the whole domain, and then removed those whose position appeared to be inside the trap. This results in the average population density of $U_0 = KL^{-2}$. Fig. 2 (right) shows the distribution obtained after 1500 steps, the probability density functions of the random walk being given by the normal distributions (1) with variance $\delta^2 = 0.02$.

Note that this individual-based modeling procedure does not contain the time intervals explicitly. For a given pdf, the evolution of the population distribution in discrete time depends on the number of steps i but not on Δt. However, here we recall that, in studies on individual animal movement, the time-discrete random walk is not inherent but is introduced as a theoretical framework to describe time-continuous movement (e.g. see the beginning of this section). The time thus appears implicitly through the value of the variance: the larger the time interval Δt between the two subsequent fixations of the animal position, the larger is the variance of the step size distribution. Moreover, time becomes explicit when the time-discrete random walk is linked to its time-continuous mean-field counterpart (see Section 2.2). With this idea in mind, we can chose a certain value of Δt; in particular, for the simulation results shown in Fig. 2 we consider $\Delta t = 0.01$.

In agreement with intuitive expectations, the trap introduces a spatially inhomogeneous perturbation into the population distribution. A visual inspection of Fig. 2 immediately reveals that the population density near the trap boundary is smaller than the density far away from the trap. This is shown more explicitly in Fig. 3. Due to the finite population size, the density fluctuates stochastically around its average value $U_0 = 1$. Considering the evolution of the population density profile, we observe that the radius of the perturbed area grows with time; as will be further explained in the next section, this transient behavior is a principle property of the system dynamics that determines the pattern in the trap counts sequence over time.

It is readily seen that this emerging spatial pattern affects the trap counts. For any given level of insects movement activity (i.e. for any given δ), the number of insects caught per unit time increases with the population density in the vicinity of the trap. Therefore, on average (up to fluctuations of stochastic origin), the number of insects caught

[2] Here we neglect the inter-individual interactions that can potentially lead to a variety of collective phenomena in movement and behavior, e.g. see [36,163].

Please cite this article in press as: Petrovskii S, et al. Multiscale approach to pest insect monitoring: Random walks, pattern formation, synchronization, and networks. Phys Life Rev (2014), http://dx.doi.org/10.1016/j.plrev.2014.02.001

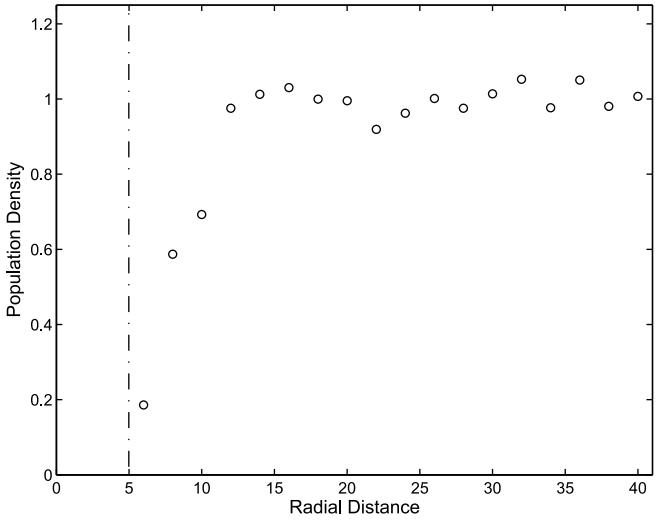

Fig. 3. Insect density as a function of the radial distance from the center of the trap corresponding to the snapshot shown in Fig. 2, right. The vertical line shows the position of the trap boundary.

per unit time should gradually decrease with time. This heuristic argument appears to be in full agreement with simulation results. Fig. 4 (top) shows the daily trap count C vs time over 3000 steps (100 steps = 1 day) obtained for initial population density $U_0 = 0.1$. The general tendency of daily counts to decrease with time can be readily seen, although the strong effect of stochasticity obscures the details of this pattern.

The pattern in the trap counts sequence is seen more clearly if, instead of daily counts, we consider a cumulative trap count J_n defined as the sum of all daily counts up to the given day n:

$$J_n = J(t_n) = \sum_{i=1}^{n} C_i, \tag{8}$$

where C_i is the trap count obtained in day i. The cumulative trap count obtained from the simulated daily counts shown in Fig. 4 (top) is shown in Fig. 4, bottom.

For a different initial distribution of the insects, both the emerging distribution and the pattern of trap counts can be completely different. Fig. 5 shows the snapshots of the insect distribution at two moments of time obtained in the case of a point-source release at the position $x = -10$, $y = -10$. Although the area occupied by the insects eventually grows in time, only very few insects reach the position of the trap boundary until approximately $t = 5$; see Fig. 6. For any earlier time, the obtained trap counts are zero.

Note that, from the mathematical point of view, the choice of the initial conditions is likely to affect only the early, transient stage of the dynamics before the system approaches some kind of 'equilibrium state'. However, in applications to pest monitoring and control, it is the transient stage – not the equilibrium state! – that is the focus of interest. Indeed, different initial population distributions correspond to different ecological situations that may require different control strategies. In particular, population aggregation (cf. Fig. 5) can arise for a variety of reasons such as a population response to environmental heterogeneity (when a favorable 'patch' has a much higher population density than the less favorable environment around it), self-organization due to spatiotemporal interspecific interactions [88], or swarming behavior [107]. The latter is especially important in the context of insect pest monitoring. Indeed, insect pest infestation often starts when an invasive or migrating swarm of pest insects lands in a small area inside an agricultural field. In this paper, we will refer to this situation as a 'point-source release'. From this initial source, the population then starts spreading over space. An early detection of the location of the population source, as well as the estimation of population size of the landed swarm, are therefore tasks of high practical importance for pest monitoring and control [58].

However, not all insect species migrate or disperse over long distances. Correspondingly, the uniform initial distribution may arise naturally from the residual pest population (e.g. over-wintered or remaining after pesticides application) dwelling in a relatively homogeneous environment.

Please cite this article in press as: Petrovskii S, et al. Multiscale approach to pest insect monitoring: Random walks, pattern formation, synchronization, and networks. Phys Life Rev (2014), http://dx.doi.org/10.1016/j.plrev.2014.02.001

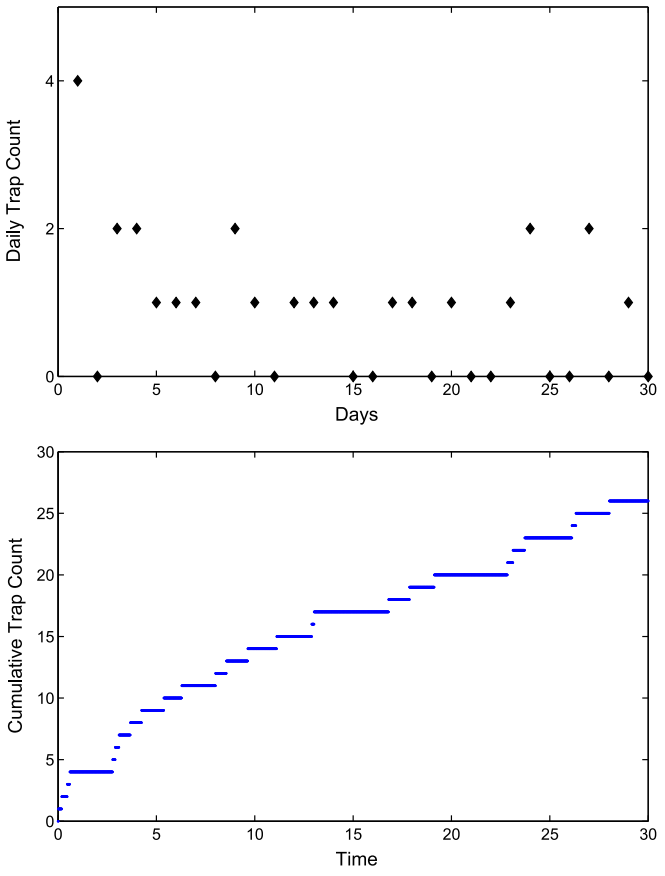

Fig. 4. Trap counts vs time (in days) obtained for $U_0 = 0.1$ (which corresponds to the total initial population size of $K = 10^3$ insects), other parameters as in Fig. 2. Top: daily trap count C; bottom: the cumulative number J of insects trapped, see Eq. (8).

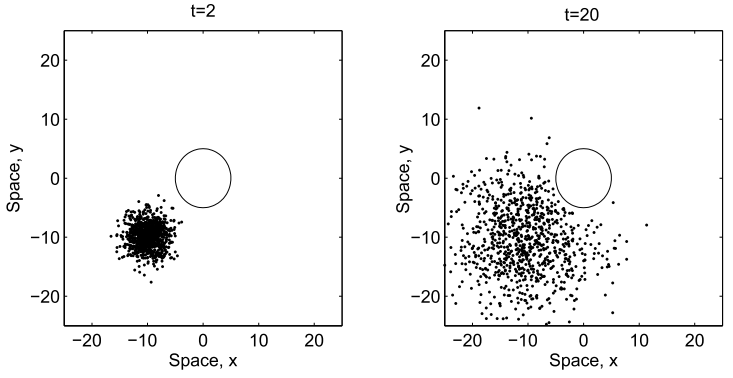

Fig. 5. Population of insects performing Brownian motion (Eqs. (1) with $\delta^2 = 0.01$); snapshots are shown at $t = 2$ (left) and $t = 20$ (right), i.e. after 200 and 2000 steps, respectively. Only a part of the computational domain is shown. The initial population consists of $K = 10^3$ insects and is released at the point $(x, y) = (-10, -10)$.

As an 'intermediate' case between the point-source release and the uniform distribution, insect pest infestation may occur as a result of short-distance migration, for instance, from an adjoint non-farmed habitat. We consider this case in detail in Section 2.3.

Now we recall that the ultimate goal of trapping is to reveal the population density distribution in the vicinity of the trap. The results shown in Figs. 4 and 6 are obtained in computer simulations where all parameters are known.

Please cite this article in press as: Petrovskii S, et al. Multiscale approach to pest insect monitoring: Random walks, pattern formation, synchronization, and networks. Phys Life Rev (2014), http://dx.doi.org/10.1016/j.plrev.2014.02.001

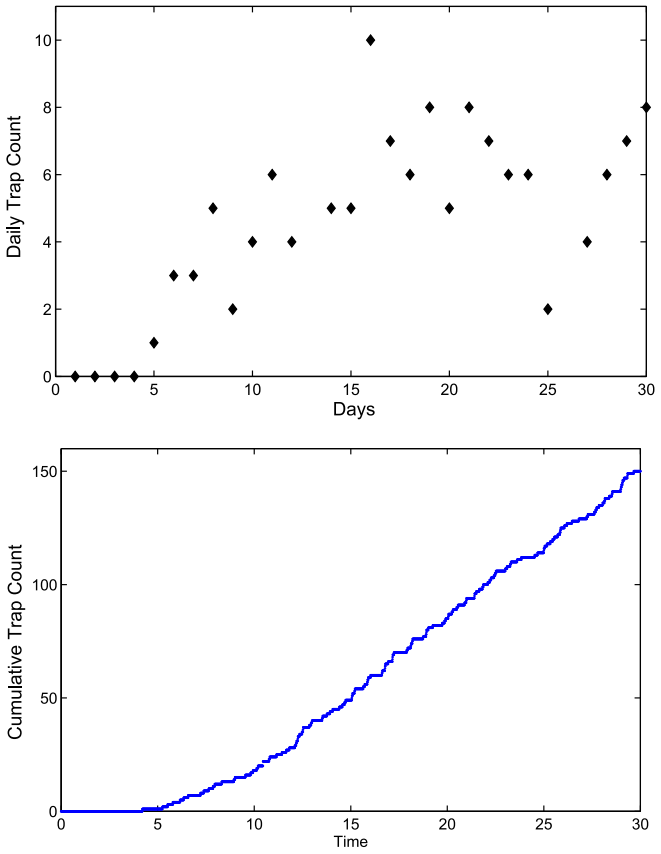

Fig. 6. Trap counts vs time (in days) obtained for a point-source release with parameters as in Fig. 5. Top: daily trap count C; bottom: the cumulative number J of insects trapped, see Eq. (8).

However, sequences of trap counts similar to Figs. 4 and 6 are routinely obtained in pest monitoring. How can we estimate the underlying population density or the location of point-source release, especially when the effects of stochasticity are so strong that they make it almost impossible to distinguish any pattern in the counts sequences? In the next section, we will show that this can be done (often with surprisingly good accuracy, sometimes using a dataset consisting of just several trap counts) by considering the stochastic trap counts together with their deterministic mean-field counterpart.

2.2. *Mean-field approach: Diffusion equation*

The individual-based approach considered in the previous section makes it possible to simulate the trap counts directly for any chosen initial distribution of insects and for any particular movement pattern as given by the probability distributions of the step length and turning angle. This makes it possible to mimic various specific situations in real-world pest control. However, a problem with the individual-based approach is that, since it is essentially simulation-based, it does not allow us to draw general conclusions about trap counts for different parameter values.

There is, however, another way to describe the trap counts. It is well known [17,33,34,107,160,168] that the population density of a system of particles performing Brownian motion is a solution of the diffusion equation. Below we give a heuristic derivation of the diffusion equation; a rigorous derivation with a detailed discussion of all subtle issues arising on the way can be found, for instance, in [52,145].

Let us consider a single insect or 'particle' randomly browsing in an infinite space. For the sake of simplicity, here we focus on the 1D case. Let $G(x,t)$ be the probability density for this random walker to be found at the position x at time t. Correspondingly, the probability to find the walker at time t in a small vicinity of x, i.e. in $(x, x+dx)$, is $P_{dx}(x,t) = G(x,t)\,dx$.

Please cite this article in press as: Petrovskii S, et al. Multiscale approach to pest insect monitoring: Random walks, pattern formation, synchronization, and networks. Phys Life Rev (2014), http://dx.doi.org/10.1016/j.plrev.2014.02.001

The evolution of the probability density is described by the master equation [10,33,160]:

$$G(x, t + \Delta t) = \int_{-\infty}^{\infty} G(x - \xi, t)\varrho(\xi, \Delta t)\, d\xi. \tag{9}$$

In the context of the previous section, we consider Eq. (9) as a discrete-time model of an inherently continuous insect movement, Δt being the timescale of (discrete) observations. The kernel $\varrho(\xi, \Delta t)$ is the probability density of the next position of the walker after time Δt, i.e. after one step in time, if its position at time t is at the origin. In ecological studies, $\varrho(\xi, \Delta t)$ defined as above is often called the dispersal kernel. Function ϱ obviously depends on Δt: increasing the time interval between the two subsequent fixations of the insect position, increases (on average) the corresponding displacement. We consider the motion to be stationary (in the statistical sense) and to be taking place in a homogeneous space, so that ϱ does not depend on x or t.

Eq. (9) is complemented by the initial condition:

$$G(x, 0) = \delta(x - x_0), \tag{10}$$

where x_0 is the position of the walker at $t = 0$.

Eq. (9) is very general and, as such, describes a variety of different stochastic processes. The type of the random walk can be specified by assuming certain properties of the function $\varrho(\xi, \Delta t)$. In particular, under certain constraints, the continuous-time limit $\Delta t \to 0$ of Eq. (9) turns into the Fokker–Planck equation, of which the diffusion equation is a special case.

With the continuous limit in mind, we consider Δt to be sufficiently small and apply the Taylor expansion to the left-hand side of (9) keeping explicitly only the first two terms, so that:

$$G(x, t + \Delta t) = G(x, t) + \frac{\partial G(x, t)}{\partial t}\Delta t + o(\Delta t), \tag{11}$$

where the notation $o(\Delta t)$ is used to refer to all small terms of a higher order, so that $o(\Delta t)/\Delta t \to 0$ when $\Delta t \to 0$.

Since $\varrho(\xi, \Delta t)$ is the probability density:

$$\int_{-\infty}^{\infty} \varrho(\xi, \Delta t)\, d\xi = 1, \tag{12}$$

hence ϱ must decay sufficiently fast at large ξ. Correspondingly, we assume that only small values of ξ contribute significantly to the right-hand side of (9) and apply the Taylor expansion to $G(x - \xi, t)$:

$$G(x - \xi, t) = G(x, t) - \frac{\partial G(x, t)}{\partial x}\xi + \cdots + \frac{(-1)^k}{k!}\frac{\partial^k G(x, t)}{\partial x^k}\xi^k + \cdots. \tag{13}$$

An important property of ϱ that distinguishes between different type of the random walk is its rate of decay at large ξ. In particular, if the rate of decay is exponential or faster, then, having substituted (11) and (13) into (9), Eq. (9) takes the following form:

$$\frac{\partial G(x, t)}{\partial t}\Delta t + o(\Delta t) = \sum_{k=1}^{\infty} \frac{(-1)^k}{k!}\frac{\partial^k G(x, t)}{\partial x^k}\langle \xi^k \rangle, \tag{14}$$

where $\langle \xi^k \rangle$ is the kth moment of the probability distribution ϱ:

$$\langle \xi^k \rangle = \int_{-\infty}^{\infty} \xi^k \varrho(\xi)\, d\xi \ < \ \infty, \quad k = 1, 2, \ldots. \tag{15}$$

We now restrict our analysis to the case where random movement is isotropic so that there is no directional bias. Correspondingly, $\varrho(\xi) = \varrho(-\xi)$ and all odd moments disappear, $\langle \xi^{2m+1} \rangle = 0$ $(m = 0, 1, \ldots)$. From (14), we then obtain:

Please cite this article in press as: Petrovskii S, et al. Multiscale approach to pest insect monitoring: Random walks, pattern formation, synchronization, and networks. Phys Life Rev (2014), http://dx.doi.org/10.1016/j.plrev.2014.02.001

$$\frac{\partial G(x,t)}{\partial t} + \frac{o(\Delta t)}{\Delta t} = \sum_{m=1}^{\infty} \frac{(-1)^k \langle \xi^{2m} \rangle}{k! \Delta t} \frac{\partial^{2m} G(x,t)}{\partial x^{2m}}. \tag{16}$$

Since ϱ depends on Δt, the moments depend on Δt as well. Their dependence on the timescale differentiates between different movement scenarios. Here we assume that the variance $\langle \xi^2 \rangle$ of the distribution ϱ does not have a singularity at $\Delta t = 0$ and that its Taylor expansion has a non-zero linear term:

$$\langle \xi^2 \rangle = 2D\Delta t + o(\Delta t), \tag{17}$$

where the numerical coefficient $2D$ has the meaning of variance per unit time.

A further standard assumption [10,52] is that, increasing the moment's order increases the power of the first non-zero term in the corresponding Taylor expansion, so that:

$$\langle \xi^{2m} \rangle = o(\Delta t) \quad \text{for } m \geqslant 2. \tag{18}$$

The random walk that satisfies conditions (15) and (17)–(18) is called Brownian motion.

From (16)–(18), considering the limit $\Delta t \to 0$, we obtain the diffusion equation:

$$\frac{\partial G(x,t)}{\partial t} = D \frac{\partial^2 G(x,t)}{\partial x^2}, \tag{19}$$

where D is the diffusion coefficient:

$$D = \lim_{\Delta t \to 0} \frac{\langle \xi^2 \rangle}{2\Delta t}.$$

Here the existence of the limit is guaranteed by (17).

The solution of the diffusion equation corresponding to initial condition (10) is well known [37]:

$$G(x - x_0, t) = \frac{1}{\sqrt{4\pi Dt}} \exp\left[-\frac{(x - x_0)^2}{4Dt} \right]. \tag{20}$$

It is readily seen that the corresponding mean squared displacement of the walker is $\langle (x - x_0)^2 \rangle \sim Dt$. This property is widely regarded as a 'fingerprint' of the Brownian motion.

Note that in the special case where the dispersal kernel is given by the normal distribution:

$$\varrho(\xi, \Delta t) = \frac{1}{\sqrt{4\pi D\Delta t}} \exp\left[-\frac{\xi^2}{4D\Delta t} \right], \tag{21}$$

the probability density for the single walker at $t = n\Delta t$, i.e. after n steps, can be found from Eq. (9) by direct calculation. The mathematical fact that the convolution of two normal distributions is also a normal distribution is used here.

An important assumption made above is that ϱ decays sufficiently fast at large ξ to ensure the existence of all moments of the distribution, see (15). It is readily seen that this is true if $\varrho(\xi, \Delta t)$ is the normal distribution. Furthermore, this holds for any kernel with the rate of decay exponential or faster. A question arises naturally as to how the random walk properties may change if this constraint is relaxed and the kernel $\varrho(\xi, \Delta t)$ is fat-tailed, so that some of the moments do not exist. An immediate example is given by the case where ϱ decays as an inverse power law, i.e. $\varrho \sim \xi^{-\alpha}$ for $\xi \to \infty$ with $\alpha > 1$. The corresponding pattern of movement is often referred to as "superdiffusion" [173] or, more broadly, as anomalous diffusion [81,174]. A detailed discussion of this phenomenon lies beyond the scope of this paper. Here we only very briefly mention some of its properties.

The situation appears to be different for $\alpha > 3$ where the kernel possesses a finite variance and for $1 < \alpha \leqslant 3$ where a finite variance does not exist. In the former case, the Central Limit Theorem applies [46], which predicts that the probability density $G(x, n\Delta t)$ of the walker after n steps (i.e. the sum of n independent identically distributed random values) converges to the normal distribution for $n \to \infty$; see Fig. 7. Interestingly, the convergence occurs non-homogeneously in space, so that, for any finite n, the rate of decay at the tail of the probability distribution $G(x, n\Delta t)$ coincides with the rate of decay of the kernel [83], that is $G \sim (x - x_0)^{-\alpha}$. Therefore, the tail of the evolving distribution remains fat. Thus, in spite of the normal distribution arising in the large-time limit, at any finite

Please cite this article in press as: Petrovskii S, et al. Multiscale approach to pest insect monitoring: Random walks, pattern formation, synchronization, and networks. Phys Life Rev (2014), http://dx.doi.org/10.1016/j.plrev.2014.02.001

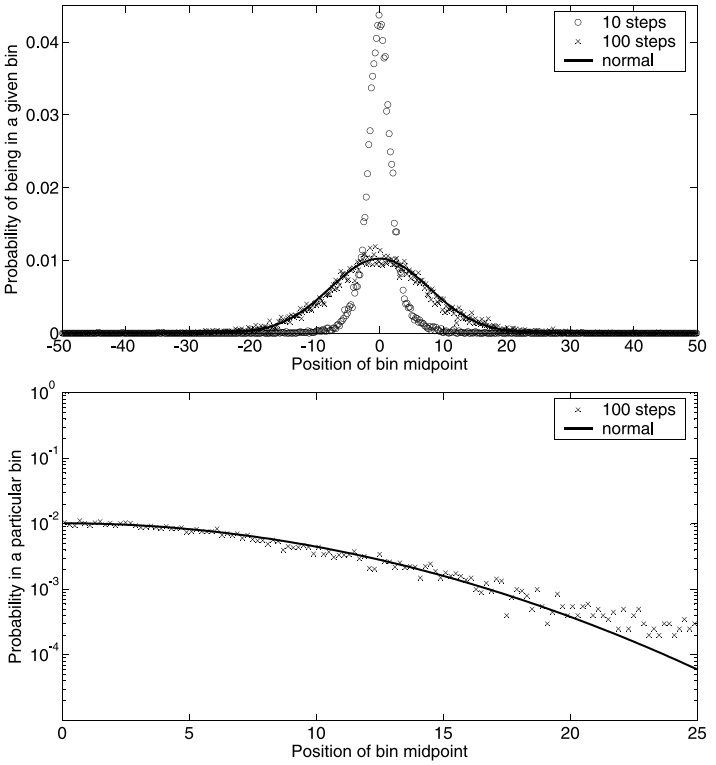

Fig. 7. Probability density distribution for the position of a random walker obtained in individual-based simulations after 10^4 realizations. At $t = 0$ the walker is released at $x = 0$. The symbols show the probability density given by the frequency per unit length in the interval or 'bin' centered at a given location x; the bin width is $\Delta x = 0.2$. The dispersal kernel used is $\varrho = C(|\xi| + \gamma)^{-\alpha}$ where $C = 0.5(\alpha - 1)$, $\alpha = 3.5$ and $\gamma = 1$. (Top) The emerging spatial distribution after 10 steps (circles) and after 100 steps (crosses). The solid curve shows the normal distribution $\mathcal{N}(0, 7.8)$. (Bottom) A fragment of the total domain showing the tail of the distribution emerging after 100 steps (in semi-logarithmic coordinates). Clearly there is a considerable deviation between the normal distribution and the actual population distribution at large x.

$t = n\Delta t$ the probability of a long jump remains high (compared to the vanishingly small probability described by the thin Gaussian tail), which results in a faster displacement [83].

For $1 < \alpha \leqslant 3$, the variance does not exist and the Central Limit Theorem does not hold so there is no convergence to the normal distribution. The corresponding random process is called a Levy walk. At any time t, the asymptotical rate of decay in the probability density G is the same as in the kernel, i.e. $G(x, t) \sim (x - x_0)^{-\alpha}$. An interesting special case is given by the Cauchy distribution [52]:

$$\varrho(\xi, \Delta t) = \frac{\nu \Delta t}{\pi[\xi^2 + (\nu \Delta t)^2]} = \frac{1}{\pi \nu \Delta t}\left[1 + \left(\frac{\xi}{\nu \Delta t}\right)^2\right]^{-1}, \tag{22}$$

where ν is the distribution parameter. A direct calculation (cf. [83]) shows that the probability density distribution G of the random walker with the dispersal kernel (22) is the Cauchy distribution at all time, i.e. after any number n of steps in time:

$$G(x, t = n\Delta t) = \frac{\nu n \Delta t}{\pi[(x - x_0)^2 + (\nu n \Delta t)^2]}. \tag{23}$$

For most of this paper (except Section 2.5), we assume that insects perform Brownian motion. Let us consider a point-source release of $K \gg 1$ independent identical walkers, the movement of each of them being described by Eq. (19). Since all the walkers are identical and independent, we may regard it as the same stochastic event repeated K times. Correspondingly, the number dK of the walkers to be found at time t in the vicinity of x is given by $dK(x, t) = KP_{dx}(x, t) = KG(x, t)\,dx$. Having defined the population density in the usual way as $u(x, t) = dK(x, t)/dx = KG(x, t)$, we find that it should be a solution of the same equation as G, i.e. of the diffusion equation:

Please cite this article in press as: Petrovskii S, et al. Multiscale approach to pest insect monitoring: Random walks, pattern formation, synchronization, and networks. Phys Life Rev (2014), http://dx.doi.org/10.1016/j.plrev.2014.02.001

$$\frac{\partial u(x,t)}{\partial t} = D\frac{\partial^2 u(x,t)}{\partial x^2}. \tag{24}$$

The diffusion equation (19) for the probability density of a single walker is precise in the continuous limit $\Delta t \to 0$. However, one can expect that it remains valid, at least approximately, for a small but finite value of Δt. In the corresponding approximate expression for the diffusion coefficient:

$$D \approx \frac{\delta^2}{2\Delta t}, \tag{25}$$

δ^2 is the variance of the probability density ϱ of the next step's length for the given value of Δt. This is obviously the same δ^2 that was used in the individual-based simulations in Section 2.1. Therefore, the diffusion coefficient links the "microscale" of an individual walker to the "macroscale" of the population density. We mention here that the diffusion equation for the population density could be derived in a completely different way based on Fick's law relating population flux to the density gradient [17,37]. However, in that case the relationship between micro- and macro-scales would remain obscure.

We mention here that, in mathematical terms, Eq. (19) (or (24)) should be classified as deterministic because it does not contain any random values. Although the random walk is a paradigm of stochastic dynamics, it is described by a purely deterministic diffusion equation. Therefore, the stochastic nature of the process does not necessarily require an explicitly stochastic model. This observation is well known in physics[3] but it is less commonly appreciated in biological applications.

In fact, an explicitly stochastic model may only be required if we are interested in fluctuations, i.e. the deviations from the mean. In the particular case of Brownian motion, by virtue of the Central Limit Theorem the relative magnitude of the fluctuations is:

$$\frac{\Delta u}{u} \sim \frac{1}{\sqrt{u}}.$$

Hence fluctuations are negligible for large population densities but may become important at small densities.

In the case of a point-source release, the initial condition for Eq. (24) is given by $u(x,0) = K\delta(x - x_0)$ and the spatial distribution of the population density is immediately obtained from (20) as $u(x,t,x_0) = KG(x - x_0, t)$. In a more general case, $u(x,0) = u_0(x)$ where $u_0(x)$ is a certain function, it is straightforward to see (cf. [37]) that the solution of the diffusion equation is

$$u(x,t) = \int_{-\infty}^{\infty} G(x-\xi,t)u_0(\xi)\,d\xi. \tag{26}$$

In practical applications concerned with trapping of walking or crawling insects, the diffusion equation should be considered on a 2D domain (on a 3D domain for flying insects). However, it is instructive to begin with a 1D case when the population density depends on one spatial coordinate only. Moreover, the traps used in pest monitoring often have the shape of a long narrow slot ([21]; also [49]) and in that case 1D approximation can be expected to provide not only a qualitative but also a quantitative insight into the problem.

When the trap is installed, the movement space is not infinite anymore and the diffusion equation must be complemented with the boundary conditions. Let us consider a population of randomly walking insects in a field of size L. For the moment, we assume L is very large, $DTL^{-2} \ll 1$ where T is the characteristic trapping time. Correspondingly, we consider the diffusion equation in the semi-infinite domain $0 < x < \infty$ (the effects of finiteness will be addressed later) where the trap is installed at the left-hand side so that $x = 0$ corresponds to the trap boundary. Since there are no live insects in the trap, the relevant boundary condition is:

$$u(0,t) = 0. \tag{27}$$

The corresponding solution of the diffusion equation is:

[3] The Schrödinger equation would be another good example.

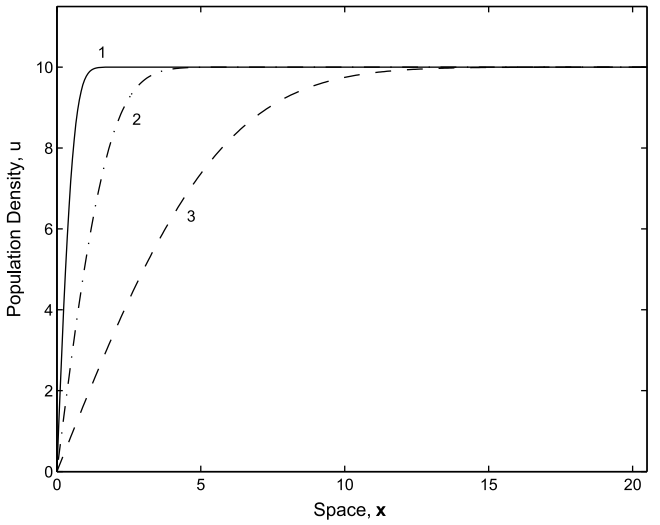

Fig. 8. Population density vs space as given by the solution (33) of the diffusion equation (24) at $t = 0.1$ (solid curve 1), $t = 1$ (dashed-and-dotted curve 2) and $t = 10$ (dashed curve 3) for parameters $D = 1$ and $U_0 = 10$. From [127], with permissions.

$$u(x,t) = \int_0^\infty \big[G(x-\xi,t) - G(x+\xi,t)\big] u_0(\xi)\, d\xi \tag{28}$$

(e.g. see [37]) where G is given by (20).

Once the solution is known, the cumulative trap count over time t can be calculated as:

$$J(t) = \int_0^t \big|j(\tau)\big|\, d\tau, \tag{29}$$

where:

$$j(t) = -D \frac{\partial u(x,t)}{\partial x}\bigg|_{x=0} \tag{30}$$

is, according to Fick's law, the diffusive flux of population density through the trap boundary.

Considering (29)–(30) together with (28), after some standard calculations we obtain:

$$J(t) = \int_0^\infty u_0(\xi)\left[1 - \mathrm{erf}\left(\frac{\xi}{\sqrt{4Dt}}\right)\right] d\xi, \tag{31}$$

where $\mathrm{erf}(z)$ is the error function.

The properties of J as a function of time can therefore be different for different initial population distributions. In the special but ecologically meaningful case of a homogeneous distribution $u_0(x) = U_0 = const$, from Eq. (31) we readily obtain:

$$J(t) = \frac{2U_0}{\sqrt{\pi}} \sqrt{Dt}. \tag{32}$$

The corresponding solution of the diffusion equation is given by:

$$u(x,t) = U_0\, \mathrm{erf}\left(\frac{x}{\sqrt{4Dt}}\right) \tag{33}$$

and is shown in Fig. 8. Note that the size of the spatial perturbation induced by the trap grows with time as $\sim \sqrt{Dt}$.

Please cite this article in press as: Petrovskii S, et al. Multiscale approach to pest insect monitoring: Random walks, pattern formation, synchronization, and networks. Phys Life Rev (2014), http://dx.doi.org/10.1016/j.plrev.2014.02.001

Another relevant case is given by a distribution with constant gradient U_1, i.e. $u_0(\xi) = U_0 + U_1\xi$. This type of initial distribution may account for the migration of the pest species through the domain boundary; see Section 2.3. In this case, from (31) we obtain:

$$J(t) = \frac{2U_0}{\sqrt{\pi}}\sqrt{Dt} + U_1 Dt. \tag{34}$$

A somewhat different case is given by the initial condition where the population is aggregated at a certain position in space ('point source release', cf. Section 2.1), i.e. $u_0(x) = K\delta(x - x_0)$ with K the total number of insects released at $t = 0$ at location x_0 and δ is the Dirac function. In this case, Eq. (31) becomes:

$$J(t) = K\left[1 - \mathrm{erf}\left(\frac{x_0}{\sqrt{4Dt}}\right)\right] = K\,\mathrm{erfc}\left(\frac{x_0}{\sqrt{4Dt}}\right). \tag{35}$$

Recall that in the pest monitoring problem we are mostly interested in small time dynamics. Also, the position x_0 of the insects' release is unlikely to be in close vicinity of the trap, so x_0 can be regarded as large. Correspondingly, of particular interest is the limiting case where the argument z of $\mathrm{erfc}(z)$ is large. We can then make use of the following asymptotic expansion [1]:

$$\mathrm{erfc}(z) \simeq \frac{1}{\sqrt{\pi}}e^{-z^2}\left[\frac{1}{z} + o\left(\frac{1}{z}\right)\right]. \tag{36}$$

Retaining only the leading term, from (35) and (36), we obtain:

$$J(t) \simeq \frac{K}{\sqrt{\pi}}\frac{\sqrt{4Dt}}{x_0}\exp\left(-\frac{x_0^2}{4Dt}\right). \tag{37}$$

Eq. (37) gives the small-time dependence of the cumulative trap count in the case of a point-source release.

Coming back to the main goal of the single-trap scale of pest monitoring, now we are going to consider how Eqs. (31)–(35) can be used for the estimation of the population density or size of the monitored species. Indeed, predictions obtained from the diffusion equation result in smooth, continuous, deterministic curves while the trap count data are given by a discrete/discontinuous set often wildly oscillating due to stochastic effects, e.g. see Fig. 4. In order to answer this question, we recall that, given that the individual insect movement can be regarded (at least on a certain time scale) as a Brownian walk, the oscillations seen in the data occur around the value predicted by the diffusion equation. The unknown population density or total population size can be obtained by looking for the best fit between theory and data [127]. This best fit can be found by using appropriate statistical tools.

The choice of the statistical tools is a controversial issue. The recent trend is to calculate the maximum likelihood function and Akaike weights [29,56] as they are regarded as more reliable than other approaches. In this paper, however, in order to avoid unnecessary complexity, we use a simpler method of nonlinear regression [41] and the parameter estimation is done by using NLREG statistical software.[4] Also, since our goal here is more to justify the concept rather than to develop a ready-to-use practical toolkit, we restrict the analysis to a 1D case. Extension of the results onto a more realistic 2D case is discussed at the end of this section.

In order to simulate the trap counts in the 1D case, we apply the procedure described in Section 2.1. Fig. 9a shows a population of $K = 10^3$ insects that at $t = 0$ is distributed uniformly (in the statistical sense) over the domain $0 < x < L = 100$. Note that the actual values of the population density (defined as the number of insects inside a 'bin' of a certain width Δx) oscillates rather wildly around the mean value $U_0 = 10$. The trap is installed at the left-hand end of the domain so that any insect crossing $x = 0$ falls into the trap, and the right-hand side boundary is reflecting. Since Eq. (32) was obtained for the semi-infinite domain, we chose L large enough in order to minimize finite size effects. Fig. 9b shows the corresponding daily trap counts over the period of 30 days, i.e. consisting of 30 data points, simulated from Brownian motion with $D = 1$. The cumulative trap counts are shown in Fig. 9c; the best fit approximation of the data by Eq. (32) is obtained for $U_0 = 10.6$. Therefore, our approach (originally proposed in [127] and further developed here) makes it possible to estimate the value of the population density in the vicinity of the trap with a very good accuracy, i.e. with a relative error of just a few percent. This approach works with good accuracy for a shorter dataset as well. Fig. 9d shows the result of best fitting the data by Eq. (32) if only the first 10 data points are used; the corresponding estimate for the population density is $U_0 = 9.6$.

[4] © Phillip H. Sherrod; a demonstration version is available from http://www.nlreg.com.

Please cite this article in press as: Petrovskii S, et al. Multiscale approach to pest insect monitoring: Random walks, pattern formation, synchronization, and networks. Phys Life Rev (2014), http://dx.doi.org/10.1016/j.plrev.2014.02.001

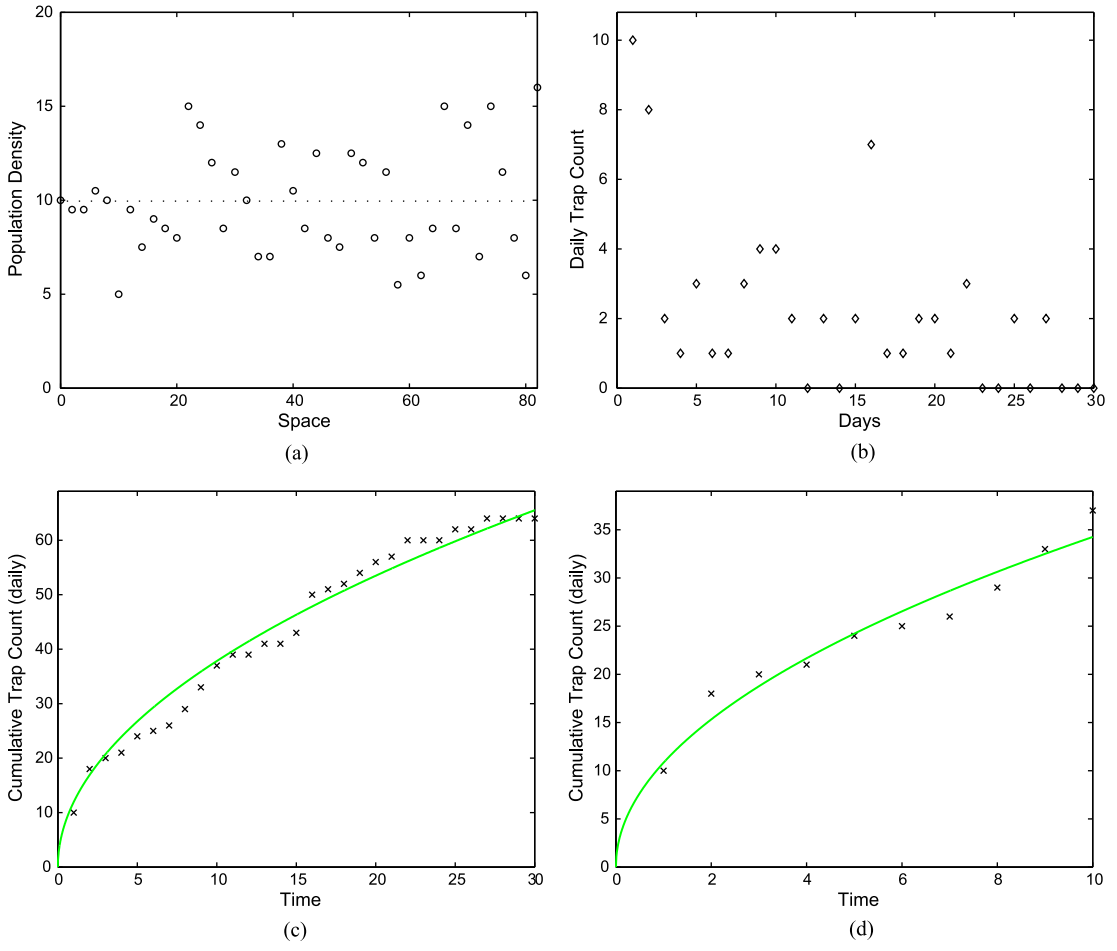

Fig. 9. (a) The initial statistically-uniform distribution of the population of size $K = 10^3$: the circles show the number of insects per unit length after they are binned with the width $\Delta x = 2$, the dotted curve shows the mean value of the population density $U_0 = 10$; (b) the daily trap counts; (c) the corresponding cumulative trap counts (shown by crosses) and their best-fit by the mean-field model (32) (shown by the solid curve), the best fit is obtained for $U_0 = 10.6$; (d) the results of data fitting in case of a smaller dataset, the best fit is obtained for $U_0 = 9.6$.

Use of the more general formula (34) also allows the parameters (in this case, U_0 and U_1) to be obtained with reasonable accuracy. In particular, having applied it to the data shown in Fig. 9d (i.e. the trap counts after the first ten days), we find that the best fit is reached for $U_0 = 9.5$ and $U_1 = 0.04$ where the latter is not significantly different from 0. In general, data fitting with a two-parameter formula is more demanding and, in order to reach a good accuracy, application of (34) may require a longer dataset compared to the one-parameter fit.

Our approach works well for aggregated initial conditions (point-source release) as well. As an example, let us consider the 1D domain $0 < x < 100$ where at $t = 0$ the population of $K = 1000$ insects is aggregated at $x = 10$. Fig. 10a shows the daily trap counts resulting from the Brownian motion with $D = 1$. Fig. 10b shows the corresponding cumulative trap counts and their best fit with the theoretical expression (35). The best fit is obtained for $K = 1176$ and $x_0 = 10.6$ which are parameter estimates of reasonable accuracy. Therefore, we are able not only to get an estimate of the pest population size but also its location, which is an important issue for practical applications [58]. As above, the need to estimate two parameters rather than one makes the accuracy somewhat worse than in the basic case (32). However, in the case shown in Fig. 10c it still provides a reasonable estimate for the parameter values based on just 15 datapoints, despite the fact that the counts over the first several days are either zero or very small and hence do not contribute much.

Please cite this article in press as: Petrovskii S, et al. Multiscale approach to pest insect monitoring: Random walks, pattern formation, synchronization, and networks. Phys Life Rev (2014), http://dx.doi.org/10.1016/j.plrev.2014.02.001

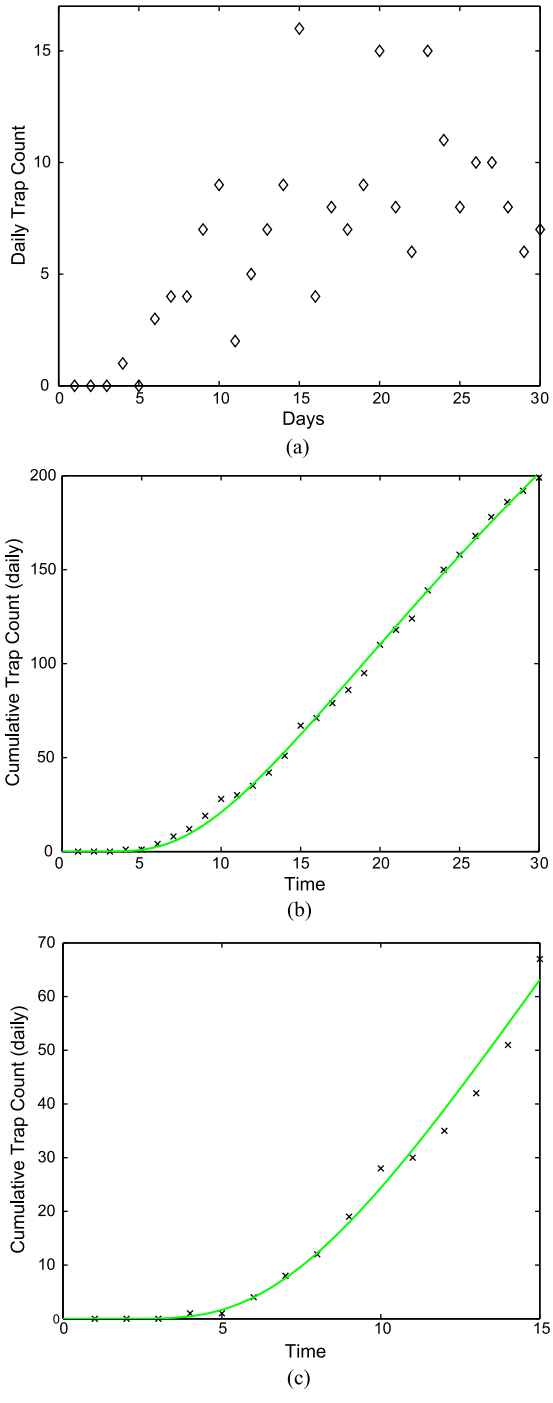

Fig. 10. (a) The daily trap counts obtained for a point-source release of $K = 1000$ insects at a distance of $x_0 = 10$ from the trap; (b) the corresponding cumulative trap counts (shown by crosses) and their best-fit by the mean-field model (35) (shown by the solid curve), the best fit is obtained for $K = 1176$ and $x_0 = 10.6$; (d) the results of data fitting in case of a smaller dataset, the best fit is obtained for $K = 848$ and $x_0 = 9.8$.

The domain used above was assumed to be large enough that the effect of the 'external' domain's boundary at $x = L$ could be neglected. If this does not hold, one needs to define the boundary condition and consider the solution of the corresponding boundary problem. Here we assume that there is no migration through the external field boundary:

Please cite this article in press as: Petrovskii S, et al. Multiscale approach to pest insect monitoring: Random walks, pattern formation, synchronization, and networks. Phys Life Rev (2014), http://dx.doi.org/10.1016/j.plrev.2014.02.001

$$\frac{\partial u(L,t)}{\partial x} = 0. \tag{38}$$

Applying the method of variable separation [37] to diffusion equation (24) with boundary conditions (27) and (38), we obtain the solution u in the form of an infinite series:

$$u(x,t) = \frac{4U_0}{\pi}\sum_{k=1}^{\infty}\frac{1}{(2k-1)}\sin\left(\frac{(2k-1)\pi x}{2L}\right)\exp\left(-\frac{(2k-1)^2\pi^2 Dt}{4L^2}\right). \tag{39}$$

From (30) and (39), we arrive at the expression for the diffusion flux at the trap boundary:

$$j(t) = -D\frac{\partial u(0,t)}{\partial x} = -\frac{2DU_0}{L}\sum_{k=1}^{\infty}\exp\left(-\frac{(2k-1)^2\pi^2 Dt}{4L^2}\right), \tag{40}$$

so that the number of insects trapped over time t is then obtained using (29):

$$J(t) = \frac{8LU_0}{\pi^2}\sum_{k=1}^{\infty}\frac{1}{(2k-1)^2}\left[1-\exp\left(-\frac{(2k-1)^2\pi^2 Dt}{4L^2}\right)\right], \tag{41}$$

where LU_0 is the total initial number of insects in the domain.

Expression (41) is valid for any t. The more compact expressions obtained above for the semi-infinite domain still apply, albeit approximately, if the observation time is not very large. In particular, in the case of a homogeneous initial distribution, we find that the same formula (32) works with a good accuracy until the perturbation from the trap reaches the outside boundary, i.e. unless t becomes very large or else L is small [127].

The above results were obtained for a 1D system. A straightforward consideration of the diffusion equation in the 2D case poses considerable technical difficulties; the corresponding solution is given by a series of the Bessel functions where an explicit expression for the coefficients is not known. An extension of the 1D results onto the 2D case was done in [127] based on scaling and dimensions analysis and a relatively simple, semi-empirical formula for the trap counts was obtained. The formula predicts that, in an infinitely large domain, the cumulative trap count $J(t)$ should become a linear function of time in the large-time limit. However, in a general case where the finiteness of the system cannot be neglected, J appears to be a linear combination of the small-time ($\sim\sqrt{t}$) and large-time ($\sim t$) asymptotics. The use of the formula to best-fit simulation data using nonlinear regression was shown to return an estimate of the corresponding population density with a reasonable accuracy of about 20% [127].

2.3. Boundary forcing

The goal of insect pest monitoring is to obtain information about pest abundance, in particular, with the purpose to detect signs of the pest population growth and hence to provide timely advice on pesticide application. An increase in the pest population size in a given agricultural field can occur because of the within-field population dynamics such as population multiplication due to reproduction. However, an increase in the pest density can also occur due to migration of the species to the field from the outside areas. This leads to the questions of (i) how this effect of pest immigration can affect the trap counts, (ii) whether it may be possible to distinguish between the effects of the native and immigrating populations, and (iii) what is the relevant timescale of trap counts collection? Mathematically, immigration can be taken into account by imposing relevant conditions at the domain boundary, e.g. by defining the value of the in-flowing flux of the population density. Correspondingly, we will refer to the effect of pest immigration as boundary forcing.

In Sections 2.1 and 2.2, pest immigration was taken into account indirectly by considering a point source release, i.e. the spatially aggregated initial population distribution. However, that only accounts for one possible ecological scenario where a swarm of insects arrives and lands at a certain location in the field. Another typical scenario occurs when the given agricultural field adjoins a non-farmed area such as grassland or meadow. Non-farmed areas are rarely treated against pests; as a result, such areas often become a refuge for pest species. The insects may then start spreading from their refuge into the neighboring field(s).

Spreading can take place in different ways. If individual insects move around in a random manner, the migration from the refuge to an adjoint farm-field goes against the population density gradient as described by Fick's law.

Please cite this article in press as: Petrovskii S, et al. Multiscale approach to pest insect monitoring: Random walks, pattern formation, synchronization, and networks. Phys Life Rev (2014), http://dx.doi.org/10.1016/j.plrev.2014.02.001

Alternatively, there can be a directed movement towards the farm-field, for instance due to the transport with the favorable wind (for airborne species) or as a response to an odor emanating from the culture grown in the field.

We first consider the case where immigration occurs due to a directed movement. Transport through the field boundary is then described by the population flux $\mathbf{j}_b = \mathbf{v}U_b$ where $\mathbf{v}$ is the velocity of the advection/migration and U_b is the population density outside (i.e. in the non-farmed habitat). Assuming that inside the field the insects move in a diffusive manner, the corresponding boundary condition is:

$$-D\frac{\partial u(\mathbf{r},t)}{\partial \mathbf{n}}\bigg|_{\Lambda} = (\mathbf{j}_b, \mathbf{n}), \tag{42}$$

where Λ is the field boundary and $\mathbf{n}$ is a unit normal vector pointing outside.

In the analysis below, we focus on a 1D case where the field is described by the domain $0 < x < L$. The trap is installed at $x = 0$ and $x = L$ is the external boundary where immigration occurs. Condition (42) then turns into the following Neumann-type boundary condition at $x = L$:

$$\frac{\partial u(L,t)}{\partial x} = G, \tag{43}$$

where G is the value of the density gradient. For the sake of simplicity, here we assume that both $\mathbf{v}$ and U_b are constant, and hence G is constant as well.

Using the method of variable separation [37], it is relatively straightforward to obtain the solution of the diffusion equation with the boundary conditions (43) and (27) and to calculate the trap counts accordingly:

$$J(t)^{Neu} = DGt + \frac{16GL^2}{\pi^3}\sum_{k=1}^{\infty}\frac{(-1)^k}{(2k-1)^3}\left[1-\exp\left(-\frac{D(2k-1)^2\pi^2 t}{4L^2}\right)\right] + \frac{8U_0 L}{\pi^2}\sum_{k=1}^{\infty}\frac{1}{(2k-1)^2}\left[1-\exp\left(-\frac{D(2k-1)^2\pi^2 t}{4L^2}\right)\right], \tag{44}$$

where the product DG is the population density flux through the external boundary of the domain at $x = L$. In the special case of an impenetrable boundary, i.e. for $G = 0$, (44) coincides with (41).

Note that the first term in Eq. (44) corresponds to the large-time asymptotics. The linear increase of the trap count indicates the steady-state behavior. Indeed, it is readily seen that the large-time, steady-state limit of the diffusion equation,

$$\frac{d^2 u_s(x)}{dx^2} = 0 \quad \text{where } u_s(x) = \lim_{t\to\infty} u(x,t), \tag{45}$$

considered together with the boundary conditions (43) and (27), has the solution $u_s(x) = Gx$ and hence the density gradient du_s/dx is constant and equal to G over the whole domain. The second and third terms in (44) thus describe the transient phase of the system. Here the third term describes the impact of the initial conditions (as it contains U_0 but not G) and the second term describes the transient boundary forcing (as it contains G but not U_0).

Recall that, for t sufficiently small, the third term in (44) behaves like $\sqrt{t}$ (see the end of Section 2.2 and also [127] for more details) and hence is the leading term. Thus, the dynamics of the trap counts is a transition between the two different asymptotics, i.e. between the small-time behavior $J(t)^{Neu} \simeq \sqrt{t}$ and the large-time linear behavior $J(t)^{Neu} \simeq DGt + const$. This is clearly seen in the graphs of $J(t)$ shown in Fig. 11. Note that this transitional dynamics may result in a curve of sigmoidal shape if G is sufficiently large, e.g. see the topmost curve in Fig. 11a.

The duration of the early stage dominated by the initial conditions depends on the distance L between the trap and the external boundary of the domain, cf. Figs. 11a and 11b. The boundary condition at $x = L$ will not have any significant impact on the trap counts until a certain time t_*; increasing L increases t_*. This is readily seen from the fact that, in the diffusion equation, time can be scaled as $t' = tDL^{-2}$ (for a general discussion of scaling and its implications see [12]). Note that, in the examples shown in Fig. 11, the horizontal axis shows time in abstract units because the diffusion coefficient is scaled to one. Therefore, the relatively large $t_* \approx 500$ for $L = 45$, see Fig. 11a, when the effect of the boundary forcing becomes important does not necessarily translate to a long time of trap collection in a real-world system.

Please cite this article in press as: Petrovskii S, et al. Multiscale approach to pest insect monitoring: Random walks, pattern formation, synchronization, and networks. Phys Life Rev (2014), http://dx.doi.org/10.1016/j.plrev.2014.02.001

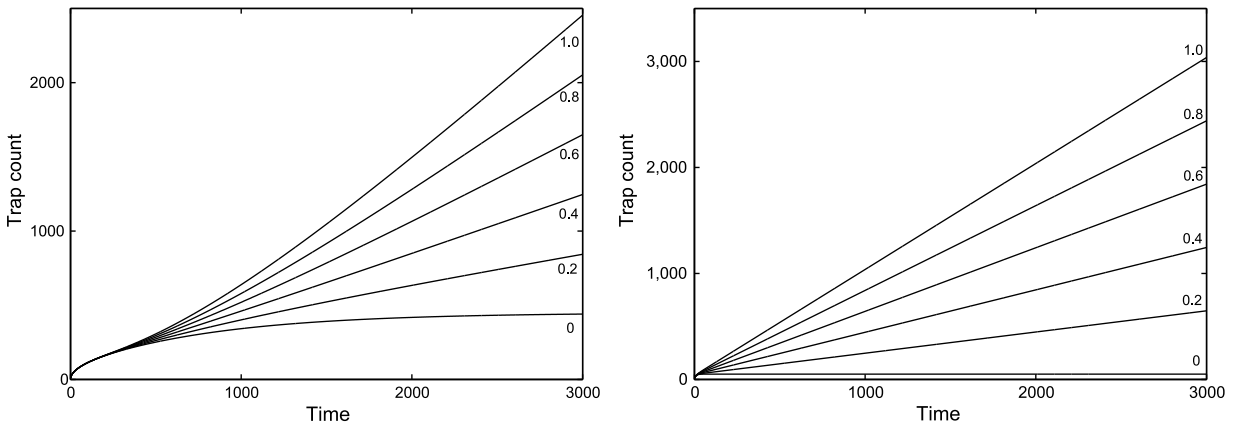

Fig. 11. Trap count vs time in the case of Neumann-type boundary forcing, see Eq. (43), for initial population density $U_0 = 10$ and for different sizes of the domain, (a) for $L = 45$, (b) for $L = 5$. Different curves correspond to different values of the gradient G as it varies between 0 and 1 (bottom to top, respectively).

Now we consider another case of boundary forcing where immigration to the field occurs due to random movement of individual insects. The boundary condition at $x = L$ is then described by the Dirichlet-type condition:

$$u(L,t) = U_b, \tag{46}$$

where U_b has the meaning of the pest population density in the adjoint non-farmed habitat. For the sake of simplicity, we assume that U_b is constant.

Using the method of the variable separation, we arrive at the following expression for the trap counts:

$$J(t)^{Dir} = \frac{DU_b}{L}t + \frac{2U_bL}{\pi^2}\sum_{k=1}^{\infty}\frac{(-1)^k}{k^2}\left[1 - \exp\left(-\frac{Dk^2\pi^2 t}{L^2}\right)\right] + \frac{4U_0L}{\pi^2}\sum_{k=1}^{\infty}\frac{1}{(2k-1)^2}\left[1 - \exp\left(-\frac{D(2k-1)^2\pi^2 t}{L^2}\right)\right]. \tag{47}$$

The expression (47) has a structure similar to (44), i.e. the first term corresponds to the large-time steady-state solution of the diffusion equation, $u_s(x) = U_b x/L$, and the third term accounts for the effect of the initial conditions. The dependence of trap counts on time exhibits similar features, too, showing a transition between the square-root behavior at small time and the linear large-time asymptotics; see Fig. 12a. Furthermore, as in the case of Neumann-type forcing, the duration of the early stage depends on L and, for a smaller domain, can be almost imperceptible (Fig. 12b).

An interesting question is which type of boundary forcing may result in a faster build-up of the pest population and hence may be more potentially dangerous? Intuitively, it seems reasonable to expect that the case of directed movement should result in faster growth. However, the reality appears to be somewhat more complicated. The type of forcing which results in a faster population growth appears to depend on the relation between the initial density U_0 and the boundary density U_b.

In order to make the two cases comparable, we first set $G = U_b/L$ thus making the large-time rate of the trap count increase the same in both cases. Fig. 13 shows the trap counts for the two cases, (44) and (47). As can be expected, the trap counts are the same during the early stage when the boundary forcing has no impact at all. At a later stage, Neumann-type forcing is more efficient when U_b is equal to U_0 (or just slightly higher, not shown here); see Fig. 13a. However, if U_b is much larger than U_0, Dirichlet-type forcing becomes more efficient; see Fig. 13b.

Correspondingly, one can expect that Dirichlet-type forcing should always result in larger trap counts if the domain is initially un-infested and the only source of the pest population is immigration. This indeed appears to be a property of the expressions (44) and (47). Fig. 14 shows the two courses of trap counts calculated for $U_0 = 0$. The relative efficiency of different types of forcing does not depend on the distance L. Fig. 15 shows the moments of time t_1 when

Please cite this article in press as: Petrovskii S, et al. Multiscale approach to pest insect monitoring: Random walks, pattern formation, synchronization, and networks. Phys Life Rev (2014), http://dx.doi.org/10.1016/j.plrev.2014.02.001

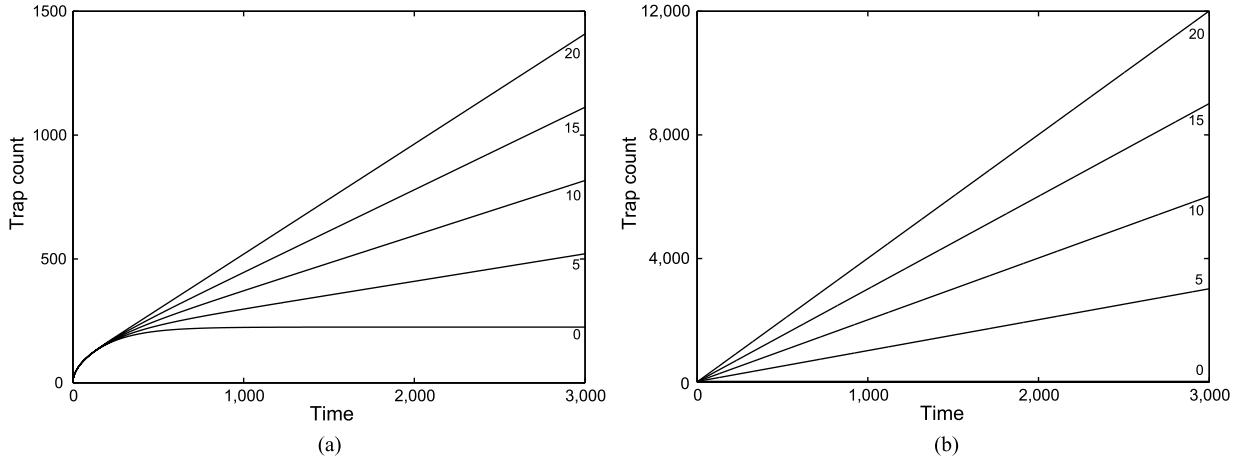

Fig. 12. Trap count vs time in the case of Dirichlet-type boundary forcing, see Eq. (46), for the initial population density $U_0 = 10$ and for different sizes of the domain, (a) for $L = 45$, (b) for $L = 5$. Different curves correspond to different values of U_b as it varies from 0 to 20 (bottom to top, respectively).

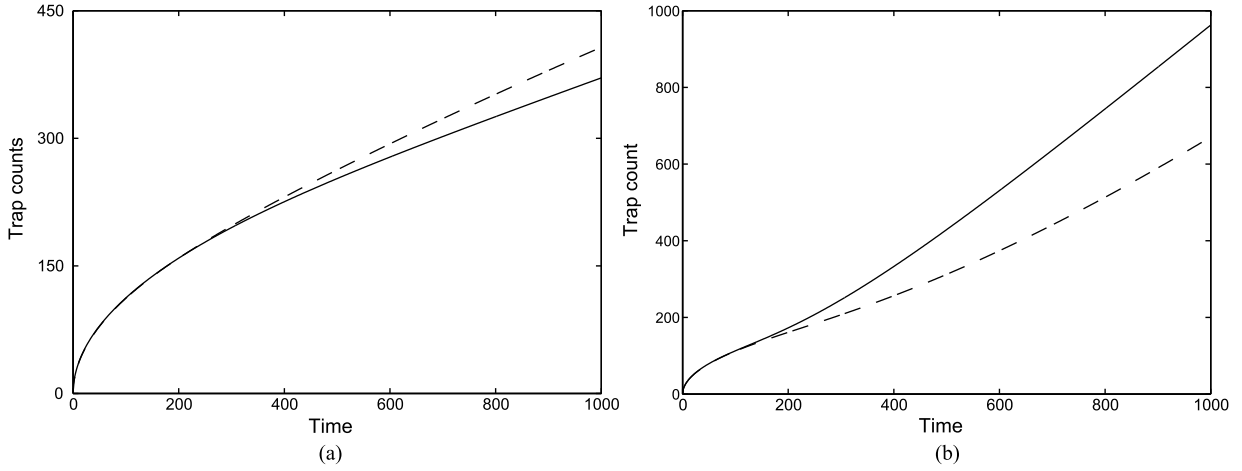

Fig. 13. Trap counts obtained from for (a) $U_b = 10$, and (b) $U_b = 50$. Other parameters are $D = 1$, $L = 45$, $U_0 = 10$ and $G = U_b/L$. Dashed curve for the Neumann forcing, solid curve for the Dirichlet forcing, Eqs. (44) and (47) respectively.

the trap count for the first time exceeds 1, i.e. when $J(t_1) = 1$ (this corresponds, approximately, to the time when the first migrating insect is caught). It is readily seen that this time is always shorter for Dirichlet-type forcing.

For the sake of simplicity, the analysis above was restricted to the 1D case. The 2D case is technically much more complicated and will be considered elsewhere [14]. Here we mention that, as we have observed in numerous numerical simulations (not shown here), the results described in this section are generic and most of them remain valid, at least qualitatively, in the 2D case.

2.4. *Random walk of non-identical dispersers*

The analysis of the population dispersal above has been done under an implicit assumption that all individuals are identical. In reality, this is not the case and in fact this is one of the main factors that makes the laws of living matter significantly different from those of physical particles or substances. No two individuals are identical; this basic observation has a variety of important implications, in particular for movement and dispersal. Indeed, consider the following illuminating example: select a group of men born on the same day, of a similar disposition and life-style, and make them run a mile; their times will be different and for some of them it will be strikingly different! Differences

Please cite this article in press as: Petrovskii S, et al. Multiscale approach to pest insect monitoring: Random walks, pattern formation, synchronization, and networks. Phys Life Rev (2014), http://dx.doi.org/10.1016/j.plrev.2014.02.001

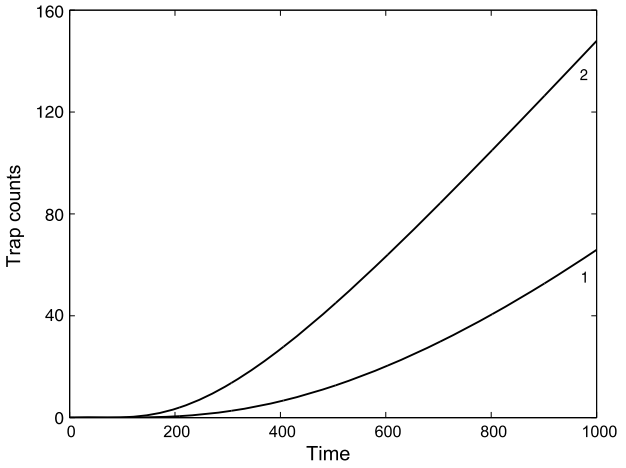

Fig. 14. Trap counts obtained for parameters $D = 1$, $L = 45$, $U_b = 10$, $U_0 = 0$. Curve 2 for Dirichlet-type boundary forcing, curve 1 for Neumann-type boundary forcing with $G = U_b/L = 0.45$.

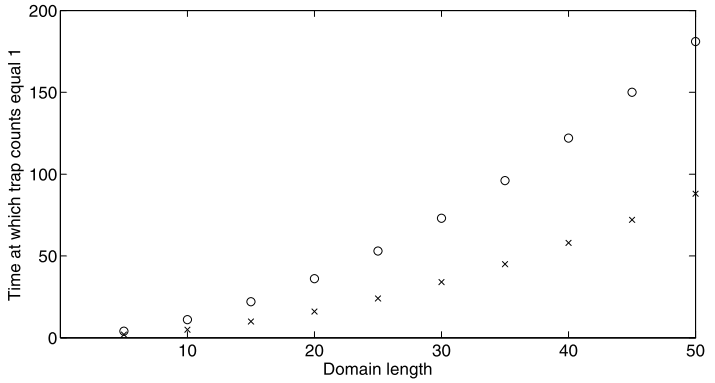

Fig. 15. Plot of time t_1 (y-axis) at which trap counts $J(t_0) = 1$ against length of domain (x-axis). Crosses for Dirichlet-type forcing, circles for Neumann-type forcing. Parameters are: $D = 1$, $U_0 = 0$, $U_b = 10$ and $G = U_b/L$.

between two invertebrates taken from the same cohort may be not as obvious as between humans, yet there is always a certain inherent variation of their traits (such as body size, wings span, etc.) which affects their movement behavior [40,62,105].

As an immediate consequence, when dispersal is considered in a population, i.e. when the details of individual animal movement (e.g. the probability distribution of the step size along the path) are pooled together, their description with a single parameter such as the diffusion coefficient D may become grossly oversimplified. In order to take into account the fact that individuals can have different dispersal abilities and hence a different value of D, the concept of a "statistically structured population" was introduced [121,124,125]. Variability of dispersal abilities is described by the probability density $\chi(D)$ that, for a randomly chosen individual, its diffusivity will have a given value D.

Consider a population of animals performing 1D Brownian motion, so that the probability density of making the step of length ξ is given by the normal distribution, cf. Eqs. (1) and (21), which we write down in the following form:

$$\varrho_D(\xi) = \frac{1}{\sqrt{4\pi D\Delta t}} \exp\left(-\frac{\xi^2}{4D\Delta t}\right), \tag{48}$$

where we consider Δt to be a fixed parameter. If all animals are identical, the distribution of the step size obtained by pooling from all individuals will coincide with (48). However, if the diffusivity D is a random variable distributed with probability density $\chi(D)$, the resulting distribution of the step size becomes [121,125]:

Please cite this article in press as: Petrovskii S, et al. Multiscale approach to pest insect monitoring: Random walks, pattern formation, synchronization, and networks. Phys Life Rev (2014), http://dx.doi.org/10.1016/j.plrev.2014.02.001

$$\varrho(\xi) = \int_0^\infty \varrho_D(\xi)\chi(D)\,dD = \int_0^\infty \frac{1}{\sqrt{4\pi D\Delta t}} \exp\left(-\frac{\xi^2}{4D\Delta t}\right)\chi(D)\,dD. \tag{49}$$

Clearly, apart from the singular case $\chi(D) \sim \delta(D - D_0)$ (which corresponds to an unstructured population of identical individuals), the distribution ϱ is not normal anymore. The properties of the step size distribution $\varrho(\xi)$ in a population of non-identical dispersers will depend on the properties of $\chi(D)$. Available data [62,124] suggest that, at least in the intermediate range of diffusivity values, $\chi(D)$ is well approximated by an inverse power law and this is in agreement with theoretical arguments [121]. Therefore, we assume here that $\chi(D) \sim D^{-\gamma}$ for D not very small and $\gamma > 1$ a positive parameter.

The singularity of the inverse power law at $D = 0$ is hardly realistic. (Recall that the integral $\int_0^\infty \chi(D)\,dD$ must converge because $\chi(D)$ has the meaning of a probability density.) Function χ should therefore include a factor suppressing the singularity. Moreover, if we assume that the power law decay is generic and hence can possibly take place with different values of the exponent γ (e.g. for different species), then the decay at $D = 0$ should be faster than any power law, i.e. at least exponential. Correspondingly, we consider $\chi(D)$ as follows:

$$\chi(D) = \frac{\alpha^{\gamma-1}}{\Gamma(\gamma-1)} \cdot D^{-\gamma} \exp\left(-\frac{\alpha}{D}\right), \tag{50}$$

for $D > 0$ and $\chi(0) = 0$, where α is an auxiliary parameter and Γ is the gamma function.

Eq. (49) then becomes:

$$\varrho(\xi) = \frac{1}{\sqrt{4\pi\Delta t}} \cdot \frac{\alpha^{\gamma-1}}{\Gamma(\gamma-1)} \int_0^\infty \frac{1}{D^{\gamma+\frac{1}{2}}} \exp\left[-\left(\alpha + \frac{\xi^2}{4\Delta t}\right)\frac{1}{D}\right] dD. \tag{51}$$

The integral in (51) can be readily calculated resulting in:

$$\varrho(\xi) = \frac{1}{\sqrt{4\pi\Delta t}} \cdot \frac{\alpha^{\gamma-1}\Gamma(\gamma-\frac{1}{2})}{\Gamma(\gamma-1)} \left(\alpha + \frac{\xi^2}{4\Delta t}\right)^{-\gamma+\frac{1}{2}}. \tag{52}$$

Obviously, for any fixed Δt and for sufficiently large ξ (so that $\xi^2 \gg \alpha\Delta t$), we obtain from (52):

$$\varrho(\xi) \sim \xi^{-2\gamma+1}. \tag{53}$$

Thus, function $\chi(D)$ given by (50) results in a step size distribution with large-distance asymptotical behavior described by a power law. We mention here that, in a more ecologically realistic 2D case, the analysis is similar and also leads to a fat-tailed distribution of the step size with a power law rate of decay [121]. Estimates of the exponent γ from data indicate that it lies between 1 and 2 [62,124]. The power law decay at large step size with these values of the exponent (where the variance does not exist) is usually regarded as a fingerprint of a Levy walk. Remarkably, in our case the underlying individual movement is perfectly Brownian! For $\gamma = 1.5$, Eq. (52) formally coincides with the Cauchy distribution which is a common model of the Levy-type random walk [174]. Interestingly, while in the Levy flight described by the Cauchy distribution (22) the jump size ξ is scaled linearly by the interval Δt [52,83,174], in our case the emerging dispersal kernel exhibits diffusion-type scaling given by $\xi^2/\Delta t$.

In the context of this paper, our primary aim here is to understand how the inherent variation of the dispersal traits may affect the trap counts. As in the above analysis, expression (31) for the trap counts should now be considered as the contribution from the population fraction consisting of individuals with diffusivity D. The actual trap count is then obtained by integrating over the whole range of possible diffusivity values:

$$J(t) = \int_0^\infty \chi(D) J_D(t)\,dD. \tag{54}$$

We now focus on two ecologically relevant cases where the initial spatial population distribution is either uniform or aggregated; see Eqs. (32) and (35), accordingly. It is readily seen that in the uniform case the dependence on time remains the same, $J(t) \sim \sqrt{t}$, the changes only affect the coefficient. However, the situation is different in the case of population aggregation. In this case, from (35) and (54) we immediately obtain:

Please cite this article in press as: Petrovskii S, et al. Multiscale approach to pest insect monitoring: Random walks, pattern formation, synchronization, and networks. Phys Life Rev (2014), http://dx.doi.org/10.1016/j.plrev.2014.02.001

$$J(t) = K \int_0^\infty \chi(D)\,\mathrm{erfc}\left(\frac{x_0}{\sqrt{4Dt}}\right) dD, \tag{55}$$

where K is the initial population size. With $\chi(D)$ given by (50), Eq. (55) becomes:

$$J(t) = \frac{K\alpha^{\gamma-1}}{\Gamma(\gamma-1)} \int_0^\infty D^{-\gamma} \exp\left(-\frac{\alpha}{D}\right) \mathrm{erfc}\left(\frac{x_0}{\sqrt{4Dt}}\right) dD. \tag{56}$$

Having introduced a new variable as $z = x_0/\sqrt{4Dt}$, Eq. (56) takes the following form:

$$J(t) = \frac{2K\alpha^{\gamma-1}}{\Gamma(\gamma-1)} \cdot \left(\frac{4t}{x_0^2}\right)^{\gamma-1} \int_0^\infty z^{2\gamma-3} \exp\left(-\frac{4\alpha t}{x_0^2} z^2\right) \mathrm{erfc}(z)\, dz. \tag{57}$$

Unfortunately, integral (57) can only be calculated analytically if $2\gamma - 3 = 1$, i.e. for $\gamma = 2$. In this case, from (57) we obtain:

$$J(t) = K\left[1 - \left(1 + \frac{4\alpha t}{x_0^2}\right)^{-\frac{1}{2}}\right]. \tag{58}$$

In the small-time limit (and/or for large x_0), Eq. (58) becomes:

$$J(t) \simeq \frac{2\alpha K}{x_0^2} t, \tag{59}$$

which is completely different from the time dependence expected in the corresponding unstructured population, cf. Eq. (37).

2.5. *Trapping of Levy-walking insects: time-dependent diffusion as an alternative framework?*

In the previous sections, we presented a theory that allows the estimation of the parameters of a monitored population such as the population density in the vicinity of a trap (or the population size and the position of the point-source release) from trap counts. A presumption of our analysis is that the insects perform Brownian motion. Although this is in many cases true [74,76,109,124], there has also been growing evidence that, under certain conditions, animals of some species can follow a different movement pattern, such as Levy flight or walk[5] [143,172,173]. An essential difference between the two patterns is that the relative frequency of long steps along the movement path is much higher in a Levy walk than in Brownian motion. Correspondingly, it can result in a faster dispersal, the phenomenon that is known as "superdiffusion" [81,154].

In mathematical terms, a higher frequency of long steps means a lower rate of probability density decay at large distances, a property often referred to as a 'fat tail' (in contrast to the 'thin tail' of the normal distribution). Note that having a probability density distribution with a fat tail is not by itself sufficient for having a Levy walk. Due to the Central Limit Theorem [46], a sum of independent identical distributions, the first three moments of which are finite, converges to a normal distribution when the number of steps n tends to infinity (but preserving the power law decay at the distribution's tail for any finite n, see Fig. 7 and also [83]). Therefore, in a 1D case, a genuine Levy walk only occurs if the probability density $\varrho(\xi)$ of the step size ξ behaves at large ξ as $\varrho \sim \xi^{-\alpha}$ with $\alpha \leqslant 3$. Obviously such a stochastic process is fat tailed and has no variance; random walks with this property are usually referred to as being 'scale-free', although this terminology can be confusing [78].

Whether animals really perform Levy walk or not remains a highly controversial issue [16,167]. Some cases that were originally branded as evidence of Levy walk [172] were later re-classified as Brownian motion [43] and then have recently been re-classified as Levy walk again [142]. Standard statistical tools may sometimes fail to distinguish between power law and exponential rate of decay in the step size distribution [137]. The 'observed' movement type

[5] Due to a long-standing confusion that has almost turned into a tradition, what is called a Levy walk in ecology often corresponds to what is known as a Levy flight in physics [154].

Please cite this article in press as: Petrovskii S, et al. Multiscale approach to pest insect monitoring: Random walks, pattern formation, synchronization, and networks. Phys Life Rev (2014), http://dx.doi.org/10.1016/j.plrev.2014.02.001

can depend on technical details of data collection such as the time scale of the study [13] and/or the time resolution at which the data are obtained [78]. Pooling together movement tracks of non-identical individuals (of the same species) can create the appearance of a Levy flight [124]. In some cases, a correlated random walk can be mistaken for a Lévy walk as it results in a similar pattern [141]. Also, animals of different taxa often employ more than one movement mode [96,103]; if each of those modes is a Brownian walk, their mixture results in a composite Brownian walk that can have the appearance of a Levy flight [40,69].

To the best of our knowledge, none of the cases provided in the ecological literature as evidence of a Levy walk appear to be free of criticism and, in principle, all of them allow different interpretation. Convincing evidence from movement data is still lacking. Also the theoretical argument in support of Levy flights/walks is sometimes rather metaphysical, for instance, operating with irrelevant objects like moving robots and using unrealistic assumptions like an infinitely fine resolution of animal's location [54]. Moreover, there are growing doubts as to whether unambiguous evidence can be obtained at all because of the complexity and variability of the behavioral response that animals exhibit to inherently stochastic environmental factors.

Along with this intense and sometimes even heated ongoing debate, there is also an emerging feeling that this discussion is going nowhere. Behind elaborated pro- and contra-arguments and the subtleness of advanced statistical analysis, some important questions seem to be almost forgotten: whichever pattern occurs, what are its ecological implications? How much should we care about the type of the movement pattern in the context of a specific problem? Levy walks are thought to be essentially different from Brownian motion but does it necessarily mean that the corresponding mathematical framework should always be different too? Let us consider the single-trap scale of the pest monitoring problem. In this section, we show that, even in case of a genuine Levy walk, the problem of trap counts interpretation can still be addressed based on the diffusion equation [2,3].

As a specific model, we consider a population where individual insects perform a random walk with the step length drawn from the Cauchy distribution:

$$\varrho_k(\xi) = \frac{1}{\pi k[1 + (\xi/k)^2]}, \tag{60}$$

where k is the distribution parameter; $\xi = k$ is the distance where the probability density $\varrho_k(\xi)$ falls twice compared to its maximum value at $\xi = 0$. Obviously, as k increases so does the relative frequency of long steps.

We consider the 1D domain $0 < x < L$ with a trap installed at $x = 0$. For each of the insects, its position at $t_{i+1} = t_i + \Delta t$ is calculated as $x_{i+1} = x_i + \xi$ where, in accordance with Eq. (60), the random step ξ is computed as:

$$\xi = k\Delta t \ \tan\left[\pi\left(\zeta - \frac{1}{2}\right)\right], \tag{61}$$

where ζ is a random number uniformly distributed in (0, 1). The corresponding trap counts obtained in the individual-based simulations are shown in Fig. 16a for a few values of k.

Intuitively, as the frequency of long jumps increases, the contribution from remote parts of the population to the trap counts also increases. Correspondingly, in the case where the insects perform a Levy walk, the trap counts can be expected to grow faster with time than they do for Brownian motion. However, the last statement is not necessarily true if the diffusivity changes with time:

$$\frac{\partial u(x,t)}{\partial t} = D(t)\frac{\partial^2 u(x,t)}{\partial x^2}, \tag{62}$$

where u is the population density. Indeed, since the diffusion coefficient is a measure of the dispersal rate, e.g. see Eq. (25), if D grows with time then the trap counts will likely grow faster than in the standard case $D = const$.

This can be shown in a more formal way. It is readily seen that, by introducing a new variable:

$$\tau = \int_0^t D(t')\,dt', \tag{63}$$

Eq. (62) turns into the standard diffusion equation with $D = 1$:

$$\frac{\partial u(x,t)}{\partial \tau} = \frac{\partial^2 u(x,t)}{\partial x^2}, \tag{64}$$

Please cite this article in press as: Petrovskii S, et al. Multiscale approach to pest insect monitoring: Random walks, pattern formation, synchronization, and networks. Phys Life Rev (2014), http://dx.doi.org/10.1016/j.plrev.2014.02.001

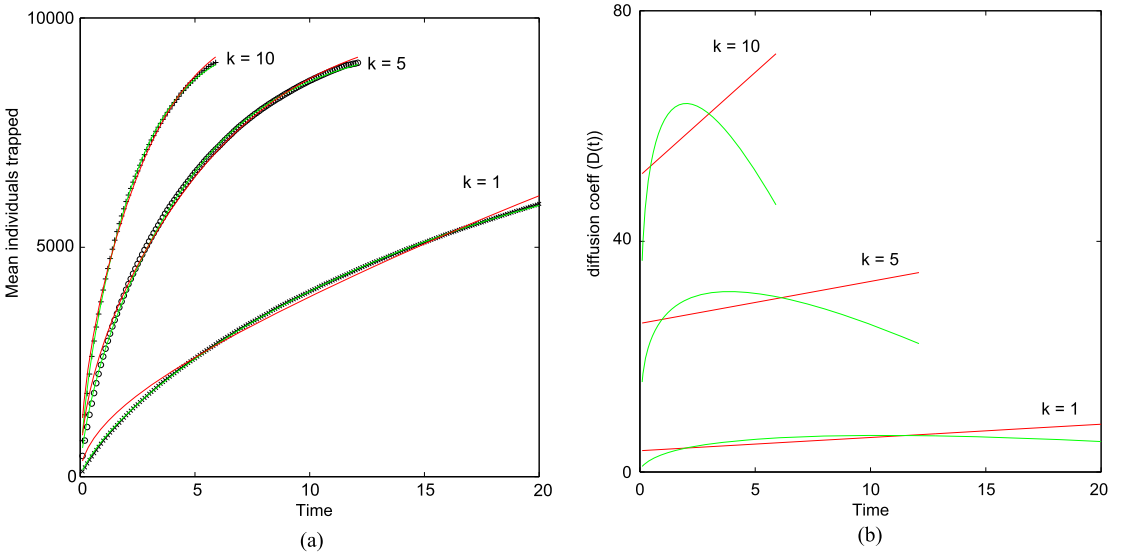

Fig. 16. (a) Trap counts simulated for Levy walks as given by (60)–(61) (different symbols correspond to different values of k) and their approximation with time-dependent diffusion for linear $D(t)$ (red curves) and nonlinear $D(t)$ (green curves). Simulations were stopped when the number of trapped insects reached 90% of the total population. Ten realizations of the system were averaged to obtain each trap count series. (b) The diffusion coefficient D as a function of time for the simulations shown in (a). At $t = 0$ the population of $K = 10^4$ insects is distributed uniformly over the domain of size $L = 20$. (For interpretation of the references to color in this figure legend, the reader is referred to the web version of this article.)

and hence the results of Section 2.2 immediately apply, up to the change $t \to \tau(t)$, so that the cumulative trap count is given by:

$$J(t) = \frac{2U_0}{\sqrt{\pi}} \sqrt{D\tau(t)}. \tag{65}$$

Therefore, if $\tau(t)$ increases faster than a linear function, the trap counts are going to grow faster than in the time-independent case and hence may mimic the superdiffusive pattern.

What is an appropriate choice of $D(t)$ is a subtle issue [2] and will be considered in detail elsewhere [3]. Here we only consider two tentative examples:

$$\text{(i) } D(t) = at + b \quad \text{and} \quad \text{(ii) } D(t) = at + bt^H, \tag{66}$$

where a, b and H are parameters. Note that (66i) is a special case of (66ii) for $H = 0$ but we want to keep the linear case separate as the simplest possible extension to the time-independent case.

Now we want to check whether time-dependent diffusion can really provide a reasonable approximation of the Levy-walking population and to find the appropriate values of the parameters. For this purpose, we look for the best-fit approximation of the simulation data with the analytical solution of the mean-field model using D given by either (66i) or (66ii), in a similar way to that used in Section 2.2. Trap counts are simulated for 12 different values of k such as $k = 0.1, 0.5, 1, 2, \ldots, 10$. The results of fitting for three values of k are shown in Fig. 16 by the solid curves. We therefore conclude that the time-dependent diffusion equation with $D(t)$ given by the nonlinear function (66ii) can provide an almost perfect fit for the Levy walk, with the relative error being consistently within one percent for all considered values of k. We also observe that the accuracy of the approximation is, in fact, rather robust to the choice of $D(t)$: while the linear function (66i) gives lower accuracy, it still provides a reasonably good fit to the data.

A technical problem with this approach is that, before it could be applied to real data, we have three parameters to determine. However, results of the regression analysis show that the best-fitting value of H does not change much for different k; its value remains close to $1/3$. We therefore fix $H = 1/3$.

Moreover, parameter b can be obtained analytically. Let $u_{i-1}(x)$ be the population density distribution over space after $(i-1)$ steps of the random walk. Then, for any probability density distribution $\varrho(\xi)$ of the step size ξ, the expected (mean) number K_i of insects trapped as a result of the next (ith) step is:

Please cite this article in press as: Petrovskii S, et al. Multiscale approach to pest insect monitoring: Random walks, pattern formation, synchronization, and networks. Phys Life Rev (2014), http://dx.doi.org/10.1016/j.plrev.2014.02.001

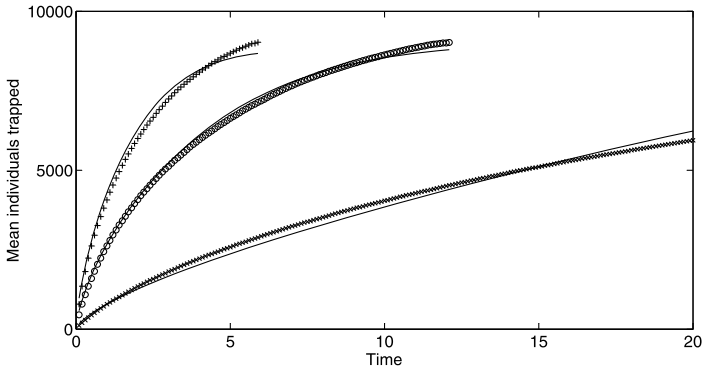

Fig. 17. Time dependent diffusion curves fitted to Levy walk trap counts, where $H = 1/3$, and b is determined from the first datapoint (at $t = 0.1$). Other parameters are the same as in Fig. 16a. Ten realizations of the system were averaged to obtain each trap count series.

$$K_i = \int_0^L dx \cdot u_{i-1}(x) \int_{-\infty}^0 dx' \varrho\big(x - x'\big). \tag{67}$$

Since $u_{i-1}(x)$ is unknown, an explicit analytical expression for K_i for an arbitrary i does not seem possible to obtain. However, it is not difficult to find the number of insects caught after the first step because $u_0(x)$ is given by the initial condition. Here we focus on the case $u_0(x) = U_0 = const$. Applying Eq. (67) to the Levy walk with the Cauchy distributed step size (60), we obtain:

$$K_1^{(L)} = \left(\frac{U_0}{\pi k}\right) \int_0^L dx \int_{-\infty}^0 \frac{dx'}{1 + ((x - x')/k)^2}, \tag{68}$$

where we add the superscript (L) in order to emphasize that (68) is obtained for the Levy walk. By calculating the integral, (68) is simplified to:

$$K_1^{(L)} = \frac{U_0 L}{2} - \frac{U_0 L}{\pi} \arctan\left(\frac{L}{k}\right) + \frac{U_0 k}{2\pi} \log\left(1 + \frac{L^2}{k^2}\right). \tag{69}$$

On the other hand, the number of insects trapped after the first step can be obtained from the diffusion equation:

$$K_1^{(D)} = \frac{2U_0}{\sqrt{\pi}} \left[\int_0^{\Delta t} D\big(t'\big)\, dt'\right]^{1/2} = \frac{2U_0}{\sqrt{\pi}} \left[\frac{a}{2}(\Delta t)^2 + \frac{b}{1+H}(\Delta t)^{1+H}\right]^{1/2}, \tag{70}$$

cf. Eq. (65), where we have assumed that L is not very small so that the effect of domain finiteness can still be neglected at time Δt.

Setting $K_1^{(L)} = K_1^{(D)}$, from (70) we obtain the expression for b:

$$b = \frac{\pi(1+H)}{4} \left(\frac{K_1^{(L)}}{U_0 L}\right)^2 \cdot \frac{L^2}{(\Delta t)^{1+H}} - \frac{a(1+H)}{2} \cdot (\Delta t)^{1-H}. \tag{71}$$

Here $K_1^{(L)}/(U_0 L)$ is the fraction of the total population trapped at the first step.

Correspondingly, the diffusion equation with D given by (66ii) has now only one parameter to be determined, i.e. a. Note that, with just one free parameter instead of three, the accuracy of the best-fitting approximation of the Levy walk data with time-dependent diffusion remains very good; see Fig. 17.

Therefore, we have a one-parameter solution of the diffusion equation which, for an appropriate choice of a, approximates very well the one-parameter stochastic model (60)–(61). We hypothesize that there is a relation between a and k, i.e. $a = a(k)$. Indeed, the existence of such relation seems obvious from Fig. 18a that shows the best-fitting values of a obtained for different k. Although we cannot calculate this relation analytically, the data shown in Fig. 18a

Please cite this article in press as: Petrovskii S, et al. Multiscale approach to pest insect monitoring: Random walks, pattern formation, synchronization, and networks. Phys Life Rev (2014), http://dx.doi.org/10.1016/j.plrev.2014.02.001

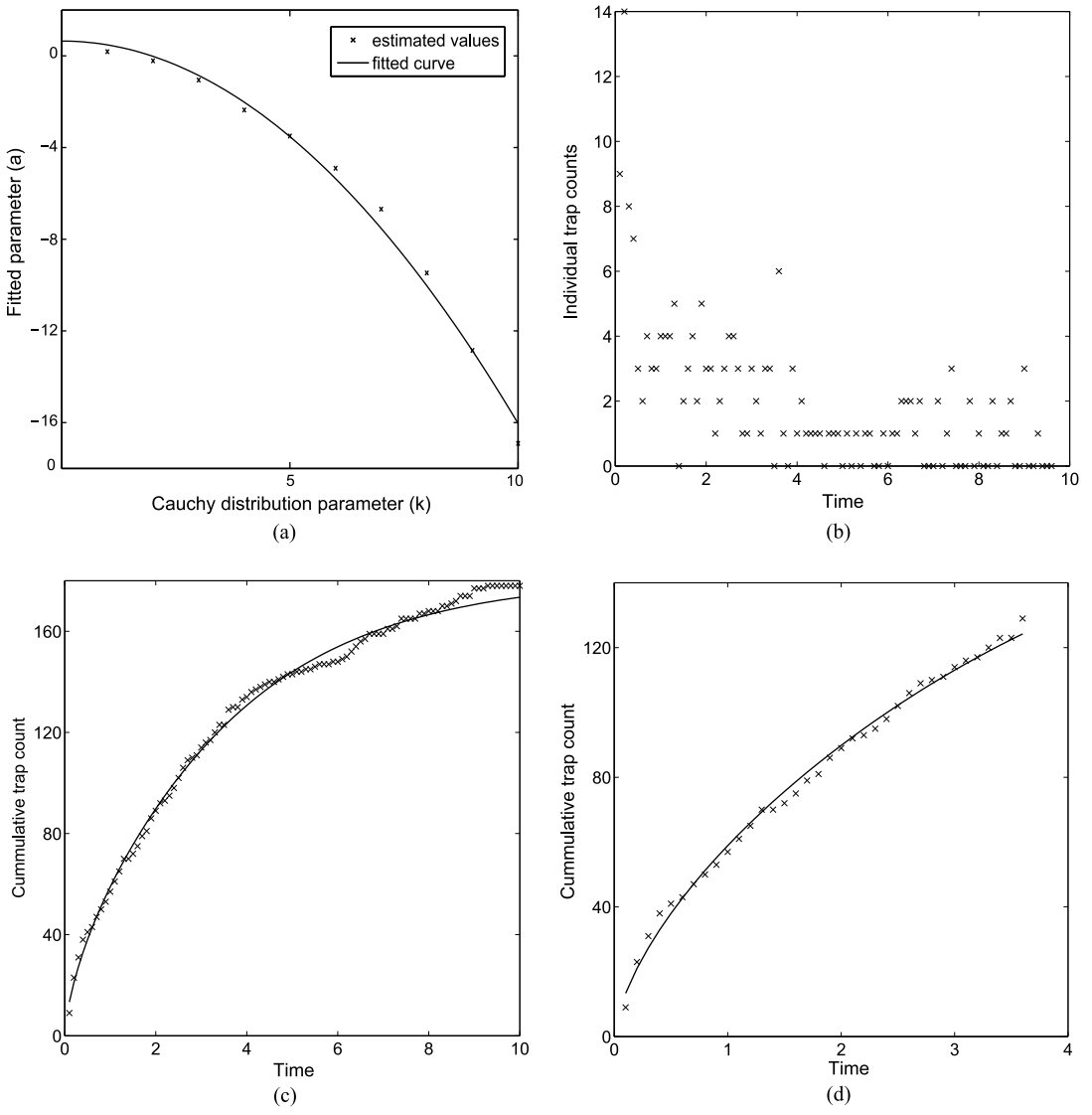

Fig. 18. (a) Variation of parameter a with k. The solid curve is the best-fitting quadratic polynomial. (b) The daily trap counts obtained for the Levy-walking population (60)–(61) that at $t = 0$ is distributed uniformly (in the statistical sense) over the domain $0 < x < 20$ with mean density $U_0 = 10$; (c) the corresponding cumulative trap counts (shown by crosses) and their best-fit (shown by the solid curve) by the mean-field model with time-dependent diffusion, the best fit is obtained for $U_0 = 9.7$; (d) the results of data fitting for a smaller dataset, the best fit is obtained for $U_0 = 9.3$.

are very well approximated by a square polynomial $a = 0.64k - 0.36k^2$ (shown by the solid curve). This completes our analysis. For any specific value of k, say k_0, associated with a particular population of Levy walking individuals, we can calculate the corresponding value of a, i.e. $a_0 = a(k_0)$. The population density in the vicinity of the trap is then obtained in the same way as in Section 2.2, i.e. by best-fitting the data with the corresponding mean-field solution.

As an example of this approach, we consider a set of trap counts simulated using the Levy-walking population (60)–(61) with $k = 5.5$; see Fig. 18b. The corresponding cumulative trap counts are approximated by the mean-field solution, see Fig. 18c, the best fit is obtained for $U_0 = 9.7$ which therefore provides an excellent accuracy with a relative error of just 3%. As a drawback, we notice that this very good estimate of the population density is obtained based on a large number of trap counts. However, the best-fit approximation of a shorter dataset, see Fig. 18d, still provides a good estimate of U_0 with a relative error of about 7%.

Please cite this article in press as: Petrovskii S, et al. Multiscale approach to pest insect monitoring: Random walks, pattern formation, synchronization, and networks. Phys Life Rev (2014), http://dx.doi.org/10.1016/j.plrev.2014.02.001

3. Single field problem: multiple traps

In the previous section, we showed how the population density of a pest insect can be evaluated based on the trap counts obtained by a single trap. However, the information obtained in this way is local in the sense that it only reflects the pest abundance in a certain vicinity of the trap. Indeed, typical dispersal distances for walking insects are estimated to be on the order of 1 meter or less per day [171], which obviously corresponds to the diffusion coefficient $D \sim 1\ \mathrm{m}^2\,\mathrm{day}^{-1}$. Assume that counts are collected daily. It was shown in Section 2.2 that ten trap counts are usually enough to obtain a population density estimate of good accuracy. Therefore, consider the total time T of trap exposure to be ten days. The mean squared displacement over this time is $\langle x^2\rangle = 2DT \sim 20\ \mathrm{m}^2$, thus giving the characteristic radius of the catchment area as 4.5 m. Agricultural fields rarely have area less than 1 ha, which gives a typical linear size of around 100 m or more, whereas the spatial scale of variations in the population density distribution for walking insects is known to be 30–40 meters [47,65]. Therefore, an accurate monitoring may require more than one trap.

Correspondingly, we now consider the situation where the data are collected with several traps that are installed at certain locations $\mathbf{r}_i$, $i = 1, \ldots, N$. That gives N values of the population density, $u_1, \ldots, u_N$, where $u_i = u(\mathbf{r}_i)$. The question is how to estimate the average population density based on this information. The approach that is usually employed in ecology suggests that it can be calculated by the arithmetic mean [38,159]:

$$m(N) = \frac{1}{N}\sum_{i=1}^{N} u_i. \tag{72}$$

An approximate value of the pest population size I can then be found by multiplying the sample mean by the area of the field A, that is:

$$I \approx m(N)A. \tag{73}$$

For convenience, below we will refer to (72)–(73) as the statistical rule.

Reliability of the estimate (72) remains a disputable issue though [24,27]. One way to improve the accuracy is to ensure that the size of the data set is large enough, i.e. that enough traps are installed. In theory, the sample mean value given by Eq. (72) is known to converge to the exact value of the population size when N tends to infinity (cf. [46]). Hence we can expect better accuracy of the estimate when N gets larger. In practice, however, there is a trade-off between the number of traps needed to achieve sufficient accuracy and the number that can be afforded. If trapping is used in ecological research, the number N of traps per given area can be made quite large, e.g. on the order of hundreds. Meanwhile, in routine pest monitoring programs N rarely exceeds twenty [91] and, in some cases, it can be as small as just one or a few traps per field [104]. There are several reasons why the number of traps cannot be made large. An increase in the number of traps or samples equates to an increase in the amount of labour and hence finances required. In any real-world situation, such resources are limited. Besides, traps introduce a disturbance into the field and installing a large number of them can damage the corresponding agricultural product.

Another problem with Eq. (72) is that it is spatially implicit, i.e. it takes into account neither the spacing between the traps (which, generally speaking, can be variable) nor any information about the properties of the population spatial distribution. Clearly, a spatially-explicit generalization of (72) is likely to provide, for the same number of traps, a better quality estimate of the average population density.

The essence of the problem can be seen from Fig. 19. For the sake of simplicity, we show it in a hypothetical 1D domain. Five traps are installed over the field. However, their location misses the high-density peak between the second and third traps. As a result, the estimate obtained with (72) is going to underestimate the actual average density considerably. The questions therefore arise as to (i) whether the existence of the peak could possibly be better accounted for if a more advanced approach is used instead of Eq. (72) and (ii) how the number of the traps and/or their location can be optimized with respect to the population spatial distribution. These two issues will be the main focus of this section.

Interestingly, the problem of evaluation of the average population density based on local density values, if addressed formally, almost coincides with the problem of numerical integration. One important difference is that, for the reasons mentioned above, the number of the grid nodes (i.e. traps) cannot be made large as is usually assumed in the numerical integration theory. This brings to the fore the challenging problem of integration on coarse grids. In recent years, intensive study of numerical integration methods for ecological applications has been carried out [44,45,114–116, 118,119] and here we briefly summarize our experience and highlight the main results obtained.

Please cite this article in press as: Petrovskii S, et al. Multiscale approach to pest insect monitoring: Random walks, pattern formation, synchronization, and networks. Phys Life Rev (2014), http://dx.doi.org/10.1016/j.plrev.2014.02.001

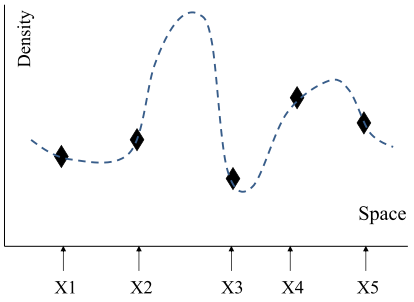

Fig. 19. A sketch of data collection with multiple traps. The diamonds gives the value of the density at the location of the traps $X1, \ldots, X5$ whilst the dashed curve shows the actual population distribution.

3.1. Evaluation of pest insect abundance from discrete data

In this section, we briefly revisit the basics of numerical integration. Consider the domain Ω where the pest insect monitoring is carried out (e.g. a farm-field). Let N be the total number of traps installed across the field Ω. Let us assume that we have already reconstructed the pest population density $u_i \equiv u(\mathbf{r}_i)$ at the trap locations $\mathbf{r}_i$, $i = 1, \ldots, N$ (e.g. using the approaches described in Section 2). Hence our next goal is to evaluate pest abundance I from the pest population density values $u_i \equiv u(\mathbf{r}_i)$.

If we had a continuous pest population density function $u(\mathbf{r})$ defined at any point $\mathbf{r} = (x, y)$ of the domain Ω, then the pest abundance I in the field would, by the definition of density, be given by the following integral:

$$I = \iint\limits_{\Omega} u(\mathbf{r})\, d\mathbf{r}. \tag{74}$$

However, the pest population density is only available to us at a discrete set of points $\mathbf{r}_i$, $i = 1, \ldots, N$. Consequently the above integral cannot be evaluated exactly and is instead approximated by means of numerical integration. A generic numerical integration formula is given by (e.g. see [39]):

$$I \approx I_a(N) = \sum_{i=1}^{N} \omega_i u_i, \tag{75}$$

where $I_a(N)$ is an approximation of the exact integral I, and ω_i, $i = 1, \ldots, N$, are weight coefficients that define a particular method of integration. Correspondingly, in the context of numerical integration, the set of points $\{\mathbf{r}_i\}$ is called the numerical grid.

For any chosen method of numerical integration and any fixed number of traps N used to collect the data, the accuracy of an approximation $I_a(N)$ is assessed by analyzing the integration error. Let us assume that the exact value I of the pest abundance (74) is known to us. The relative integration error $e(N)$ is defined as:

$$e(N) = \frac{|I - I_a(N)|}{I}. \tag{76}$$

The integration error $e(N)$ (also known as the approximation error) emerges because we replace a continuous function $u(\mathbf{r})$ with a discrete function u_i, $i = 1, \ldots, N$. The less data we use in the approximation (75), the bigger the integration error we should expect. The aim of pest monitoring is to obtain a reliable estimate of the pest abundance; therefore, large values of the approximation error are unacceptable. The largest acceptable value of the error e is called the tolerance τ of the estimate. In other words, the relative error (76) should satisfy the following condition:

$$e(N) \leqslant \tau, \tag{77}$$

where τ is a specified tolerance. In ecological applications, the tolerance of $\tau \sim 0.2$–0.5 is usually considered as acceptable accuracy [111,152].

The integration error (76) depends on the number of the grid nodes N (i.e. the number of traps) but it also depends on the definition of weight coefficients in the formula (75). For a given N, different methods of numerical integration

Please cite this article in press as: Petrovskii S, et al. Multiscale approach to pest insect monitoring: Random walks, pattern formation, synchronization, and networks. Phys Life Rev (2014), http://dx.doi.org/10.1016/j.plrev.2014.02.001

can result in a different value of $e(N)$. Below we will briefly discuss the choice of weight coefficients in several methods of numerical integration.

In a general case, the definition of weight coefficients depends on the location of the traps. The most straightforward case is that the traps are located at the nodes of a regular Cartesian grid. Suppose that an agricultural field where traps have been installed has a rectangular shape. A linear transformation then maps the original domain onto the unit square $\Omega_1 = [0, 1] \times [0, 1]$ where a Cartesian grid is generated as the tensor product of two one-dimensional (1D) grids. Namely, let us consider a set of points x_i, $i = 1, \ldots, N_1$, at the interval $[0, 1]$, where we require that $x_1 = 0$, $x_{i+1} = x_i + h_1$, $i = 1, \ldots, N_1 - 1$, and the grid step size h_1 is defined as $h_1 = 1/(N_1 - 1)$. Similarly, a set of points y_j, $j = 1, \ldots, N_2$, in the domain $[0, 1]$ generates a 1D grid in the y-direction as $y_1 = 0$, $y_{j+1} = y_j + h_2$, $j = 1, 2, \ldots, N_2 - 1$, where $h_2 = 1/(N_2 - 1)$. The grid node position in the unit square is then given by (x_i, y_j). In the simplest case when $h_1 = h_2 \equiv h$, we have a grid of square elements $c_{ij} = [x_i, x_{i+1}] \times [y_j, y_{j+1}]$.

Since the Cartesian grid is defined as the tensor product of 1D grids, it suffices to design weight coefficients for a 1D problem and then extend their definition to the 2D problem. Let the function $u(x)$ be given to us at the nodes x_i, $i = 1, \ldots, N$, of a 1D grid generated with a constant grid step size h over the unit interval $[0, 1]$. The most straightforward way to define the weight coefficients is to consider piecewise polynomial approximation of the continuous function $u(x)$. Consider a polynomial $p_k(x)$ of the degree k, where we require that $p_k(x_n) = u(x_n)$ for $n = i, i + 1, \ldots, i + k$. In other words, we consider a polynomial passing through $k + 1$ consecutive points where the function values are available. We then approximate:

$$\int_{x_i}^{x_{i+k}} u(x)\,dx \approx I_i = \int_{x_i}^{x_{i+k}} p_k(x)\,dx, \tag{78}$$

and the resulting integral I is computed by summation of all integrals I_i. Consideration of the polynomial degree $k = 1$ and $k = 2$ in the formula (78) with consecutive summation results in the composite trapezoidal rule and the composite Simpson's rule of integration, respectively. The integration formula for the composite trapezoidal rule is:

$$I = \int_0^1 u(x)\,dx \approx I_a(N) = \frac{h}{2}\left[u_1 + 2\sum_{i=2}^{N-1} u_i + u_N\right], \tag{79}$$

where $u_i \equiv u(x_i)$. It is clear from comparison of (79) and (75) that the weight coefficients are given by $\omega_1 = \omega_N = h/2$ and by $\omega_i = h$ for $i = 2, \ldots, N - 1$. The composite Simpson rule of integration is only defined for an odd number of grid nodes, $N = 2m + 1$. Integration of a quadratic polynomial over a sub-interval $[x_i, x_{i+2}]$ with the subsequent summation results in:

$$I = \int_0^1 u(x)\,dx \approx I_a(N) = \frac{h}{3}\left[u_1 + 2\sum_{i=1}^{m-1} u_{2i+1} + 4\sum_{i=1}^{m} u_{2i} + u_N\right]. \tag{80}$$

The weight coefficients in the Simpson rule are therefore given by $\omega_i = 4h/3$ for $i = 2, 4, \ldots, 2m$, $\omega_i = 2h/3$ for $i = 3, 5, \ldots, 2m - 1$, and $\omega_i = h/3$ for $i = 1$, $i = N$.

Consideration of the approach (78) for an arbitrary polynomial degree $k > 0$ leads to the derivation of the Newton–Cotes formulae of numerical integration [39]. The trapezoidal rule ($k = 1$) and the Simpson rule ($k = 2$) discussed above represent the first two rules in the Newton–Cotes family on regular grids. Let us note that the idea of interpolating the integrand function $u(x)$ by a polynomial $p_k(x)$ of degree k can be further generalized to take irregular grids into consideration, albeit derivation of weight coefficients on irregular grids is not so straightforward (cf. [117]) as they should be re-computed every time an irregular grid is generated. For example, the trapezoidal rule on irregular grids is given by:

$$I \approx I_a(N) = \sum_{i=1}^{N-1} h_i \frac{(u_i + u_{i+1})}{2}, \tag{81}$$

where the grid step size $h_i = x_{i+1} - x_i$ is variable rather than fixed. Similarly, the Simpson rule on irregular grids is:

Please cite this article in press as: Petrovskii S, et al. Multiscale approach to pest insect monitoring: Random walks, pattern formation, synchronization, and networks. Phys Life Rev (2014), http://dx.doi.org/10.1016/j.plrev.2014.02.001

$$I \approx I_a(N) = \sum_{i=1}^{\frac{N-1}{2}} \frac{h_{2i-1} + h_{2i}}{6}(u_{2i-1} + 4u_{2i} + u_{2i+1}), \tag{82}$$

which also relies on the variable grid step size $h_i = x_{i+1} - x_i$. As with the conventional Simpson rule (80), the number of grid nodes N is required to be odd.

Once the integration techniques have been designed in the 1D case, they can be extended to the two-dimensional (2D) case. Namely:

$$I = \int_0^1 \int_0^1 u(x, y)\, dx\, dy = \sum_{i,j} I_{ij}, \tag{83}$$

where:

$$I_{ij} = \int_{x_i}^{x_{i+1}} \int_{y_j}^{y_{j+1}} u(x, y)\, dx\, dy. \tag{84}$$

Hence, the integration problem is reduced to the evaluation of the integral in each sub-domain $c_{ij} = [x_i, x_{i+1}] \times [y_j, y_{j+1}]$ of the Cartesian grid. Integration on rectangular elements c_{ij} can, in turn, be further reduced to consecutive application of the 1D formulae. Consider, for example, the simplest case of a regular grid with a constant grid step size h in both directions x and y. The integration technique is as follows. First, the integral (84) is re-written as:

$$I_{ij} = \int_{y_j}^{y_{j+1}} U(y)\, dy, \tag{85}$$

where $U(y) = \int_{x_i}^{x_{i+1}} u(x, y)\, dx$. We then employ 1D Newton–Cotes formulae in order to evaluate the function $U(y)$ in the square cell c_{ij}. Once the values of $U(y)$ have been computed, the same integration rule can be applied to approximate the 1D integral (85). For example, the trapezoidal rule of integration implies the approximation of $u(x, y)$ by a linear function on each sub-domain c_{ij}. Correspondingly, the integral I_{ij} is evaluated as:

$$I_{ij} \approx \frac{h^2}{4}[u_{ij} + u_{i+1,j} + u_{i,j+1} + u_{i+1,j+1}], \tag{86}$$

where $u_{ij} \equiv u(x_i, y_j)$. The application of the Simpson rule in the cell c_{ij} requires that the data $u(x, y)$ are available at points (x_{i+q}, y_{j+r}), where $q = 0, 1, 2$ and $r = 0, 1, 2$. The function $u(x, y)$ is then integrated in the cell c_{ij} as:

$$\begin{aligned} I_{ij} \approx \frac{h^2}{36}\big[&u_{ij} + u_{i,j+2} + u_{i+2,j} + u_{i+2,j+2} \\ &+ 4(u_{i,j+1} + u_{i+1,j} + u_{i+2,j+1} + u_{i+1,j+2}) + 16u_{i+1,j+1}\big]. \end{aligned} \tag{87}$$

Note that, like in the 1D case, integration by the Simpson rule requires an odd number of nodes N in each direction x and y of the 2D regular grid.

For irregular grids, numerical integration in the 2D case can be significantly more difficult compared to 1D integration. If the irregular grid is of Cartesian type (with a variable grid step size in each direction) then an approach similar to the one described above for regular grids (cf. Eq. (85)) can still be applied. However, the situation becomes much more complicated when the traps are located arbitrarily so that the grid of traps cannot be mapped onto a regular Cartesian grid in the unit square. In scientific computing, such 'truly irregular' grids are called *unstructured grids*. An unstructured grid normally appears in a 2D problem as a set of non-overlapping triangles that covers the entire domain [32]. There are two situations when such grids may be needed. First, the domain can in some cases have a sophisticated geometry so that installation of traps at nodes of a Cartesian grid may not well resolve a curvilinear boundary of the domain. Second, an irregular grid may be required in order to avoid a bias in the trap counts [5,91] if there is a reason to believe that such a bias can significantly affect the data, e.g. when the environment has its own regular structure as would an orchard or plantation.

Please cite this article in press as: Petrovskii S, et al. Multiscale approach to pest insect monitoring: Random walks, pattern formation, synchronization, and networks. Phys Life Rev (2014), http://dx.doi.org/10.1016/j.plrev.2014.02.001

On an unstructured 2D grid, Eq. (85) obviously does not apply and a different approach should be used. After the triangulation of the domain, the vertices of each triangle are considered as grid nodes where the function $u(x, y)$ is defined (i.e. where the traps are installed). One can then use local polynomial reconstruction of the integrand $u(x, y)$ by a least-squares method and integrate the resulting polynomial in each triangle. The least-squares technique for polynomial reconstruction of the integrand function has been discussed in our previous work [119].

Numerical integration on an unstructured grid is, in principle, an efficient technique to evaluate the population size from discrete data collected with any random spatial distribution of traps. However, to the best of our knowledge irregular grids remain relatively rare in ecological applications, even when used or considered in a broader context [64, 67,166,177]. One problem with the use of unstructured grids, in particular in the pest abundance evaluation problem, is that the accuracy of polynomial reconstruction on such grids can depend heavily on the grid geometry [112,113]. The issue of accuracy of numerical integration on unstructured grids therefore requires further careful investigation before they can be employed for numerical integration of the pest population density. For these reasons, in this paper we mostly focus on the application of regular grids.

Our discussion in this section has mostly been concerned with the definition of the weight coefficients based on the idea that the integrand function $u(x, y)$ is replaced with a polynomial. It is worth mentioning here that there exists a big class of alternative methods of numerical integration, Gauss quadrature being perhaps the most well-known of them [39]. However, we are not aware of any cases where those methods have been applied to ecological problems and hence we do not discuss them in this paper.

3.2. Evaluation of population abundance on coarse grids

Application of numerical integration methods to the problem of insect pest abundance evaluation was first considered in [116] and then further developed in [44,114,115,118,119]. Examples of numerical integration of either field data or ecologically meaningful simulation data can be found in [115–117,119] where a detailed discussion of the numerical procedure and the related issues has been provided. Several methods of numerical integration have been considered. In particular, the trapezoidal rule and the Simpson rule of integration have been discussed thoroughly both in the 1D and 2D cases. Also, methods based on reconstruction of the integrand function by higher order polynomials were studied in [116,117] for a 1D problem and were briefly discussed in [119] in the 2D case. Given the variety of available numerical integration techniques, questions arise with regard to their relative accuracy and efficiency: are some methods better than others and, if yes, what is a criterion for the selection of the best one?

The standard theory of numerical integration is based on the concept of *convergence rate*. The key requirement of any method of numerical integration is that weight coefficients should satisfy the following condition:

$$I_a(N) \to I \quad \text{for } N \to \infty, \tag{88}$$

where N is the number of the grid nodes. The design of weight coefficients in any method of numerical integration is based on this condition. Meanwhile, apart from the convergence as such, it is also important to understand how fast the approximate value $I_a(N)$ actually approaches the exact value of the integral I when N increases. Different methods of numerical integration can have different convergence rates.

In order to illustrate the concept, let us consider a 1D problem on a regular grid. The idea of convergence rate can be broadly described by the following relation:

$$e(N) \simeq Ch^p = O\big(h^p\big), \tag{89}$$

where h is the distance between grid nodes, and the coefficient C and the exponent p depend on the method of numerical integration used in the problem. In particular, p is fully determined by the choice of weight coefficients. On a regular Cartesian grid $h = 1/(N-1)$ and Eq. (88) can be re-written in terms of the grid step size h as $I_a(h) \to I$ for $h \to 0$. Eq. (89) described how the integration error $e(h)$ tends to zero for a particular method of numerical integration, and in particular the speed of this process. We emphasize here that the theory of numerical integration normally deals with asymptotic convergence so that, strictly speaking, Eqs. (88)–(89) are only valid when h is sufficiently small.

The theory states [39] that the statistical rule (72)–(73) has convergence rate $O(h)$ while the convergence of the composite Simpson rule (80) is $O(h^4)$; see Fig. 20. This means that doubling the number of grid nodes will decrease the error of the Simpson method by a factor of 16, while the error of the statistical rule is only halved. Therefore, a much bigger number of grid nodes (i.e. much larger number of traps) is required to achieve the same accuracy τ

Please cite this article in press as: Petrovskii S, et al. Multiscale approach to pest insect monitoring: Random walks, pattern formation, synchronization, and networks. Phys Life Rev (2014), http://dx.doi.org/10.1016/j.plrev.2014.02.001

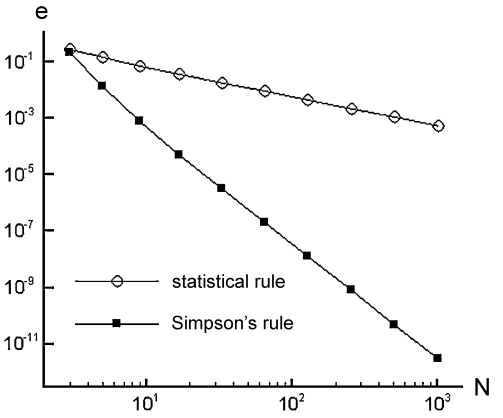

Fig. 20. Comparison of convergence rates. The relative integration error (76) is calculated as a function of the number of the grid nodes N in a regular grid with $h = 1/(N-1)$. The open circles (dashed line) and the closed squares (solid line) show the error (on the logarithmic scale) for the statistical rule (72)–(73) and the Simpson rule (80), respectively.

(cf. Eq. (77)) if the statistical rule is employed in the evaluation of insect abundance compared to the Simpson rule. In other words, for the same number of grid nodes, the Simpson rule will give a much better accuracy.

The above consideration clearly leads to the conclusion that, when choosing from available methods of numerical integration with which to evaluate the total pest population size, the method with the fastest convergence rate (89) must be employed and other methods should simply be ignored. If we approximate the integrand function by a polynomial, the convergence rate will depend on the polynomial degree, higher order polynomial approximation having faster convergence [39]. For example, the 1D composite Simpson method with the convergence $O(h^4)$ should always be more accurate than the 1D composite trapezoidal rule with the convergence $O(h^2)$, and both Simpson and trapezoidal rules are superior to the statistical rule (72)–(73) which has the convergence rate as $O(h)$. Similar conclusions about the convergence rate can also be drawn in the 2D case [39].

The convergence criterion is conventionally used whenever several methods of numerical integration are compared. Other factors such as the complexity of a numerical integration algorithm, speed of computation of the weight coefficients in the method etc. should be taken into account too, especially in multi-dimensional problems. However, the convergence rate remains the most important requirement that ultimately guarantees the best accuracy of numerical integration.

Unfortunately, the convergence rate criterion does not always work in ecological applications. This is because, strictly speaking, the error estimate (89) only holds if the grid step size h is sufficiently small, i.e. if the number of grid nodes (traps) N is sufficiently large. In this case we can say that we have a *fine* grid where we can rely upon the error estimate (89). Meanwhile, if N is small, Eq. (89) may become invalid and we cannot readily tell which integration method is better based on their convergence rate (89). Correspondingly, a *coarse* grid is defined as a grid where the error estimate (89) is not valid because h is not small enough (or N is not large enough). The question therefore arises as to how to evaluate the accuracy of integration on such grids.

The failure of the criterion (89) is a serious problem of pest abundance evaluation as coarse grids are common in pest monitoring, for the reasons that are explained at the beginning of Section 3. Here we want to emphasize that this difficulty arises not only for more advanced methods like the trapezium rule or the Simpson rule but also for the baseline method (72)–(73) as the latter effectively coincides with the simplest 'mid-point rule' of numerical integration. Note that, if we are not happy with accuracy of the original estimate, we cannot just increase the number of traps and repeat trapping. A repeated trapping would be done under different environmental conditions and would be subject to a different (unknown) population density distribution. This difficulty is, in fact, related to a more fundamental problem with replicated experiments in ecology, e.g. see [119]. Hence in the pest abundance evaluation problem we normally have to deal with a coarse grid of traps where we cannot readily draw any conclusions about the accuracy of the integration method.

The issue of accuracy of pest abundance evaluation from sparse sampled data has been the focus of ecological research for a long time [42,175,176]. Some recommendations have been provided for the minimum number of traps required to obtain a reliable estimate. However, those recommendations are heavily based on the assumption that

Please cite this article in press as: Petrovskii S, et al. Multiscale approach to pest insect monitoring: Random walks, pattern formation, synchronization, and networks. Phys Life Rev (2014), http://dx.doi.org/10.1016/j.plrev.2014.02.001

the population density distribution is approximately homogeneous [18,73,161]. While the above assumption is often true, there are also many cases where the pest density is strongly heterogeneous and can be aggregated into several patches [11,48]. In the latter case there are no recommendations about the minimum number of traps required to achieve desirable accuracy. For a heterogeneous spatial population distribution, it is very likely that a small number of traps (as is normally used in the routine monitoring) may be insufficient to resolve highly localized sub-domains (or "patches") of high population density, and we can anticipate an inaccurate estimate of the total pest population size. This generic problem of accuracy control on grids of traps where the error estimate (89) does not apply has been dubbed as a "coarse grid" problem in [116] and then further investigated in [116,119,117]. Below we provide several examples illustrating the challenges of insect abundance evaluation on coarse grids.

Let us first consider the problem in the 1D case [116]. Although our final goal is to develop a method of evaluation of the pest population size from spatially discrete data, in order to reveal the properties of the course grid problem, we now consider a hypothetical case where the population density $u(x)$ is continuous. The value of u is then available for any x, so that we can compare the accuracy obtained on different grids. For this purpose, a continuous population density can be obtained from a relevant model. Figs. 21a and 21c show the population density versus space obtained from a spatially explicit predator–prey model with the Allee effect [88,101,169]. The equations of the model have been solved numerically on a very fine spatial grid; details of the model and the numerical procedure as well as parameter values and the initial and boundary conditions used in simulations can be found in [116]. The properties of the spatial distribution $u(x)$ obtained from this model[6] are known to be determined by the diffusion coefficient D [88,118,123]. For $D \sim 1$ or larger, the initial density distribution normally evolves to a monotone function, e.g. as shown in Fig. 21a. For $D \ll 1$, the model describes pattern formation: the initial conditions evolve to a function with a complicated, multi-peak structure (see Fig. 21c), smaller values of D result in a larger number of peaks in the domain [122,123].

In order to look into the issue of accuracy, the two population density distributions shown at the left-hand side of Fig. 21 are integrated numerically on a sequence of regular grids with different (increasing) N using the statistical rule (72)–(73) and the Simpson rule (80); the corresponding integration error (76) is shown at the right-hand side of Fig. 21. For the monotone distribution of Fig. 21a, the error of the statistical rule exhibits its asymptotical behavior already for a very small number of grid nodes (Fig. 21b). In contrast, for the same range of N between 3 and 17, the error of the Simpson rule behaves quite erratically, having nothing to do with the prediction of Eq. (89). In spite of this, integration by the Simpson rule gives very accurate results even on a grid with a very small number of grid nodes ($N = 3$), while the statistical rule (72)–(73) generates a much bigger error.

The situation becomes very different for the population density distribution $u(x)$ shown in Fig. 21c. The convergence curves for the statistical rule and the Simpson rule are shown in Fig. 21d. It is readily seen that, regardless of which integration rule is used, we have a coarse grid problem where the density $u(x)$ is not well approximated on a grid with the number of nodes in the considered range. In particular, the Simpson rule appears to have a bigger error in comparison with the method (72)–(73) on grids with 3, 5 and 9 nodes. Only when the number of grid nodes increases to $N = 17$ does the error of the Simpson rule become smaller than the error of the statistical rule.

One important observation that can be drawn from the above example is that the accuracy of integration depends on the properties of the spatial density distribution. For the same number of grid nodes, the same method can provide a good accuracy in one case and a very poor accuracy in another. Correspondingly, the same grid can appear to be a fine grid in one case, i.e. for a spatial population distribution with simple properties (for instance, for a smooth monotone function, see Fig. 21a) but a coarse grid in another case, i.e. for a population distribution with a more complicated structure, cf. Fig. 21c. Indeed, in the former case the error of the statistical rule (72)–(73) is already close to asymptotic behavior (89) on the grid with just 3–5 nodes, whilst in the latter case it only approaches its asymptotics for $N = 17$.

This observation is further confirmed by considering numerical integration in the 2D case. The 2D examples shown in Fig. 22 are generated from the same mathematical model (see also [119]). Again, we consider two spatial density distributions with qualitatively different properties. The population density $u(x, y)$ shown in Fig. 22a consists of a single wide peak with a steep gradient at one side but a shallow gradient at all other sides. In contrast, the population density shown in Fig. 22c consists of many narrow peaks separated by areas where the population density is very small; this type of the spatial pattern is characteristic of the late stage of patchy invasion [126,128].

[6] The spatial population density distribution obtained from this model depends also on time; here by $u(x)$ we denote the population density obtained at a certain moment of time.

Please cite this article in press as: Petrovskii S, et al. Multiscale approach to pest insect monitoring: Random walks, pattern formation, synchronization, and networks. Phys Life Rev (2014), http://dx.doi.org/10.1016/j.plrev.2014.02.001

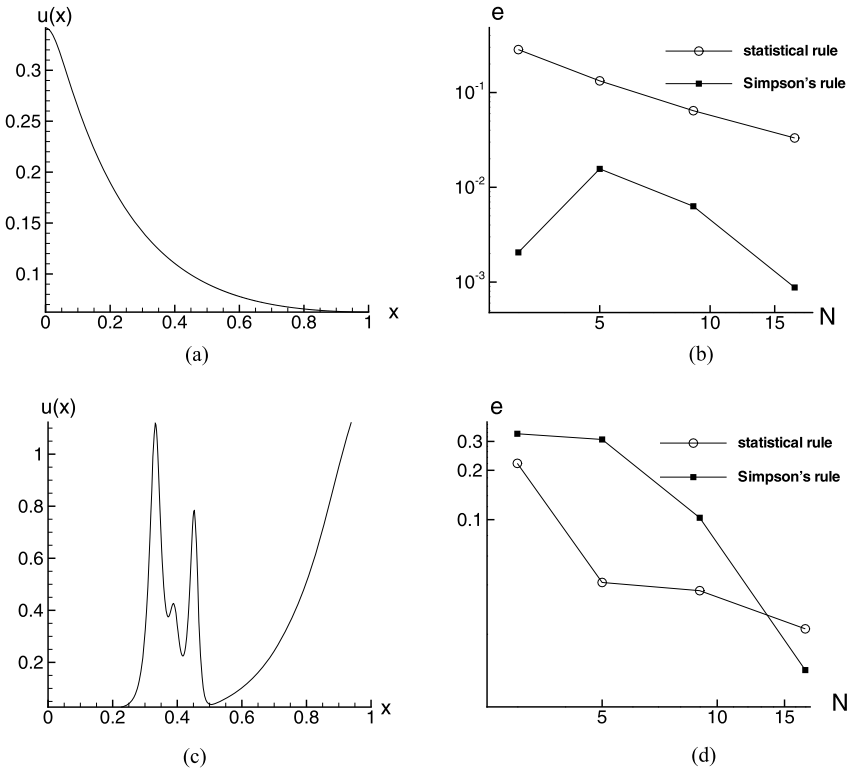

Fig. 21. The coarse grid problem. (a) A monotone spatial distribution of the pest population density $u(x)$ obtained for the dimensionless diffusion coefficient $D = 10^{-4}$. Other parameters along with the initial and boundary conditions used to generate one-dimensional density distributions are discussed in [116]. (b) The integration error (76) arising from numerical integration of the distribution in (a) using the statistical rule (72)–(73) (solid line, open circle) and the Simpson rule (80) (solid line, closed square). The error is shown on the logarithmic scale. (c) A 'multi-peak' density distribution obtained for the diffusion coefficient $D = 10^{-5}$. (d) The integration error (76) corresponding to (c), the legend is the same as in (b).

The error of numerical integration by methods (72)–(73) and (87) is shown in the right-hand side of Fig. 22. Integration is carried out on regular grids with the grid step size $h = const$ in each direction. It is readily seen from the figure that integration of the population distribution of Fig. 22a already gives good accuracy[7] on grids with a small number of nodes ($N = 3$ or $N = 5$ in each direction, which corresponds to the total number of nodes/traps as $3 \times 3 = 9$ or $5 \times 5 = 25$) even though the range of the asymptotical convergence (89) has obviously not yet been reached, i.e. the grids are coarse. The Simpson method remains consistently a more accurate method of integration on all considered grids.

Meanwhile, the more complex spatial structure of the density distribution shown in Fig. 22c requires a larger number of grid nodes to provide reasonable accuracy. On the coarse grids with $N = 3$, the error is large for both statistical and Simpson rule; see Fig. 22d. Interestingly, in this particular case, the statistical rule (72)–(73) appears to be slightly more accurate than the Simpson rule. However, any conclusion about accuracy on a particular method of integration is not reliable on coarse girds. It does not follow from the above result that the rule (72)–(73) is always more accurate on a coarse grid of 3×3 nodes. As we will see below, for the same numerical integration method, a slight change in the spatial pattern may result in a large increase in the integration error.

Let us now consider how numerical integration works for field data and what factors may affect its accuracy. Numerical integration techniques have been applied to field data of ecological monitoring in [115,119] and here we discuss some of their results. Fig. 23a shows one of the six cases of different population density distributions of the New Zealand flatworm (*Arthurdendyus triangulatus*) analyzed in [119] based on the field data collected by Murchie

[7] Recall that in ecological studies a relative error of up to 50% (i.e. $e \sim 0.5$) is often deemed as acceptable, while an error $e < 0.3$ is usually regarded as small, cf. [111,152].

Please cite this article in press as: Petrovskii S, et al. Multiscale approach to pest insect monitoring: Random walks, pattern formation, synchronization, and networks. Phys Life Rev (2014), http://dx.doi.org/10.1016/j.plrev.2014.02.001

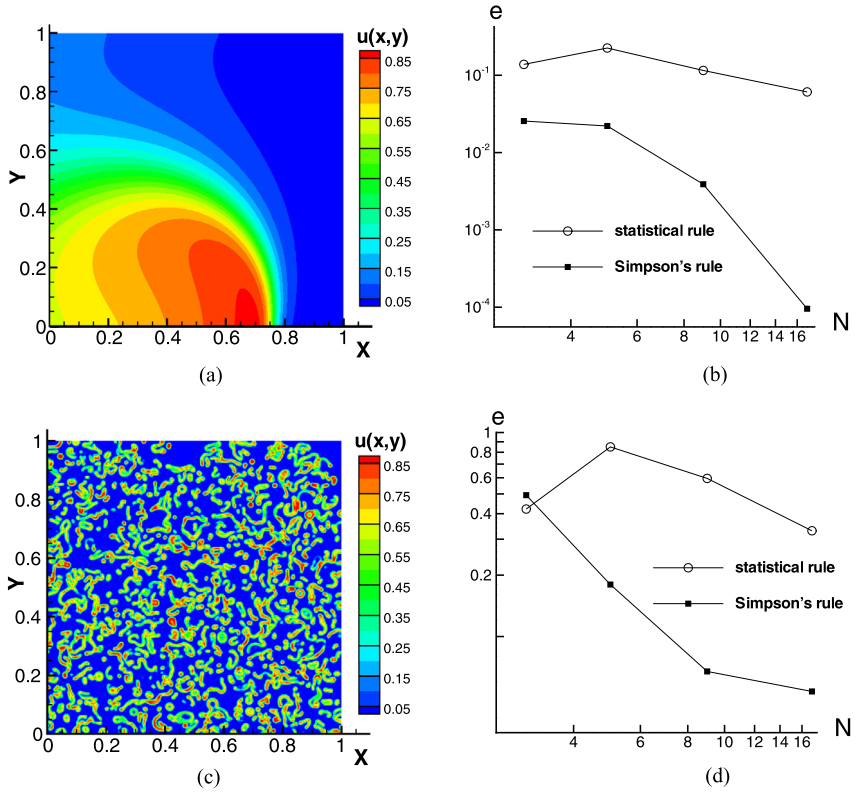

Fig. 22. The coarse grid problem in the 2D case. (a, c) Population density $u(x, y)$ obtained from a mathematical model of population dynamics (see details in the text), (b, d) the corresponding integration error (76) shown on the logarithmic scale, N is the number of nodes in each direction x and y of a regular Cartesian grid. (a) A single peak population distribution typical for the values of the diffusion coefficient $D \sim 1$ or larger. (b) The integration error for the statistical rule (solid line, open circle) and the Simpson rule (solid line, closed square) corresponding to (a). (c) A snapshot of a patchy population density distribution typical for $D \ll 1$. (d) The integration error corresponding to (c), the legend is the same as in (b).

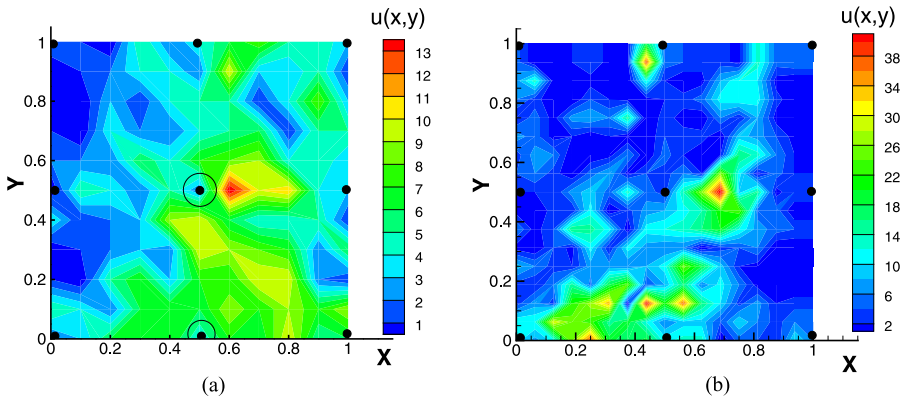

Fig. 23. Numerical integration of field data on a coarse regular grid of 3×3 nodes, the nodes are shown as large black dots. (a) The population density $u(x, y)$ based on the field data collected in [100] (see also [119]). The two circled grid nodes fall into small patches of lower density. Since the density values at those locations are not representative ("outliers"), 2/9 of the total information is lost and hence numerical integration results in a large integration error. (b) The density function $u(x, y)$ based on the field data by [5]; see details in the text. (For interpretation of the references to color in this figure, the reader is referred to the web version of this article.)

and Harrison [100]. The original data were collected with 121 traps installed at the nodes of a regular grid of 11×11 nodes. First, the values of the population density available at the nodes of this fine grid were integrated in order to obtain the 'true' value of the population size. (In Fig. 23a, the population density is shown as a continuous function

Table 1
The approximated value I_a of the total population size and the integration error e on a regular grid of 3×3 nodes for the field data. The rows marked (a) and (b) correspond to the population density distributions shown in Figs. 23a and 23b, respectively. I_a and e are computed by the statistical rule (72)–(73) (the columns I_a^{stat} and e_{stat}) and by the Simpson rule (87) (the columns I_a^{SR} and e_{SR}).

Case	I	I_a^{stat}	e_{stat}	I_a^{SR}	e_{SR}
(a)	544	289	0.469	247	0.545
(b)	1980	1507	0.239	2332	0.178

$u(x, y)$ using linear interpolation.) Then, a coarse grid of $3 \times 3 = 9$ nodes was generated by picking the first, sixth and eleventh nodes in each direction. The locations of those selected 9 traps on a coarse grid is shown in Fig. 23a by large black dots, the values of the population density at those locations were taken from the original grid. Finally, the approximate value I_a of the population size was obtained by numerical integration over that coarse grid.

The values of I_a obtained with different integration rules [see case (a) in Table 1] were compared to the 'true' value I in order to estimate the accuracy of the approach. Here we want to mention that the case shown in Fig. 23a was the one with the worst accuracy. For the other five population distributions analyzed in [119], the integration error on the coarse 3×3 grid was consistently less than 35% and the Simpson rule was shown to be more accurate (with the integration error less than 10% in three our of six cases). However, here we deliberately focus on the most difficult case shown in Fig. 23a as it is instructive to understand the reasons resulting in the relatively large integration error shown in Table 1.

First, we note that the larger error of the Simpson rule compared to the statistical rule (see Table 1, row (a)) clearly indicates that the 3×3 integration grid is indeed coarse as on a fine grid it should have been otherwise; see Fig. 20. Secondly, consistent with our analysis above, the accuracy of integration is determined by the properties of the spatial pattern in the density distribution [119]. After a careful visual examination of Fig. 23a, it becomes clear that, on the coarse grid, some information about the density function $u(x, y)$ is lost as two out of nine grid nodes are located inside small patches where the density is significantly different (lower) from the density in the surrounding areas; those nodes are circled in the figure. Hence two out of the nine available local density values used for numerical integration will make a misleading contribution to the integral I_a, no matter what integration technique is used. As a result, we have a relative integration error $e \sim 0.5$ for both statistical and Simpson rules.

For the second example, Fig. 23b presents the field data from [5] where the insect species *Pterostichus melanarius* was monitored with pitfall traps installed at the nodes of 15×15 regular Cartesian grid. The corresponding density distribution $u(x, y)$ obtained as a linear interpolation of the local density values is shown in Fig. 23b. The idea of our analysis is similar to the previous example, i.e. we obtain the 'true' value I of the population size by integrating the data on the original fine grid, construct a coarse 3×3 grid as a relevant subset of grid nodes, and then obtain an approximate value I_a by integrating the data on the coarse grid. Note that, in this case, the population distribution has not just one but several small patches of high density. Obviously, these small patches are unlikely to be well resolved on a 3×3 grid. Hence the poor resolution of the pattern can be expected to contribute to the integration error. On the other hand, there is a large area inside the domain where the density, while rather low, is approximately homogeneous (shown in various shades of blue in Fig. 23b). The population density in this area is well-resolved on the grid of 3×3 nodes and hence the contribution to the integral from this sub-domain is expected to be sufficiently accurate. Since the number of high-density patches is not large, we can therefore expect a reasonably small integration error on the coarse grid. This heuristic argument is in agreement with the results of numerical integration; case (b) of Table 1 shows that the relative error is less than 25%. Interestingly, as was shown in [115], an increase in the number of traps from 3×3 to 9×9 does not significantly increase the accuracy of integration because small patches of high density remain unresolved on those grids.

The above results lead us to the conclusion that, on a grid with a given number of nodes (traps), the accuracy of pest abundance evaluation is to a large extent determined by the properties of the spatial pattern in the density distribution. Therefore, the following simple classification can be offered:

(A) N (the number of nodes in each direction) is sufficiently large to make the grid fine for the given spatial density distribution, so the asymptotic error estimate (89) holds and the integration error is small.
(B) N is not large enough for the given spatial density distribution, so the grid is coarse and the asymptotic error estimate (89) does not hold, however the integration error appears to be small.

Please cite this article in press as: Petrovskii S, et al. Multiscale approach to pest insect monitoring: Random walks, pattern formation, synchronization, and networks. Phys Life Rev (2014), http://dx.doi.org/10.1016/j.plrev.2014.02.001

(C) N is not large enough so the spatial pattern is not well resolved, the grid is coarse and the integration error is large.

Hence, future research into numerical integration for the pest abundance evaluation problem should investigate how the information about the spatial pattern in population density, if available, can be used to correctly predict the integration error and, ultimately, to improve the integration accuracy. Note that, in real-life applications, *a priori* information about a spatial density distribution is rarely available (but see [118] for a discussion of this issue). However, it seems plausible to assume that some inferences about a typical population distribution can be made based on field data collected for a given pest species in previous years, especially for common pests where such data are likely to be abundant.

Let us assume, for the sake of the discussion only, that we know the spatial pattern $u(x, y)$ and can classify the integration error. Then, in case (A), a method based on higher order polynomial approximation of the integrand will provide much better accuracy in comparison with a low order method. Correspondingly, in this case the Simpson rule would definitely be preferred to the statistical rule (72)–(73). However, in cases (B) and (C), a better accuracy for an integration rule based on higher order polynomial approximation cannot be guaranteed and other factors should be taken into account in order to decide wisely about the choice of a numerical integration method.

Therefore, as we showed above, a population distribution with a simple structure (e.g. like those shown in Figs. 21a and 22a) is easy to integrate with a good accuracy, even on a very coarse grid consisting of just a few nodes. Conversely, a population with a complicated spatial pattern like a patchy distribution (cf. Figs. 21c, 22c and 23) is usually difficult to integrate, the accuracy of integration depending on the characteristic size of each patch and the number of patches. A generic result is that, if we have several small patches of high population density and we have to use a coarse grid, i.e. a grid with a large distance between neighboring nodes (traps), then the integration accuracy heavily depends on the location of those nodes with regard to the positions of the patches. As the positions of the patches is usually unknown, and may depend on various factors that are difficult to quantify, they can be regarded as random values. Correspondingly, the approximate value I_a of the population size calculated on a coarse grid becomes a random value, too [119]. In this situation, none of the approaches described in this section (including the baseline rule (72)–(73)) apply anymore. To extend any of the above methods to this case, the whole concept of numerical integration should be amended. Clearly, the most extreme case of integration on coarse grids is given by the population distribution consisting of a single patch of high population density where the patch characteristic width is smaller than the distance between grid nodes. In the next section, we discuss these highly aggregated density distributions in order to demonstrate that a conceptually different approach should be applied to evaluate the total population size.

3.3. Integration of high-aggregation density distributions

There are a few ecologically meaningful situations where the population of an insect species can be highly aggregated so that all of it or most of it is confined, at least temporarily, within a small area inside a given habitat. This may happen as a result of insect migrations, e.g. when a swarm lands locally onto an agricultural field (cf. "point source release" in Section 2, see Fig. 5). Alternatively, it may happen during the establishment stage of biological invasion [120,153]. Whichever is the case, timely and accurate evaluation of the insect abundance through an efficient monitoring approach is important in order to prevent potential damage to the agricultural product. At the same time, the application of numerical integration methods to highly aggregated density distributions is a very challenging task, in particular because the exact location of the high density patch is normally not known.

Highly aggregated population density distributions or "peak functions" have been defined in [114] as spatial patterns where the entire population of a given species is confined to a small single area within a (much) larger field or habitat. We will refer to this area as the patch of high density. In the context of insect monitoring, "small" here means that the typical size of the patch, say δ, is equal to or less than the characteristic distance h between the neighboring traps. The properties of the numerical integration on such "ultra-coarse" grids [119] appears to be different depending on whether the grid is regular ($h = const$) or the traps are installed randomly (h varies). Below we briefly discuss both of these cases.

An example of a peak function in the 1D case is sketched in Fig. 24a where the black dots show the position of the nodes of a regular grid that is used to evaluate the integral. It is intuitively clear that the accuracy of integration of a peak function on grids with a small number of nodes N (equivalently, for a large h, i.e. for $h \geqslant \delta$) depends

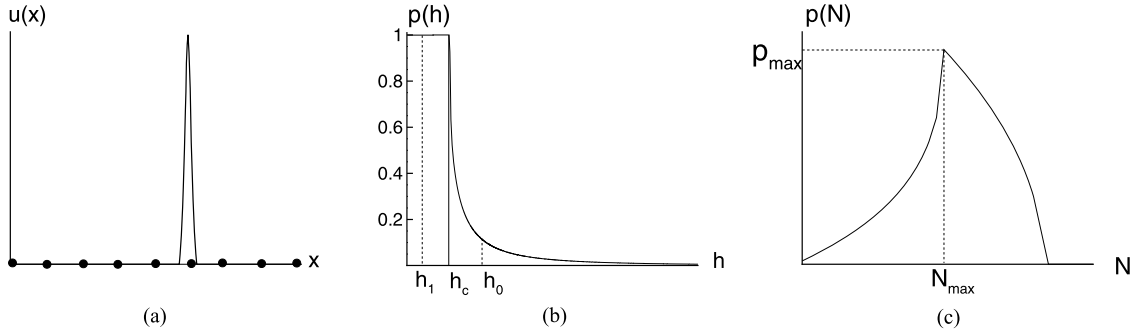

Fig. 24. (a) An example of a 1D highly aggregated distribution of the population density $u(x)$ (high density patch, peak function), black dots show the position of the grid nodes. (b) The probability of obtaining an accurate estimate of the pest population size if traps are installed at nodes of a regular grid. (c) The probability of obtaining an accurate estimate of the pest population size using the integration rule (72)–(73) on a random grid of traps under the constraint that only a single trap falls into the high density patch.

on the peak width and peak location with respect to the grid nodes. In the worst case scenario, a narrow peak can fall entirely between two neighboring nodes of the grid and then the integration gives exactly zero, which is grossly misrepresentative of the true population size. On the other hand, it is equally possible to find a peak location such that integration of the population density $u(x)$ on the same regular grid would provide a very accurate answer [118].

Correspondingly, the following issues arise: (i) what is the minimum 'critical' number N_c of nodes/traps required to achieve desirable accuracy if a highly aggregated population density distribution $u(x)$ of a given width δ is integrated on a 1D regular grid, and (ii) what is an appropriate measure of integration accuracy on a regular grid of traps where $N < N_c$? Following [114,119], we address these issues by introducing the concept of an ultra-coarse grid. An ultra-coarse grid is defined as a grid where the integration error is essentially a random variable because of insufficient information (uncertainty) about the integrand function. When numerical integration is performed on ultra-coarse grids, the integration error as such does not have much meaning as it can be very different for a slightly different position of the peak (which is unknown). Instead, one can calculate the probability p that the value of the error will remain smaller than the given tolerance τ, cf. Eq. (77).

It does not seem possible to calculate p analytically for an arbitrary population density $u(x)$. However, we recall that the spatial distribution of the population density appears as a result of movement of individual insects; see Section 2.2. Depending on the type of the movement (e.g. diffusion or superdiffusion), that will add up to either the normal distribution or the Cauchy distribution. Both distributions are dome-shaped so that the density profile around its maximum value (located at a certain $x = x_m$) is obviously described as $u(x) = u(x_m) - u''(x_m)x^2 + o(x^2)$. Correspondingly, by neglecting the tail of the density profile (which does not affect the accuracy much, see [118]), we can approximate $u(x)$ with a square polynomial.

Based on the quadratic approximation of the peak function, the probability $p(h)$ that the value of the integration error does not exceed τ was obtained in [114]. The exact shape of the graph $p(h)$ depends on the chosen integration rule, on δ and on τ; the generic shape is shown in Fig. 24b. The probability $p(h)$ appears to be a piecewise function of the grid step h; there exists a critical, threshold value h_c such that $p(h) \equiv 1$ for any $h \leqslant h_c$, and $p(h)$ is a monotonously decreasing function for $h > h_c$. It was also shown in [114] that the critical grid step size h_c is a linear function of the peak function's width:

$$h_c = \alpha_c(\tau)\delta, \tag{90}$$

where the coefficient α_c depends on the tolerance τ.

In order to illustrate how this approach works, we consider a hypothetical aggregated population density distribution $u(x)$ with the width δ, so that the corresponding probability $p(h)$ is given by the curve shown in Fig. 24b. If the data on local abundance are collected on a regular grid with the step size $h_0 > h_c$, for example, then our chance to evaluate the integral within the acceptable accuracy range τ is $p(h_0) \approx 0.15$. Therefore, for this grid with $N_0 \approx 1/h_0$ nodes, there is an 85% chance that the error of our evaluation will be larger than the maximum affordable error τ. In other words, if this grid of traps is installed in ten similar fields, it is likely that in 8 cases out of 10 the obtained estimate of the pest population size will have little to do with reality. Clearly, this is a very low quality monitoring system.

Please cite this article in press as: Petrovskii S, et al. Multiscale approach to pest insect monitoring: Random walks, pattern formation, synchronization, and networks. Phys Life Rev (2014), http://dx.doi.org/10.1016/j.plrev.2014.02.001

Consider now a regular grid with $h_1 < h_c$ and the number of nodes $N_1 \approx 1/h_1$. The error of integral evaluation is now smaller than τ, no matter where the peak is located. The probability $p(h)$ of getting the error within the accuracy range $e(N_1) < \tau$ is $p(h_1) = 1$. In this case, in all ten fields the pest population size is evaluated meaningfully.

If the grid is not regular, e.g. some of the traps are misplaced, the integration accuracy may become worse [118]. Let us consider the integration of a peak function on an irregular grid where the position of all the traps across the domain is chosen randomly (according to a certain rule to ensure that the traps are distributed uniformly – now in the statistical sense – across the whole area). Integration of a highly aggregated population density on random grids using the statistical rule (72)–(73) was studied in [44] both in 1D and 2D cases under an assumption that the total number of traps is small, so that only one trap falls within the high density patch. Note that this assumption is very important in the context of the real-life monitoring as it describes the existing typical constraints; see the beginning of Section 3. Under this assumption, in a similar way to the regular case, the grid is ultra-coarse because of the uncertainty of the peak location, and an estimate of the total population size is a random variable.

The probability p to obtain an estimate with the error $e < \tau$ was calculated in [44] basing on the quadratic approximation of the population density profile. An example of the probability p as a function of the number N of grid nodes is shown in Fig. 24c. Note that the function $p(N)$ consists of two branches. The increasing branch reflects the better averaging of the error with an increase in N. The decreasing branch of the graph $p(N)$ shows the (decreasing) probability to have exactly one trap inside the patch [44]; this range of N should therefore be regarded as unrealistic because of the constraints mentioned above. Correspondingly, under the assumption of a single trap within the high density patch, there is an optimum number N_{max} of traps that provides the maximum probability p_{max} of obtaining an accurate estimate. Interestingly, it appears that the maximum probability is always $p_{max} < 1$ [44].

The results revisited in this section demonstrate that the conventional conclusions that ecologists make about accuracy of pest abundance evaluation should be regarded with care. Ecologists are well aware that there is uncertainty in the estimation of the pest abundance, which may become worse as the number of samples decreases [18]. However, to the best of our knowledge, the idea of handling the error of the evaluation as a random variable has not been discussed in the ecological literature so far. Under the conditions that only a small number of traps are available per field and a highly aggregated population distribution is likely to occur, our results may eventually lead to a paradigm shift where the traditional ways to estimate the population abundance in individual fields give way to "probabilistic integration" across a group of fields or habitats with similar properties.

4. Landscape scale: synchronization and self-organization

The largest spatial scale in the problem of pest monitoring is the landscape scale that may include many agricultural fields as well as non-farmed habitats. Pest monitoring programs are usually region-wide or even nation-wide. For instance, aphids have been the focus of an intensive monitoring program in the U.K. Aphids rarely cause any significant damage by themselves but they are regarded as harmful species because of their high potential to transmit viruses to crops. In order to monitor aphid abundance, the U.K. Food and Environment Research Agency created a monitoring system consisting of dozens of traps installed at various locations across the country [104]. The system was set up in 2002, and for the first two years consisted of around a dozen traps in 4 geographically distinct regions (Scotland, North Yorkshire, East Anglia and Wiltshire). From 2004 onwards, the system has consisted of around 100 traps in 8 regions; see Fig. 25.

Good understanding of trends and peculiarities in the trap counts is clearly important for providing timely and reliable information about pest abundance to crops growers. A visual inspection of the map shown in Fig. 25 immediately reveals that the trap counts at different locations do not seem to be independent as the date of the first catch of the pest insect appears to be correlated across a certain area. This indicates that aphid population numbers are not entirely independent either. A question thus arises as to how typical this situation is and whether it originates in the landscape properties, in the weather conditions (e.g. seasonality) or in some inherent density-dependent population self-regulation.

Environment is known to affect the population dynamics in space and time through a variety of specific factors such as landscape structure [71,131], seasonality and solar cycles [155], weather conditions on both global and regional scales [9,138,139], etc. In many cases, the population fluctuations in different habitats appear to be, to a certain extent, correlated; the phenomenon known as synchronization [85,87]. The example of aphids considered above is therefore by no means unique. There is increasing recognition that an efficient and reliable insect pest monitoring

Please cite this article in press as: Petrovskii S, et al. Multiscale approach to pest insect monitoring: Random walks, pattern formation, synchronization, and networks. Phys Life Rev (2014), http://dx.doi.org/10.1016/j.plrev.2014.02.001

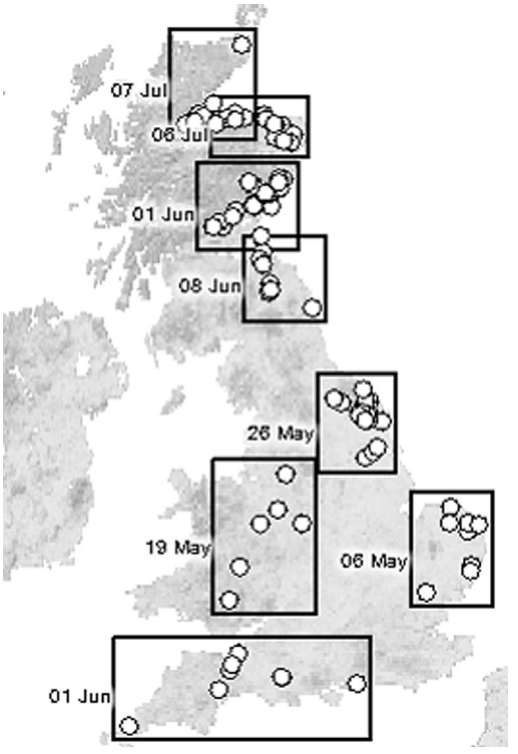

Fig. 25. A sketch of the aphid monitoring system in the U.K. showing the location of traps (circles) in different regions (boxes) in 2009. Date is first capture of peach potato aphid in the region. From [104], by courtesy of Phil Northing.

program should include consideration of scales larger than a single field scale as the importance of long-distance cross-correlations between the pest abundance in different fields has become evident [15,22,23].

Due to the landscape heterogeneity, it often happens that the population of the same species occupy disjoint habitats. Depending on the inter-habitat distance, individual mobility and the nature of the environment between habitats, these local populations may or may not interact with each other through dispersal. The inter-habitat dispersal has been identified as a synchronizing factor [85]. There is considerable evidence that dispersal coupling by just a small fraction of the population may bring population fluctuations into synchrony [59,80,144].

Dispersal coupling, however, is not the only factor that can result in population synchronization. Environmental forcing, in particular through the effect of regional (spatially correlated) transient weather conditions (that are usually regarded as environmental stochasticity or noise; e.g. see [170] and references therein), can synchronize the fluctuations of disconnected populations. This phenomenon is known as the Moran effect [97,98,140,149] and it has been widely observed in different taxa and in various environments [85].

Synchronization of population fluctuations can therefore be driven by the regional environmental stochasticity, by the interaction between local populations through dispersal, or by a mixture of both [55]. However, the relative importance of these two factors often remains obscure apart from special cases where dispersal can be ruled out completely. Synchronization has many implications across the whole range of ecological sciences, in particular, for agro-ecology [148] and pest control [20,94,178]. Understanding the coupling between different habitats is now being considered an essential prerequisite to good management practices [66]. Identifying particular factor(s) resulting in synchronization is therefore important. However, since both dispersal and the Moran effect can have a similar impact on population dynamics, it is often very difficult to distinguish between them. Differentiating the effects of stochasticity from that of dispersal is sometimes regarded as one of the greatest challenges to ecologists studying spatiotemporal population dynamics [85].

A related problem is to identify the corresponding spatial scale of the mechanisms involved. For species with low mobility, the scale of synchronization due to dispersal is known to usually be smaller than the scale induced by the regional stochasticity. In particular, in a field study on butterflies [164] it was shown that the spatial scale of dispersal

Please cite this article in press as: Petrovskii S, et al. Multiscale approach to pest insect monitoring: Random walks, pattern formation, synchronization, and networks. Phys Life Rev (2014), http://dx.doi.org/10.1016/j.plrev.2014.02.001

coupling is on the order of 5 km while population synchrony can be observed on much larger distances of up to 200 km. The larger spatial scale of synchronization is therefore likely to be linked to regional stochasticity, although this may not necessarily be true if insect dispersal is assisted by the wind [15].

Note that the large, landscape spatial scale of the insect monitoring problem allows for a different level of detail in the description of local populations. We no longer consider trap counts (like in Section 2) or population densities at particular locations (like in Section 3). Instead, each monitored unit, e.g. an agricultural field, is now described by a single variable such as the total population size or the average density of a given pest species. In terms of the mathematical framework, it means that we consider a discrete space – a lattice [7,95,146] or a network [68,150] – rather than a continuous one.

Let us consider the populations of a certain species dwelling in two fields, say, X and Y. The population census takes place at certain times, $t_1, \ldots, t_n$ (e.g. weekly, monthly or annually), and results in the two time-courses, $X_1, \ldots, X_n$ and $Y_1, \ldots, Y_n$ where X_i and Y_i are the population sizes of the monitored species in fields X and Y, respectively, at time t_i. The degree of synchronization between the two populations is usually quantified by the Pearson product moment correlation coefficient:

$$r_0(X,Y) = \frac{\sum_{i=1}^{n}(X_i - \mu_X)(Y_i - \mu_Y)}{\sqrt{(\sum_{i=1}^{n}(X_i - \mu_X)^2)(\sum_{i=1}^{n}(Y_i - \mu_Y)^2)}}, \tag{91}$$

where n is the length of the monitoring time-course and μ_X and μ_Y are the sample means of the two time series, i.e.:

$$\mu_X = \frac{1}{n}\sum_{i=1}^{n} X_i, \qquad \mu_Y = \frac{1}{n}\sum_{i=1}^{n} Y_i. \tag{92}$$

In order to demonstrate a practical application of this technique,[8] to reveal its limitations and to discuss its possible extension and/or modification, we now consider a case study [15]. The population of *T. paludosa*, a common agricultural insect pest in the British Isles, was monitored over 15 years between 1980 and 1994 across a region in South-Western Scotland; see Fig. 26. The study covered the area of approximately 200×200 km^2 with the inter-field distances varying between 2 and 200 km (Fig. 27).

Tipula paludosa is a univoltine insect species with adult emergence, under the typical U.K. weather conditions, between mid-August and mid-September. Adult *T. paludosa* are flying insects; however, their dispersal is thought to be limited as females are poor fliers, emerging gravid and laying eggs within one day. The larval stages of *T. paludosa*, known as leatherjackets, are soil dwelling and relatively lacking in mobility.

An annual census of the population abundance was taken in mid-winter (when the species is in the larval stage) in each of 38 fields shown in the map. This resulted in 38 time-courses, each containing 15 datapoints, i.e. values of the average population density over 15 years. The correlation coefficient r_0 was then calculated for all possible pairs of these time-courses. The results are shown in Fig. 28. We observe that the dependence of r_0 on distance between fields exhibits a clear intermittent behavior with: some fields being strongly positively correlated (synchronized) up to distance of 150–170 km, some fields being significantly negatively correlated, and some fields (including cases where the fields are situated very close to each other) being not correlated at all. A general trend in correlation strength vs distance can be revealed using linear regression analysis (solid line in Fig. 28), which shows a slow decay. We therefore conclude that, as such, the distance between fields does not provide sufficient information to decide whether the populations of two fields are likely to be synchronized.

A better understanding of the system's properties can be achieved if the correlation strength is linked to the actual position of the fields. Fig. 29 shows the location of all 38 fields where those that are significantly correlated, in the statistical sense, are connected by a line. Interestingly, the observed network exhibits anisotropic properties with more correlated pairs situated along the North-West to South-East direction than on other bearings. Since the terrain does not seem to possess any clear directional structure, one can hypothesize that the asymmetry in the network shown in Fig. 29 may have appeared because of the impact of the wind. Indeed, having considered the weather data (location of the weather stations is shown in Fig. 26 by the flag), a considerable similarity between the structure of the inter-field correlations and the prevailing wind directions was discovered [15].

[8] Sometimes it may be necessary first to remove the effects of density dependence from the original data before calculating the cross-correlation coefficient (91) in order to make sure that the individual time series are serially independent.

Please cite this article in press as: Petrovskii S, et al. Multiscale approach to pest insect monitoring: Random walks, pattern formation, synchronization, and networks. Phys Life Rev (2014), http://dx.doi.org/10.1016/j.plrev.2014.02.001

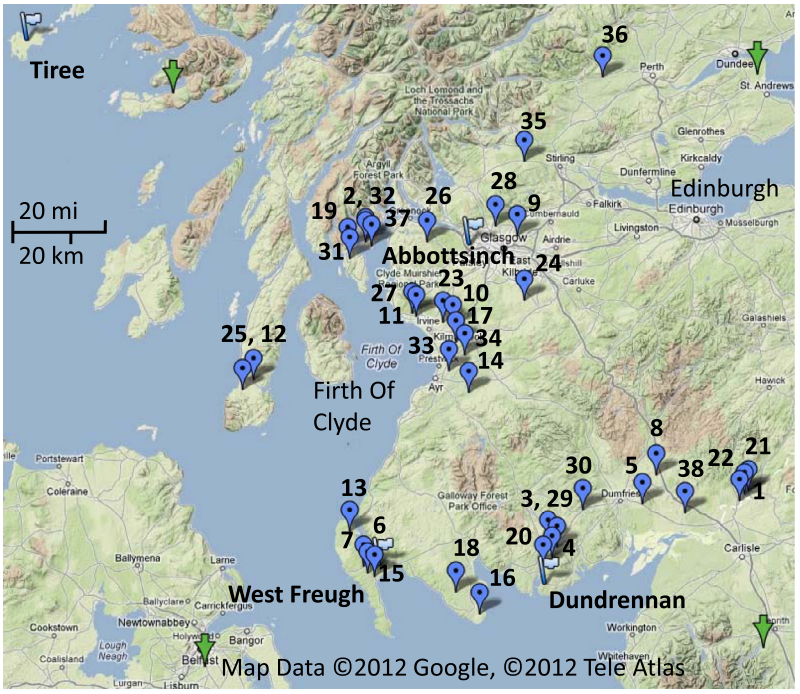

Fig. 26. Map showing the locations of fields, indicated by balloon markers, used in the case study on *T. paludosa*. The arrows provide an approximate location of the corner points of the schematic plots shown in Figs. 29, 31 and 34. Barren and rocky areas are shown in various shades of brown, while green shading is an indicator of grass cover. Relative height of terrain is indicated by the three-dimensional effect. Reproduction of the image complies with Google's FairUse principles; see http://www.google.com/permissions/geoguidelines.html. (For interpretation of the references to color in this figure legend, the reader is referred to the web version of this article.)

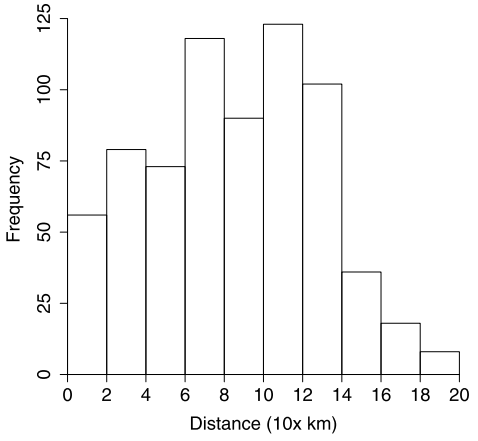

Fig. 27. Frequency of the inter-field distances in the monitoring system shown in Fig. 26.

Note that, in spite of the apparent existence of long-distance spatial correlations, not all fields are parts of the network. Inspection of Fig. 29 immediately reveals fields that are not correlated to others, even if there are fields situated close by and along the prevailing direction.

Thus, the statistical significance of correlations taken together with field positions helps to reveal the system's spatial structure. However, it still remains unclear whether these correlations are caused by the Moran effect or by wind-assisted dispersal coupling. In order to differentiate between these two factors, we consider a time-lagged correlation coefficient $r_k(X, Y)$:

Please cite this article in press as: Petrovskii S, et al. Multiscale approach to pest insect monitoring: Random walks, pattern formation, synchronization, and networks. Phys Life Rev (2014), http://dx.doi.org/10.1016/j.plrev.2014.02.001

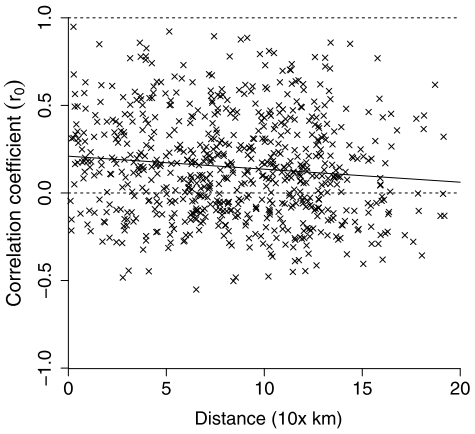

Fig. 28. Plot of the correlation coefficients, see Eq. (91), for pairs of fields against distance between those fields. The solid line indicates the trend predicted by the linear regression analysis. From [15], with permission.

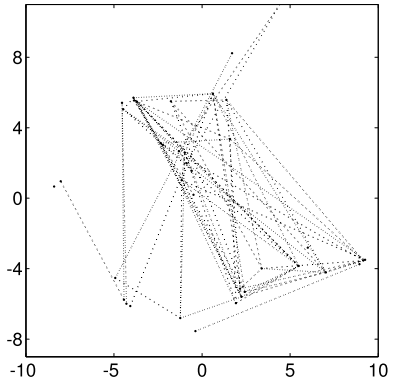

Fig. 29. Network of inter-field correlations. The dotted lines connect fields with significantly correlated populations. Further details are given in the text. Scales indicate relative position in tens of kilometers.

$$r_k(X,Y) = \frac{\sum_{i=1}^{n-k}(X_i - \mu_X)(Y_{i+k} - \mu_Y)}{\sqrt{(\sum_{i=1}^{n-k}(X_i - \mu_{X,k})^2)(\sum_{i=k+1}^{n}(Y_i - \mu_{Y,k})^2)}}, \tag{93}$$

where $\mu_{X,k}$ and $\mu_{Y,k}$ are defined as follows:

$$\mu_{X,k} = \frac{1}{n-k}\sum_{i=1}^{n-k} X_i, \qquad \mu_{Y,k} = \frac{1}{n-k}\sum_{i=k+1}^{n} Y_i. \tag{94}$$

Note that, generally speaking, $r_k(X,Y) \neq r_k(Y,X)$. The time-lagged correlation coefficient makes it possible to distinguish between the effect that the population of field X has on field Y (described by $r_k(X,Y)$) from the effect that the population of field Y may have on X (described by $r_k(Y,X)$). It therefore takes into account a possible asymmetry in the inter-field coupling which is especially relevant if insect dispersal is assisted by the wind of a prevailing direction.

There is considerable evidence that weather conditions are correlated in time, cf. [170]. It seems reasonable to distinguish between the long-term weather trends and short-term transient weather conditions as they are likely to have different effects on the population dynamics.[9] It is the short-term weather fluctuations that create the environmental stochasticity behind the Moran effect. Recall that the population census on *T. paludosa* abundance was taken once a

[9] For a discussion of this issue and an example of the possible effect of correlated weather conditions on the spatial population structure see [129].

Please cite this article in press as: Petrovskii S, et al. Multiscale approach to pest insect monitoring: Random walks, pattern formation, synchronization, and networks. Phys Life Rev (2014), http://dx.doi.org/10.1016/j.plrev.2014.02.001

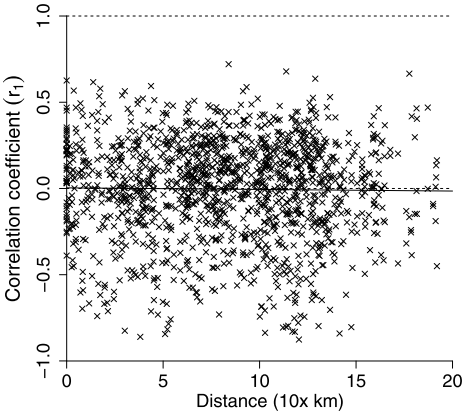

Fig. 30. Plots of correlation coefficients r_1 for pairs of distinct fields against distance between those fields calculated using a time-lag of 1 year, cf. Eq. (93) with $k = 1$. The solid line indicates the trend as predicted by linear regression analysis. From [15], with permission.

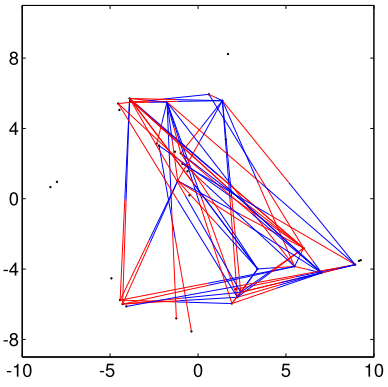

Fig. 31. Network of inter-field correlations subject to a one year delay. The lines connect fields between which significant relationships exist. The red section of each line emanates from the influencing field, the blue section terminates at the influenced field. Further details are given in the text. Scales indicate relative position in tens of kilometers. (For interpretation of the references to color in this figure legend, the reader is referred to the web version of this article.)

year. It is unlikely that synchronization due to the impact of stochasticity is subject to such a long delay. Therefore, if the synchronization pattern seen in Figs. 28 and 29 is caused by stochasticity, it is unlikely to be seen in the behavior of the time-lagged correlation coefficient r_k even for the shortest lag of $k = 1$.

In contrast, if the synchronization pattern is caused by dispersal coupling, it is likely to be captured by the coefficient r_k. The annual population census was taken in mid-winter. Dispersal is primarily associated with the flying stage of the insect species that occurs in late August/early September. Therefore, the effect of dispersal will not be seen in the census until the next year. The effect of delay is likely to be felt more strongly if dispersal is asymmetric (which is clearly the case of wind-assisted dispersal), i.e. field X delegates a fraction of its population to field Y but not vice versa.

We begin with the case where the time-lag is one year, $k = 1$, which seems to be justified by the species traits, i.e. by the fact that it produces exactly one generation per year. The correlation coefficient r_1 vs inter-field distance calculated for all pairs of fields used in the study is shown in Fig. 30. Time-lagged correlation strength vs distance therefore exhibits an intermittent behavior roughly similar to that observed on the non-lagged case (cf. Fig. 28). One important difference, however, is that the number of fields that are negatively correlated is considerably larger in the time-lagged case.

The spatial structure of the correlations is shown in Fig. 31. It is readily seen that all correlated fields are connected into a network. Since, as we have argued above, in the time-lagged case the correlations are likely to be the result of inter-field coupling by dispersal, the structure shown in Fig. 31 is the network of *T. paludosa* dispersal over the study

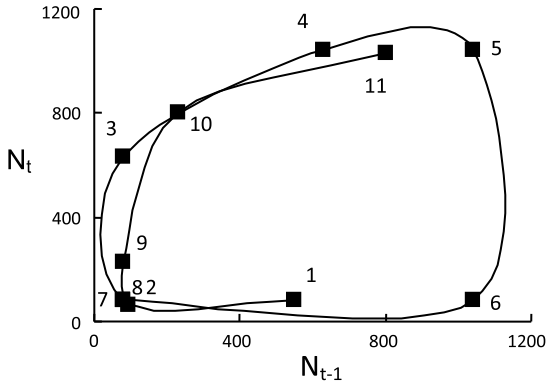

Fig. 32. Phase trajectory of annual leatherjacket population ($\times 10^3$) changes in south-west England. Black squares show the population in the current year (N_t) against the population in the previous year (N_{t-1}). The line connects points in chronological order with points numbered sequentially. Data from Fig. 3 in [91].

area. Note that, in the case of time-lagged correlations, this is a directed network as we have influencing fields and influenced fields. Furthermore, as in the non-lagged case (cf. Fig. 29), the network has clear anisotropic properties.

We mention here that species dispersal through a certain network (rather then uniformly over space) is a frequent phenomenon in ecology; e.g. see [57] and references therein. However, the dispersal network is usually related to the effect of clearly defined external factors that shape the environment geometry and connectivity, e.g. by creating corridors and/or stepping stones [79]. Well-known examples are given by dispersal of aquatic plants or animals through waterways [25] and (on a much larger spatial scale) dispersal of zooplankton by ships with ballast waters [72]. In contrast, the dispersal network observed in the study on *T. paludosa* seems to be self-organized in the sense that the location of coupled fields cannot be straightforwardly linked to the terrain structure but more likely arises as a result of an interplay between exogenous and endogenous factors. In particular, long-distance transport with the wind was proved to be important for many small biological objects like seeds, pollen and ballooning spiders [102] that have no ability to fly by themselves but can be kept in the air for a long time by turbulent air flows. Landscape heterogeneity can interact with turbulent airflows resulting in ascending currents and large travel distances [102]. Recall that adult *T. paludosa* are flying insects, although they are regarded as poor flyers. There is currently no direct evidence that *T. paludosa* can sail with the wind; however, there is plenty of evidence for many other insect species [35,53]. Moreover, insects are not always carried with the wind passively. Some insect species are known to possess navigation abilities that allow them to control the altitude of their flight and to choose the landing site [35,53]. The *T. paludosa* dispersal network is therefore likely to emerge as a result of the interplay between physical transport and the behavioral response of the insects. Indeed, an insight into the weather data shows that the orientational properties of the dispersal network agree very well with the prevailing directions of the wind [15].

Thus, the time-lag of one generation makes it possible to reveal the effect of dispersal coupling between different habitats. The question may arise whether any new insight can be made by considering a longer time-lag. There is some evidence (obtained from an earlier study [91] performed in a different region of the U.K.) that *T. paludosa* may exhibit a multi-annual cycle, see Fig. 32, although it remains unclear whether this cycle is induced by 'external' environmental factors or by 'internal' density-dependent mechanisms, or by a combination of both [23]. The population dynamics of *T. paludosa* therefore has at least two different timescales. Whichever is the origin of the multi-annual cyclic dynamics, one can expect that its effect may be seen in the behavior of the time-lagged correlation coefficient r_k for some $k > 1$.

Fig. 33 shows the coefficients r_2 and r_3 vs the interfield distance. Generally, the results are similar to those obtained for r_1. Furthermore, as above, they exhibit a complicated intermittent behavior with many fields being strongly negatively correlated up to 150–200 km. The corresponding networks of the interfield coupling is shown in Fig. 34. Interestingly, they exhibit properties somewhat different from the r_1 network. In particular, the number of cross-correlated fields in the central part of the study area has decreased but more distant fields (e.g. west-most and north-most) are now connected to the network. In the case of the r_3 network, the direction of the relationships swaps in several places, e.g. see the cluster of blue links out of the south west corner where they were mostly red in case of r_1; these fields have become "influenced" rather than "influencing".

Please cite this article in press as: Petrovskii S, et al. Multiscale approach to pest insect monitoring: Random walks, pattern formation, synchronization, and networks. Phys Life Rev (2014), http://dx.doi.org/10.1016/j.plrev.2014.02.001

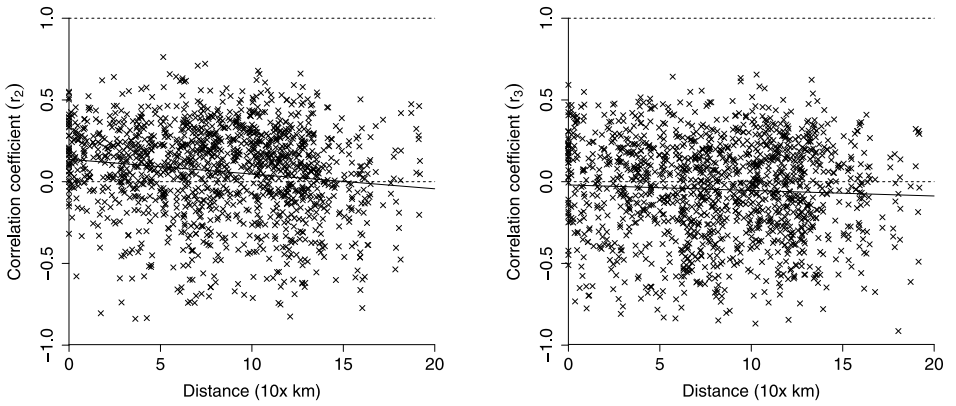

Fig. 33. Plots of correlation coefficients for pairs of distinct fields against distance between those fields calculated using a time-lag of (a) 2 years, (b) 3 years. The solid lines indicate trends predicted by linear regression analysis.

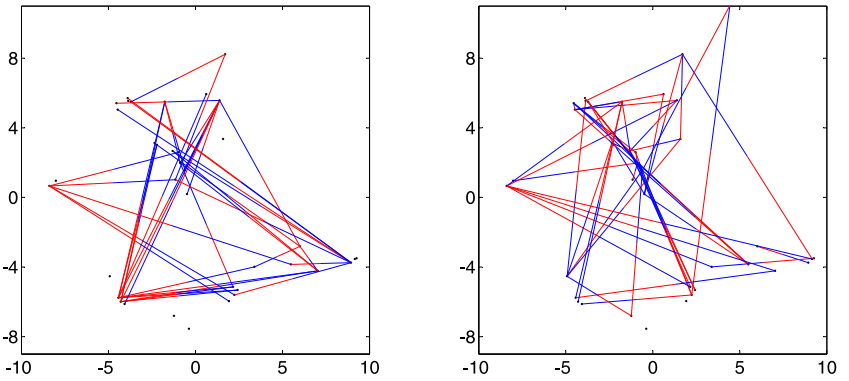

Fig. 34. Network of significant inter-field correlations calculated using a time-lag of (a) 2 years, (b) 3 years. The lines connect fields between which significant relationships exist. The red section of each line emanates from the influencing field, the blue section terminates at the influenced field. Scales indicate relative position in tens of kilometers. (For interpretation of the references to color in this figure legend, the reader is referred to the web version of this article.)

A more detailed view of the spatial structure of the time-lagged cross-correlations can also be obtained by considering the distribution of the inter-field distances between significantly correlated fields. In order to avoid bias induced by the peculiarities of the system geometry, i.e. different distance frequencies in the original system (see Fig. 27), for each distance range we scale the observed frequency by the height of the corresponding bar in the underlying distribution shown in Fig. 27. The results are shown in Fig. 35 for different values of the time delay. It is readily seen that in the non-delayed case (Fig. 35a) the distribution of distances is approximately uniform in the range 0–160 km showing just a slight tendency to decrease. The apparent minimum in the middle (in the 60–80 km bin) is likely caused by the effect of the terrain's structure. The mean distance 72.9 km is close to the median of the distribution which confirms the generic uniformity of the distribution. The corresponding network therefore does not have a characteristic spatial scale. Note that the situation where all spatial scales are represented equally complies well with our conclusion that, in the non-delayed case, synchronization is likely to occur due to the Moran effect associated with regionally correlated transient weather conditions.

Distribution of distances remains approximately uniform in the case of cross-correlations with time delay of one year (see Fig. 35b). As above, this indicates that the corresponding network does not possess a characteristic scale. This result agrees well with our earlier conclusion that the time-lagged synchronization occurs due to dispersal coupling as transport by turbulent flows is known to be scale-free.

The distribution pattern changes for a larger time-lag. For $k = 2$ (Fig. 35c), the frequency of small distances decreases dramatically. The distribution now spans over a larger spatial range 0–180 km. The relative frequency of large distances become higher, the mean distance being larger than the median of the distribution. Inspection of the

Please cite this article in press as: Petrovskii S, et al. Multiscale approach to pest insect monitoring: Random walks, pattern formation, synchronization, and networks. Phys Life Rev (2014), http://dx.doi.org/10.1016/j.plrev.2014.02.001

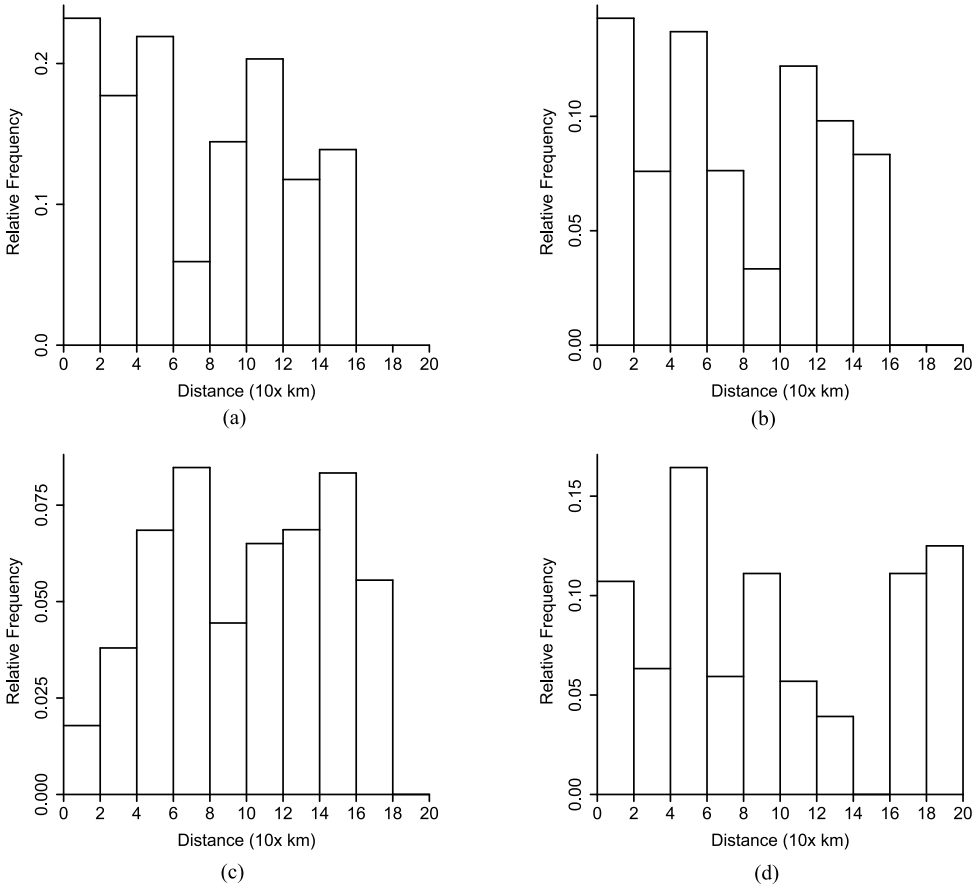

Fig. 35. Distribution of distances between significantly correlated fields as obtained for (a) r_0, (b) r_1, (c) r_2 and (d) r_3, i.e. for time-delays of none, one, two and three years, respectively. The corresponding mean distance is 72.9, 74.9, 100.0 and 94.7 kilometers.

corresponding network suggests that the higher frequency of large distances may happen because the network now includes a few more distant fields that were not connected in the cases of $k = 0$ and $k = 1$.

This tendency becomes even stronger in case of the three year delay, i.e. for $k = 3$ (Fig. 35d). The spatial range has now become even bigger (spanning between 0–200 km). The mean distance is slightly less than the median of the distribution; however, the mean distance is not informative in this case as the distribution exhibits a clear bimodal shape, i.e. the short-distance mode and the long-distance mode. Recall that *T. paludosa* exhibits multi-annual cyclic dynamics with estimated period of the cycle being about 6–7 years; see Fig. 32. The three-year delay used in Fig. 35d is on the same order which opens up the possibility of a resonance interaction. We therefore hypothesize that this change of pattern, i.e. from approximately uniform to bimodal, may be an effect of the multi-annual cycle, although we are currently not able to provide any proof of this.

5. Discussion

It is widely recognized that ecological dynamics has multiple spatial and temporal scales [19,61,84,110,151]. Ecological monitoring aims to provide information about the ecosystem's state at different times and under different conditions and hence is expected to capture the main features of the dynamics. In order to ensure that the information obtained is reliable and robust, a comprehensive monitoring program therefore needs to take into account the existence of multiple scales. This requires a careful, well-designed ecological protocol for data collection and their subsequent interpretation based on an efficient and consistent theoretical framework.

Please cite this article in press as: Petrovskii S, et al. Multiscale approach to pest insect monitoring: Random walks, pattern formation, synchronization, and networks. Phys Life Rev (2014), http://dx.doi.org/10.1016/j.plrev.2014.02.001

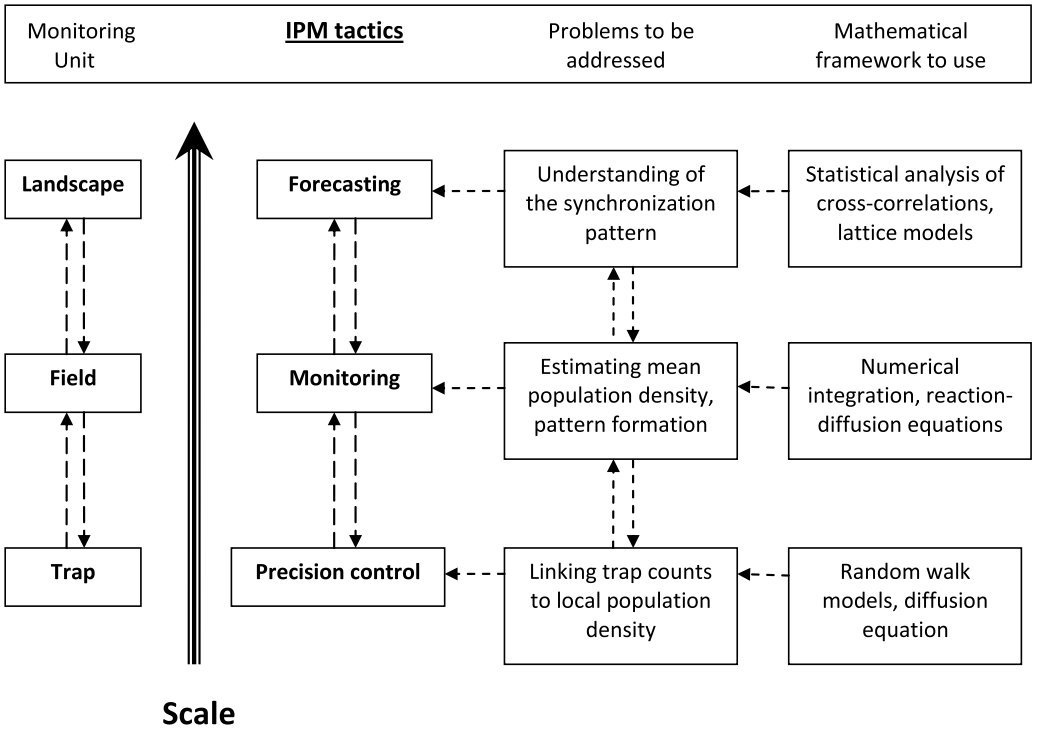

Fig. 36. A sketch of the scale-specific goals of insect pest monitoring, corresponding theoretical frameworks and mathematical tools. The arrows indicate the information flow between different scales and approaches; see details in the text.

In this paper, we focused on pest insect monitoring.[10] We showed that insect monitoring has at least three distinctly different spatial scales; throughout the paper we referred to them as the single trap scale, the single field scale and the landscape scale. Information on local insect abundance is usually obtained from trap counts. Correspondingly, the smallest scale is defined by insect movement in the vicinity of the trap. An intermediate scale comes into consideration when data are collected with multiple traps as may happen, for instance, in a large agricultural field or plantation. The information obtained at different locations then needs to somehow be 'integrated' to provide the value of total population size or average population density. The largest scale appears when pest abundance is considered over a landscape where the effects of inter-field coupling and synchronization become important.

We have shown that the theoretical framework and the mathematical approaches to modeling and data interpretation are significantly different for these three scales. The challenges are different, too. For the single trap scale, perhaps the biggest challenge is to extend the theoretical framework described in Section 2 onto baited traps as the effect of the attracting agent (e.g. light, color or pheromone) on the insects' movement behavior is not straightforward and details are often unknown. For the single field scale, the main challenge is to utilize *a priori* information about the properties of the population spatial distribution. Such information may be obtained either from previous field studies on the given species or from predictions of a relevant model and it can increase the monitoring efficiency dramatically by tuning the location of the traps. For the landscape scale, the challenge remains in identification of species-specific mechanisms of the inter-field synchronization and, in case of dispersal coupling, in revealing specific environmental and biological features that result in a dispersal network.

Note that, if considered in the context of integrated pest management (IPM) [28,82], the specific purpose of monitoring at different scales is different too; see Fig. 36. The natural monitoring unit is an agricultural field and this is the scale where the decisions on pest control measures (e.g. pesticides application) are made if/when the pest density exceeds a dangerous threshold. Methods to estimate the average pest density are therefore of primary importance; see

[10] We mention here that many of the approaches reviewed in this paper are not insect-specific and apply to monitoring of other invertebrate species as well. One good example is flatworms considered in [119]; see also Section 3.2.

Please cite this article in press as: Petrovskii S, et al. Multiscale approach to pest insect monitoring: Random walks, pattern formation, synchronization, and networks. Phys Life Rev (2014), http://dx.doi.org/10.1016/j.plrev.2014.02.001

Section 3. However, these methods use the information obtained locally from trap counts collected by a given trap; therefore, accurate estimation of the local density is an essential prerequisite. The forecasting done on the landscape scale aims to observe the regional tendencies in pest development. It also helps to identify the location of fields where potentially dangerous pest development is likely to take place (as well as, in principle, the timing of those events; see Fig. 25).

It is clear from the above that the information obtained at different scales is not independent. There are certain 'information flows' between the scales. Precision of the local density estimate affects the field-scale accuracy of the average density estimate. In turn, as the information on average population density is used to reveal regional cross-field correlations, it can affect the conclusions drawn on the landscape scale. Understanding of the processes and phenomena that can affect the accuracy of monitoring at the single-field scale is therefore crucial for insect pest monitoring as a whole. One such phenomenon is pattern formation where the distribution of the pest population density over space can become prominently heterogeneous due to the impact of some environmental and/or biological factors. For instance, a heterogeneous insect distribution can be expected to emerge as a likely response to spatially synchronized fruit production observed in large orchards [148]. In Section 3, we showed that the accuracy of the average density estimate in the single field problem can be improved significantly (or the number of traps can be decreased) if some *a priori* information is available about the spatial pattern. In other words, once the properties of the spatial pattern are known, it often becomes possible to draw conclusions about the population density at particular locations. This additional information can then be used to significantly increase the accuracy of the local density estimate at the single trap scale.

Thus, pattern formation at the intermediate, single-field level provides coupling between different spatial scales. Pattern formation in population dynamics is a complicated phenomenon that has been a focus of intensive research for a few decades [107,110,88]. It can be of different origins and controlled by different factors [6,60,89,108,147]. One factor that seems to be particularly relevant to pattern formation in the agricultural context is the geometry of the domain but the effects of the field shape seem to be largely overlooked in standard agricultural practices. Indeed, the value of a farm field often depends on its area but rarely on its shape. However, theory predicts (see below) that the properties of the pattern can depend both on the size *and* shape of the domain. Hence, the efficiency of pest monitoring (which, in its turn, can greatly affect costs of crops growing, cf. Section 1) can be significantly different in fields of different shape, or else fields of different shape may require a different monitoring protocol.

In the theoretical perspective, there are a few situations where the effects of shape either are known or can be readily seen. For the simplest example, let us consider a single-species population $U(\mathbf{r},t)$ that multiplies according to the logistic growth, $f(U)=\alpha U(1-\frac{U}{K})$, and diffuses inside a 2D domain of rectangular shape:

$$\frac{\partial U(\mathbf{r},t)}{\partial t}=D\nabla^2U(\mathbf{r},t)+f(U)\approx D\nabla^2U(\mathbf{r},t)+\alpha U(\mathbf{r},t),$$
$$\mathbf{r}=(x,y),\quad 0<x<L_x,\ 0<y<L_y, \tag{95}$$

where we have assumed, for the sake of simplicity, that $U\ll K$ and hence the growth rate is approximately linear, $f(U)\approx\alpha U$. We also assume that the environment outside of the domain is hostile so that the condition at the domain boundary Λ is of Dirichlet type, $U(\mathbf{r}\in\Lambda,t)=0$.

The linearized equation (95) can be readily solved by the method of variable separation [37]. Interestingly, the solution appears to have different properties depending on how large the domain is in the x and y directions. Namely, the solution is decreasing for:

$$\alpha-D\pi^2\left(\frac{1}{L_x^2}+\frac{1}{L_y^2}\right)<0, \tag{96}$$

which will eventually lead to population extinction, and is increasing otherwise. Obviously, for fixed values of α and D, it means that the population can only survive if *both* L_x and L_y are large enough. In particular, it means that the population will survive in a square domain $L\times L$ for:

$$L>L_{cr}=\pi\left(\frac{2D}{\alpha}\right)^{1/2}, \tag{97}$$

Please cite this article in press as: Petrovskii S, et al. Multiscale approach to pest insect monitoring: Random walks, pattern formation, synchronization, and networks. Phys Life Rev (2014), http://dx.doi.org/10.1016/j.plrev.2014.02.001

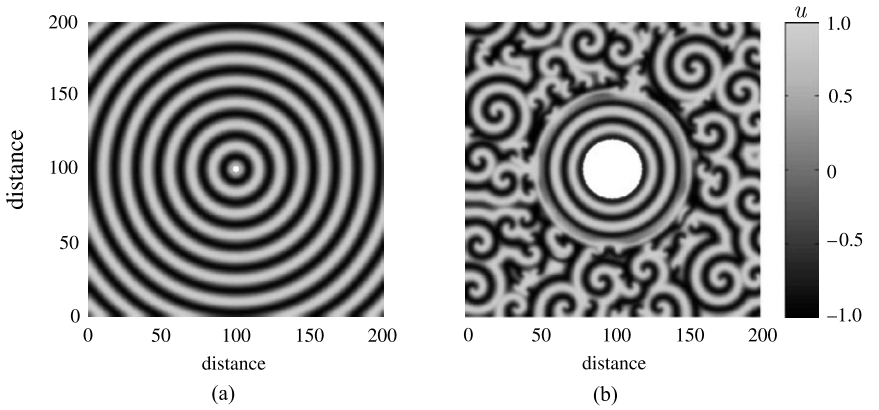

Fig. 37. The effect of obstacle size on the spatial pattern in a predator–prey system. Different shades of grey correspond to different population density. The obstacle of a larger size turns the regular pattern to a chaotic one. From [158], with permissions.

but will go extinct in a rectangular domain of the same area $L_x L_y = L^2$ where either L_x or L_y are sufficiently small. Note that, although very simple to demonstrate, this effect of the domain shape is sometimes overlooked which may result in artificial or even meaningless results, cf. [156].

More subtle effects of the domain shape and size are observed in the case of more complicated population dynamics. Consider, for instance, a predator–prey system. For cyclic dynamics, which are rather common in nature [152], the predator–prey system can exhibit two different types of spatiotemporal dynamics, i.e. either smooth patterns in space (e.g. periodical) combined with periodical oscillations in time or spatiotemporal chaos [122], the latter also being known as the "biological turbulence" [88].

Let us consider the situation where the populations occupy a ring-shaped domain, $r_0 < r < r_1$ where $r_0 \ll r_1$, i.e. there is an "obstacle" of radius r_0 at the domain center so that a part of the domain is not accessible. (In terms of a real-world system, for instance, it can be a pond or a small lake.) It was shown in [158] that the type of the system's dynamics and, correspondingly, the type of the spatial pattern then depends on the radius of the obstacle; see Fig. 37. The population spatial distribution forms a regular target-like pattern for a small obstacle but an irregular (actually, chaotic) spatiotemporal pattern for a sufficiently large obstacle. Clearly, in the former case the same number of traps will result in a much more accurate estimate of the average population density than in the latter case.

The effect of the domain shape on the dynamics of a predator–prey system was also studied in [99]. It was shown that, if considered in a rectangular domain with a sufficiently small width, the initial population distribution given by a complicated two-dimensional pattern eventually evolves to a much simpler pattern consisting of almost parallel stripes; see Fig. 38. The emerging population distribution in the form of stripes is effectively one-dimensional and hence can be monitored with a much higher accuracy; see Section 3.

Interestingly, the example shown in Fig. 38 seems to indicate that a field of an elongated shape should be easier to monitor. However, this message should be regarded with some care. The results shown in Fig. 38 were obtained under some specific assumptions about the population dynamics (see [99] for details) and it is not clear how general they are. In a broader context, a more reliable monitoring system is not yet sufficient to increase the IPM efficiency. In particular, the nature of the adjoint areas can be important. For a field of a given area, the more elongated the shape the larger the length of the field boundary. If the neighboring areas are not farmed, they can become a refuge for pest insects, and then a stripe-shaped agricultural field may appear to be more susceptible to pest migration from the adjoint habitats, cf. Section 2.3.

The domain shape therefore can act as a pattern selection mechanism and this should be taken into account when designing the monitoring program. However, the current understanding of this issue is meager and incomplete. In particular, in the above examples the domains are of a simple shape, i.e. either rectangular or with a cylindrical symmetry. One can expect that in the case of a more intricate shape the selection mechanism can also become more complex. That, along with other challenges mentioned above, should become a focus of future research.

Please cite this article in press as: Petrovskii S, et al. Multiscale approach to pest insect monitoring: Random walks, pattern formation, synchronization, and networks. Phys Life Rev (2014), http://dx.doi.org/10.1016/j.plrev.2014.02.001

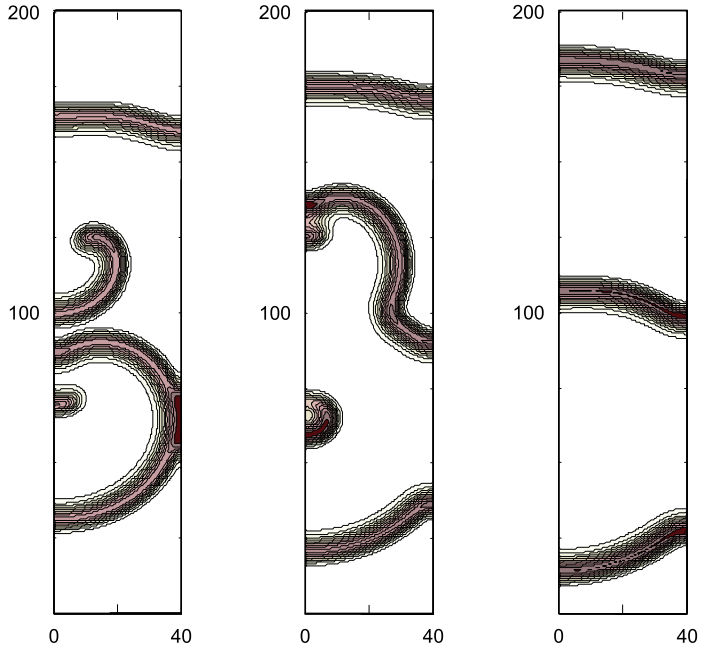

Fig. 38. The population density of prey in a predator–prey system shown for three equidistant moments. Different shades of grey correspond to different population density. As the time increases (from left to right), the irregular 2D pattern converges to an effectively 1D system of plane waves. From [99], with permissions.

Acknowledgements

The authors are thankful to Rod Blackshaw (Plymouth) for fruitful and stimulating discussions of the topic. Helpful discussions with Larissa Collins (FERA, Sand Hutton) are appreciated. The authors also acknowledge useful discussions of Sections 1 and 3 with Nina Embleton (Birmingham) and Section 2.5 with Danish Ahmed (Leicester). Thilo Gross (Bristol) read the manuscript and made many comments aimed to improve the manuscript clarity. This work was supported by The Leverhulme Trust through grant F/00-568/X. S.P. gratefully acknowledges the support given by the University of Leicester in granting an academic study leave which was essential for completion of this work.

References

[1] Abramowitz M, Stegun IA. Handbook of mathematical functions. Washington: National Bureau of Standards; 1972.
[2] Ahmed DA. Stochastic and mean-field approaches for trap counts modelling and interpretation. PhD thesis, Leicester: University of Leicester; 2014.
[3] Ahmed DA, Bearup D, Petrovskii SV. Time-dependent diffusion as a mean-field counterpart of Levy-type random walk. Math Model Nat Phenom 2014 [submitted for publication].
[4] Alavanja MCR, Ross MK, Bonner MR. Increased cancer burden among pesticide applicators and others due to pesticide exposure. CA Cancer J Clin 2013;62(2):120–42.
[5] Alexander CJ, Holland JM, Winder L, Woolley C, Perry JN. Performance of sampling strategies in the presence of known spatial patterns. Ann Appl Biol 2005;146:361–70.
[6] Alonso D, Bartumeus F, Catalan J. Mutual interference between predators can give rise to Turing spatial patterns. Ecology 2002;83:28–34.
[7] Allen JC, Schaffer WM, Rosko D. Chaos reduces species extinction by amplifying local population noise. Nature 1993;364:229–32.
[8] Alyokhin A, Baker M, Mota-Sanchez D, Dively G, Grafius E. Colorado potato beetle resistance to insecticides. Am J Potato Res 2008;85:395–413.
[9] Baars MA, Van Dijk TS. Population dynamics of two carabid beetles at a Dutch heathland. I. Subpopulation fluctuations in relation to weather and dispersal. J Anim Ecol 1984;53:375–88.
[10] Balescu R. Equilibrium and nonequilibrium statistical mechanics. New York: John Wiley; 1975.
[11] Barclay HJ. Modelling the effects of population aggregation on the efficiency of insect pest control. Res Popul Ecol 1992;34:131–41.
[12] Barenblatt GI. Scaling, self-similarity, and intermediate asymptotics. Cambridge: Cambridge University Press; 1996.
[13] Bartumeus F, Catalan J, Viswanathan GM, Raposo EP, da Luz MGE. The influence of turning angles on the success of non-oriented animal searches. J Theor Biol 2008;252:43–55.

Please cite this article in press as: Petrovskii S, et al. Multiscale approach to pest insect monitoring: Random walks, pattern formation, synchronization, and networks. Phys Life Rev (2014), http://dx.doi.org/10.1016/j.plrev.2014.02.001

[14] Bearup D, Petrovskaya NB, Petrovskii SV. Some analytical and numerical approaches to understanding trap counts resulting from pest insect immigration. Math Biosci 2014 [submitted for publication].
[15] Bearup D, Petrovskii SV, Blackshaw R, Hastings A. Synchronized dynamics of Tipula paludosa metapopulation in a South-Western Scotland agroecosystem: linking pattern to process. Am Nat 2013;182:393–409.
[16] Benhamou S. How many animals really do the Lévy walk?. Ecology 2007;88:1962–9.
[17] Berg HC. Random walks in biology. Princeton: Princeton University Press; 1983.
[18] Binns MR, Nyrop JP, Van Der Werf W. Sampling and monitoring in crop protection: the theoretical basis for designing practical decision guides. Wallingford: CABI Publishing; 2000.
[19] Bisigato AJ, Villagra PE, Ares JO, Rossi BE. Vegetation heterogeneity in Monte Desert ecosystems: a multi-scale approach linking patterns and processes. J Arid Environ 2009;73:182–91.
[20] Blackshaw RP. The annual leatherjacket survey in Northern Ireland 1965–1982, and some factors affecting populations. Plant Pathol 1983;32:345–9.
[21] Blackshaw RP. Personal communication.
[22] Blackshaw RP, Vernon RS. Spatiotemporal stability of two beetle populations in non-farmed habitats in an agricultural landscape. J Appl Ecol 2006;43:680–9.
[23] Blackshaw RP, Petrovskii SV. Limitation and regulation of ecological populations: a meta-analysis of Tipula paludosa field data. Math Model Nat Phenom 2007;2(4):46–62.
[24] Boag B, Mackenzie K, McNicol JW, Neilson R. Sampling for the New Zealand flatworm. In: Proceedings crop protection in Northern Britain 2010. 2010. p. 45–50.
[25] Bobeldyk AM, Bossenbroek JM, Evans-White MA, Lodge DM, Lamberti GA. Secondary spread of zebra mussels (Dreissena polymorpha) in coupled lake–stream systems. EcoScience 2005;12:339–46.
[26] Brown JH. Complex ecological systems. In: Cowan GA, Pines D, Melzer D, editors. Complexity: metaphors, models, and reality. Santa Fe Institute studies in the Science of Complexity, proceedings, vol. XVIII. Reading, MA: Addison-Wesley; 1994. p. 419–49.
[27] Buntin GD. Developing a primary sampling program. In: Pedigo LP, Buntin GD, editors. Handbook of sampling methods for arthropods in agriculture. Boca Raton: CRC Press; 1994. p. 99–115.
[28] Burn AJ. Integrated pest management. New York: Academic Press; 1987.
[29] Burnham KP, Anderson DR. Model selection and multimodel inference: a practical information-theoretic approach. 2nd edition. New York: Springer; 2002.
[30] Byers JA. Simulation and equation models of insect population control by pheromone-based traps. J Chem Ecol 1993;19:1939–56.
[31] Byers JA. Wind-aided dispersal of simulated bark beetles flying through forests. Ecol Model 2000;125:231–43.
[32] Carey GF. Computational grids: generation, adaptation, and solution strategies. Washington, DC: Taylor & Francis; 1997.
[33] Chorin AJ, Hald OH. Stochastic tools in mathematics and science. New York: Springer; 2006.
[34] Codling EA, Plank MJ, Benhamou S. Random walk models in biology. J R Soc Interface 2008;5:813–34.
[35] Compton SG. Sailing with the wind: dispersal by small flying insects. In: Bullock JM, Kenward RE, Hails RS, editors. Dispersal ecology. Oxford: Blackwell; 2002. p. 113–33.
[36] Couzin ID, Krause J, Franks NR, Levin SA. Effective leadership and decision-making in animal groups on the move. Nature 2005;433:513–6.
[37] Crank J. The mathematics of diffusion. 2nd edition. Oxford: Oxford University Press; 1975.
[38] Davis PM. Statistics for describing populations. In: Pedigo LP, Buntin GD, editors. Handbook of sampling methods for arthropods in agriculture. Boca Raton: CRC Press; 1994. p. 33–54.
[39] Davis PJ, Rabinowitz P. Methods of numerical integration. New York: Academic Press; 1975.
[40] De Jager M, Weissing FJ, Herman PMJ, Nolet BA, van de Koppel J. Response to Comment on "Lévy walks evolve through interaction between movement and environmental complexity". Science 2012;335:918.
[41] Dennis JE, Gay DM, Welsch RE. An adaptive nonlinear least-squares algorithm. ACM Trans Math Softw 1981;7(3).
[42] Dent D. Insect pest management. Wallingford: CABI Publishing; 2000.
[43] Edwards AM, Phillips RA, Watkins NW, Freeman MP, Murphy EJ, Afanasyev V, et al. Revisiting Lévy flight search patterns of wandering albatrosses, bumblebees and deer. Nature 2007;449:1044–8.
[44] Embleton NL, Petrovskaya NB. On numerical uncertainty in evaluation of pest population size. Ecol Complex 2013;14:117–31.
[45] Embleton NL, Petrovskaya NB. A novel approach to evaluation of pest insect abundance in the presence of noise. Bull Math Biol 2014. http://dx.doi.org/10.1007/s11538-014-9940-z [in press].
[46] Feller W. Introduction to probability theory and its applications, vol. 1. 3rd edition. New York: John Wiley & Sons; 1968.
[47] Ferguson AW, Klukowski Z, Walczak B, Perry JN, Mugglestone MA, Clark SJ, et al. The spatio-temporal distribution of adult Ceutorhynchus assimilis in a crop of winter oilseed rape in relation to the distribution of their larvae and that of the parasitoid *Trichomalus perfectus*. Entomol Exp Appl 2000;95(2):161–71.
[48] Ferguson AW, Klukowski Z, Walczak B, Clark SJ, Mugglestone MA, Perry JN, et al. Spatial distribution of pest insects in oilseed rape: implications for integrated pest management. Agric Ecosyst Environ 2003;95:509–21.
[49] Flechtmann CA, Ottati AL, Berisford CW. Comparison of four trap types for ambrosia beetles (Coleoptera, Scolytidae) in Brazilian Eucalyptus stands. J Econ Entomol 2000;93:1701–7.
[50] Gallos LK, Argyrakis P, Kehr KW. Trapping and survival probability in two dimensions. Phys Rev E 2001;63:021104.
[51] Garcia R, Moss F, Nihongi A, Strickler JR, Göller S, Erdmann U, et al. Optimal foraging by zooplankton within patches: the case of Daphnia. Math Biosci 2007;207:165–88.
[52] Gardiner CW. Handbook of stochastic methods. Springer series in synergetics, vol. 13. Berlin: Springer; 1985.
[53] Gatehouse AG. Behavior and ecological genetics of wind-borne migration by insects. Annu Rev Entomol 1997;42:475–502.

Please cite this article in press as: Petrovskii S, et al. Multiscale approach to pest insect monitoring: Random walks, pattern formation, synchronization, and networks. Phys Life Rev (2014), http://dx.doi.org/10.1016/j.plrev.2014.02.001

[54] Gautestad AO. Lévy meets Poisson: a statistical artifact may lead to erroneous recategorization of Lévy walk as Brownian motion. Am Nat 2013;181:440–50.
[55] Goldwyn EE, Hastings A. The roles of the Moran effect and dispersal in synchronizing oscillating populations. J Theor Biol 2011;289:237–46.
[56] Gotelli NJ, Ellison AM. A primer of ecological statistics. Sunderland: Sinauer Associates; 2004.
[57] Grant EH, Lowe WH, Fagan WF. Living in the branches: population dynamics and ecological processes in dendritic networks. Ecol Lett 2007;10:165–75.
[58] Guichard S, Kriticos DJ, Leriche A, Kean JM, Worner SP. Individual-based modelling of moth dispersal to improve biosecurity incursion response. J Appl Ecol 2012;49:287–96.
[59] Haydon D, Steen H. The effects of large and small-scale random events on the synchrony of metapopulation dynamics: a theoretical analysis. Proc R Soc Lond B 1997;264:1375–81.
[60] Hastings A, Harrison S, McCann K. Unexpected spatial patterns in an insect outbreak match a predator diffusion model. Proc R Soc Lond B 1997;264:1837–40.
[61] Hastings A, Petrovskii SV, Morozov A. Spatial ecology across scales. Biol Lett 2011;7:163–5.
[62] Hapca S, Crawford JW, Young IM. Anomalous diffusion of heterogeneous populations characterized by normal diffusion at the individual level. J R Soc Interface 2009;6:111–22.
[63] Higley LG, Pedigo LP. Economic thresholds for integrated pest management. Omaha: University of Nebraska Press; 1996.
[64] Holland EP, Aegerter JN, Dytham C, Smith GC. Landscape as a model: the importance of geometry. PLoS Comput Biol 2007;3(10):e200.
[65] Holland JM, Perry JN, Winder L. The within-field spatial and temporal distribution of arthropods in winter wheat. Bull Entomol Res 1999;89:499–513.
[66] Holland JM, Thomas CFG, Birkett S, Southway S, Oaten H. Farm-scale spatiotemporal dynamics of predatory beetles in arable crops. J Appl Ecol 2005;42:1140–52.
[67] Huret M, Runge JA, Chen C, Cowles G, Xu Q, Pringle JM. Dispersal modeling of fish early life stages: sensitivity with application to Atlantic cod in the western Gulf of Maine. Mar Ecol Prog Ser 2007;347:261–74.
[68] Jacoby DMP, Brooks EJ, Croft DP, Sims DW. Developing a deeper understanding of animal movements and spatial dynamics through novel application of network analyses. Methods Ecol Evol 2012;3:574–83.
[69] Jansen VAA, Mashanova A, Petrovskii SV. Model selection and animal movement: comment on "Levy walks evolve through interaction between movement and environmental complexity". Science 2012;335:918.
[70] Jopp F, Reuter H. Dispersal of carabid beetles – emergence of distribution patterns. Ecol Model 2005;186:389–405.
[71] Kaitala V, Ranta E, Lundberg P. Self-organized dynamics in spatially structured populations. Proc R Soc Lond B 2001;268:1655–60.
[72] Kaluza P, Kölzsch A, Gastner MT, Blasius B. The complex network of global cargo ship movements. J R Soc Interface 2010;7:1093–103.
[73] Karandinos MG. Optimum sample size and comments on some published formulae. Bull Entomol Soc Am 1976;22:417–21.
[74] Kareiva PM. Local movement in herbivorous insecta: applying a passive diffusion model to mark-recapture field experiments. Oecologia 1983;57:322–7.
[75] Kareiva PM. Population dynamics in spatially complex environments: theory and data. Philos Trans R Soc Lond B 1990;330:175–90.
[76] Kareiva PM, Shigesada N. Analyzing insect movement as a correlated random walk. Oecologia 1983;56:234–8.
[77] Kawai R. Sampling rate of spatial stochastic processes with independent components in modeling random search paths. Phys Rev E 2012;85:021907.
[78] Kawai R, Petrovskii SV. Multi-scale properties of random walk models of animal movement: lessons from statistical inference. Proc R Soc A 2012;468:1428–51.
[79] Keitt TH, Urban DL, Milne BT. Detecting critical scales in fragmented landscapes. Conserv Ecol 1997;1(1):4 [online]. Available from http://www.consecol.org/vol1/iss1/art4/.
[80] Kendall BE, Bjornstad ON, Bascompte J, Keitt TH, Fagan WF. Dispersal, environmental correlation, and spatial synchrony in population dynamics. Am Nat 2000;155:628–36.
[81] Klafter J, Sokolov IM. Anomalous diffusion spreads its wings. Phys World 2005;18:29–32.
[82] Kogan M. Integrated pest management: historical perspectives and contemporary developments. Annu Rev Entomol 1998;43:243–70.
[83] Kot M, Lewis MA, van der Driessche P. Dispersal data and the spread of invading organisms. Ecology 1996;77:2027–42.
[84] Lewis M, Maini P, Petrovskii SV. Dispersal, individual movement, and spatial ecology: a mathematical perspective. Lecture notes in mathematics, vol. 2071. Berlin: Springer; 2013.
[85] Liebhold A, Koenig WD, Bjornstad ON. Spatial synchrony in population dynamics. Annu Rev Ecol Evol Syst 2004;35:467–90.
[86] Loehle C. Challenges of ecological complexity. Ecol Complex 2004;1:3–6.
[87] Lundberg P, Ranta E, Ripa J, Kaitala V. Population variability in space and time. Trees 2000;15:460–4.
[88] Malchow H, Petrovskii SV, Venturino E. Spatiotemporal patterns in ecology and epidemiology: theory, models, simulations. Boca Raton: Chapman & Hall/CRC Press; 2008.
[89] Maron JL, Harrison S. Spatial pattern formation in an insect host-parasitoid system. Science 1997;278:1619–21.
[90] Mashanova A, Oliver TH, Jansen VAA. Evidence for intermittency and a truncated power law from highly resolved aphid movement data. J R Soc Interface 2010;7:199–208.
[91] Mayor JG, Davies MH. A survey of leatherjacket populations in south-west England, 1963–1974. Plant Pathol 1976;25:121–8.
[92] Metcalf RL. Introduction to insect pest management. London: Wiley; 1982.
[93] Metzler R, Klafter J. The random walk's guide to anomalous diffusion: a fractional dynamics approach. Phys Rep 2000;339:1–77.
[94] Milne A, Laughlin R, Coggins RE. The 1955 and 1959 population crashes of the leatherjacket, *Tipula paludosa* Meigen, in Northumberland. J Anim Ecol 1965;34:529–34.

Please cite this article in press as: Petrovskii S, et al. Multiscale approach to pest insect monitoring: Random walks, pattern formation, synchronization, and networks. Phys Life Rev (2014), http://dx.doi.org/10.1016/j.plrev.2014.02.001

[95] Mistro DC, Rodrigues LAD, Petrovskii SV. Spatiotemporal complexity of biological invasion in a space- and time-discrete predator–prey system with the strong Allee effect. Ecol Complex 2012;9:16–32.
[96] Morales JM, Haydon DT, Frair J, Holsinger KE, Fryxell JM. Extracting more out of relocation data: building movement models as mixtures of random walks. Ecology 2004;85:2436–45.
[97] Moran PAP. The statistical analysis of the Canadian lynx cycle. I. Structure and prediction. Aust J Zool 1953;1:163–73.
[98] Moran PAP. The statistical analysis of the Canadian lynx cycle II. Synchronization and meteorology. Aust J Zool 1953;1:291–8.
[99] Morozov A, Li BL. On the importance of dimensionality of space in models of space-mediated population persistence. Theor Popul Biol 2007;71:278–89.
[100] Murchie AK, Harrison AJ. Mark-recapture of 'New Zealand flatworms' in grassland in Northern Ireland. In: Proceedings crop protection in Northern Britain 2004. 2004. p. 63–7.
[101] Murray JD. Mathematical biology. Berlin: Springer; 1989.
[102] Nathan R, Sapir N, Trakhtenbrot A, Katul GG, Bohrer G, Otte M, et al. Long-distance biological transport processes through the air: can nature's complexity be unfolded in silico?. Divers Distrib 2005;11:131–7.
[103] Newlands NK, Lutcavage ME, Pitcher TJ. Analysis of foraging movements of Atlantic bluefin tuna (*Thunnus thynnus*): individuals move with two modes of searching. Popul Ecol 2004;46:39–53.
[104] Northing P. Extensive field based aphid monitoring as an information tool for the UK seed potato industry. Asp Appl Biol 2009;94:31–4.
[105] Nottingham SF, Hardie J. Migratory and targeted flight in seasonal forms of the black bean aphid, *Aphis fabae*. Physiol Entomol 1989;14:451–8.
[106] Oerke EC. Crop losses to pests. J Agric Sci 2006;144:31–43.
[107] Okubo A. Diffusion and ecological problems: mathematical models. Berlin: Springer; 1980.
[108] Okubo A. Dynamical aspects of animal grouping: swarms, schools, flocks and herds. Adv Biophys 1986;22:1–94.
[109] Okubo A, Chiang HC. An analysis of the kinematics of swarming of *Anarete pritchardi* Kim (Diptera: Cecidomyiidae). Res Popul Ecol 1974;16:1–42.
[110] Okubo A, Levin SA. Diffusion and ecological problems: modern perspectives. Berlin: Springer; 2001.
[111] Pascual MA, Kareiva P. Predicting the outcome of competition using experimental data: maximum likelihood and Bayesian approaches. Ecology 1996;77:337–49.
[112] Petrovskaya NB. The accuracy of least-squares approximation on highly stretched meshes. Int J Comput Methods 2008;5:449–62.
[113] Petrovskaya NB. Quadratic least-squares solution reconstruction in a boundary layer region. Commun Numer Methods Eng 2010;26:1721–35.
[114] Petrovskaya NB, Embleton NL. Evaluation of peak functions on ultra-coarse grids. Proc R Soc A 2013;469:20120665. http://dx.doi.org/10.1098/rspa.2012.0665.
[115] Petrovskaya NB, Embleton NL. Computational methods for accurate evaluation of pest insect population size. In: Godoy WAC, Ferreira CP, editors. Ecological modelling applied to entomology. Berlin: Springer; 2014 [in press].
[116] Petrovskaya NB, Petrovskii SV. The coarse-grid problem in ecological monitoring. Proc R Soc A 2010;466:2933–53.
[117] Petrovskaya NB, Venturino E. Numerical integration of sparsely sampled data. Simul Model Pract Theory 2011;19:1860–72.
[118] Petrovskaya NB, Embleton NL, Petrovskii SV. Numerical study of pest population size at various diffusion rates. In: Lewis M, Maini P, Petrovskii SV, editors. Dispersal, individual movement, and spatial ecology: a mathematical perspective. Berlin: Springer; 2013. p. 355–86.
[119] Petrovskaya NB, Petrovskii SV, Murchie AK. Challenges of ecological monitoring: estimating population abundance from sparse trap counts. J R Soc Interface 2012;9:420–35.
[120] Petrovskii SV, Li BL. Exactly solvable models of biological invasion. Boca Raton: Chapman & Hall/CRC Press; 2006.
[121] Petrovskii SV, Morozov AY. Dispersal in a statistically structured population: fat tails revisited. Am Nat 2009;173:278–89.
[122] Petrovskii SV, Malchow H. Wave of chaos: new mechanism of pattern formation in spatio-temporal population dynamics. Theor Popul Biol 2001;59:157–74.
[123] Petrovskii SV, Li BL, Malchow H. Quantification of the spatial aspect of chaotic dynamics in biological and chemical systems. Bull Math Biol 2003;65:425–46.
[124] Petrovskii SV, Mashanova A, Jansen VAA. Variation in individual walking behavior creates the impression of a Lévy flight. Proc Natl Acad Sci USA 2011;108:8704–7.
[125] Petrovskii S, Morozov A, Li BL. On a possible origin of the fat-tailed dispersal in population dynamics. Ecol Complex 2008;5:146–50.
[126] Petrovskii SV, Morozov A, Venturino E. Allee effect makes possible patchy invasion in a predator–prey system. Ecol Lett 2002;5:345–52.
[127] Petrovskii SV, Bearup D, Ahmed DA, Blackshaw R. Estimating insect population density from trap counts. Ecol Complex 2012;10:69–82.
[128] Petrovskii SV, Malchow H, Hilker FM, Venturino E. Patterns of patchy spread in deterministic and stochastic models of biological invasion and biological control. Biol Invasions 2005;7:771–93.
[129] Petrovskii SV, Morozov A, Malchow H, Sieber M. Noise can prevent onset of chaos in spatiotemporal population dynamics. Eur Phys J B 2010;78:253–64.
[130] Phillips ADG, Wyatt TD. Beyond origami: using behavioural observations as a strategy to improve trap design. Entomol Exp Appl 1992;62:67–74.
[131] Pickett S, Thompson J. Patch dynamics and the design of nature reserves. Biol Conserv 1978;13:27–37.
[132] Pimentel D. Amounts of pesticides reaching target pests: environmental impacts and ethics. J Agric Environ Ethics 1995;8:17–29.
[133] Pimentel D. Techniques for reducing pesticide use: economic and environmental benefits. New York: John Wiley & Sons; 1997.
[134] Pimentel D. Pesticides and pest control. In: Peshin R, Dhawan AK, editors. Integrated pest management: innovation-development process, vol. 1. Berlin: Springer; 2009. p. 83–8.
[135] Pimentel D, Greiner A. Environmental and socio-economic costs of pesticide use. In: Pimentel D, editor. Techniques for reducing pesticide use: economic and environmental benefits. New York: John Wiley & Sons; 1997.

Please cite this article in press as: Petrovskii S, et al. Multiscale approach to pest insect monitoring: Random walks, pattern formation, synchronization, and networks. Phys Life Rev (2014), http://dx.doi.org/10.1016/j.plrev.2014.02.001

[136] Pimentel D, Pimentel M. Food, energy and society. Boca Raton: CRC Press; 2008.
[137] Plank MJ, Codling EA. Sampling rate and misidentification of Lévy and non-Lévy movement paths. Ecology 2009;90:3546–53.
[138] Post E, Forchhammer MC. Synchronization of animal population dynamics by large scale climate. Nature 2002;420:168–71.
[139] Raimondo S, Liebhold AM, Strazanac JS, Butler L. Population synchrony within and among Lepidoptera species in relation to weather, phylogeny, and larval phenology. Environ Entomol 2004;29:96–105.
[140] Ranta E, Kaitala V, Lindstrom K, Helle E. Moran effect and synchrony in population dynamics. Oikos 1997;78:136–42.
[141] Reynolds AM. Bridging the gulf between correlated random walks and Lévy walks: autocorrelation as a source of Lévy walk movement patterns. J R Soc Interface 2010;7:1753–8.
[142] Reynolds AM. Olfactory search behaviour in the wandering albatross is predicted to give rise to Lévy flight movement patterns. Anim Behav 2012;83:1225–9.
[143] Reynolds AM, Smith AD, Menzel R, Greggers U, Reynolds DR, Riley JR. Displaced honey bees perform optimal scale-free search flights. Ecology 2007;88:1955–61.
[144] Ripa J. Analysing the Moran effect and dispersal: their significance and interaction in synchronous population dynamics. Oikos 2000;89:175–87.
[145] Risken H. The Fokker–Planck equation: methods of solution and applications. 2nd edition. Berlin: Springer; 1989.
[146] Rodrigues LAD, Mistro DC, Petrovskii SV. Pattern formation in a space- and time-discrete predator–prey system with a strong Allee effect. Theor Ecol 2011;7:77–88.
[147] Rohani P, Lewis TJ, Grünbaum D, Ruxton GD. Spatial self-organization in ecology: pretty patterns or reality?. Trends Ecol Evol 1997;12:70–4.
[148] Rosenstock TS, Hastings A, Koenig WD, Lyles DJ, Brown PH. Testing Moran's theorem in an agroecosystem. Oikos 2011;120:1434–40.
[149] Royama T. Analytical population dynamics. London: Chapman & Hall; 1992.
[150] Sander LM, Warren CP, Sokolov IM, Simon C, Koopman J. Percolation on heterogeneous networks as a model for epidemics. Math Biosci 2002;180:293–305.
[151] Schweiger O, Maelfait JP, Van Wingerden W, Hendrickx F, Billeter R, Speelmans M, Augenstein I, et al. Quantifying the impact of environmental factors on arthropod communities in agricultural landscapes across organisational levels and spatial scales. J Appl Ecol 2005;42:1129–39.
[152] Sherratt JA, Smith MJ. Periodic travelling waves in cyclic populations: field studies and reaction–diffusion models. J R Soc Interface 2008;5:483–505.
[153] Shigesada N, Kawasaki K. Biological invasions: theory and practice. Oxford: Oxford University Press; 1997.
[154] Shlesinger MF, Zaslavsky GM, Klafter J. Strange kinetics. Nature 1993;363:31–7.
[155] Sinclair ARE, Gosline JM. Solar activity and mammal cycles in the Northern hemisphere. Am Nat 1997;149:776–84.
[156] Soboleva TK, Shorten PR, Pleasants AB, Rae AL. Qualitative theory of the spread of a new gene into a resident population. Ecol Model 2003;163:33–44.
[157] Sohrabi F, Shishehbor P, Saber M, Mosaddegh MS. Lethal and sublethal effects of imidacloprid and buprofezin on the sweetpotato whitefly parasitoid *Eretmocerus mundus* (Hymenoptera: Aphelinidae). Crop Prot 2013;45:98–103.
[158] Smith MJ, Sherratt JA, Armstrong NJ. The effects of obstacle size on periodic travelling waves in oscillatory reaction–diffusion equations. Proc R Soc A 2008;464:365–90.
[159] Snedecor GW, Cochran WG. Statistical methods. Ames: The Iowa State University Press; 1980.
[160] Sornette D. Critical phenomena in natural sciences. 2nd edition. Berlin: Springer; 2004.
[161] Southwood TRE, Henderson PA. Ecological methods. 3rd edition. Blackwell Science; 2000.
[162] Stern VM. Economic thresholds. Annu Rev Entomol 1973;18:259–80.
[163] Sumpter DJT. Collective animal behavior. Princeton: Princeton University Press; 2010.
[164] Sutcliffe OL, Thomas CD, Moss D. Spatial synchrony and asynchrony in butterfly population dynamics. J Anim Ecol 1996;65:85–95.
[165] Thomas CFG, Parkinson L, Marshall EJP. Isolating the components of activity-density for the carabid beetle Pterostichus melanarius in farmland. Oecologia 1998;116:103–12.
[166] Tischendorf L. Modelling individual movements in heterogeneous landscapes: potentials of a new approach. Ecol Model 1997;103:33–42.
[167] Turchin P. Fractal analyses of animal movement: a critique. Ecology 1996;77:2086–90.
[168] Turchin P. Quantitative analysis of movement. Sunderland: Sinauer; 1998.
[169] Turchin P. Complex population dynamics: a theoretical/empirical synthesis. Princeton: Princeton University Press; 2003.
[170] Vasseur DA, Yodzis P. The color of environmental noise. Ecology 2004;85:1146–52.
[171] Vinatier F, Chailleux A, Duyck PF, Salmon F, Lescourret F, Tixier P. Radiotelemetry unravels movements of a walking insect species in heterogeneous environments. Anim Behav 2010;80:221–9.
[172] Viswanathan GM, Afanasyev V, Buldyrev SV, Murphy EJ, Prince PA, Stanley HE. Lévy flight search patterns of wandering albatrosses. Nature 1996;381:413–5.
[173] Viswanathan GM, Raposo EP, da Luz MGE. Lévy flights and superdiffusion in the context of biological encounters and random searches. Phys Life Rev 2008;5:133–50.
[174] Viswanathan GM, da Luz MGE, Raposo EP, Stanley HE. The physics of foraging: an introduction to random searches and biological encounters. Cambridge, UK: Cambridge University Press; 2011.
[175] Vlug HJ, Paul H. Sampling leatherjackets. Meded Fac Landbouwwet Rijksuniv Gent 1986;51:939–42.
[176] Ward SA, Rabbinge R, Mantel WP. The use of incidence counts for estimation of aphid populations. 1. Minimum sample size for required accuracy. Eur J Plant Pathol 1985;91:93–9.
[177] Wiegand K, Jeltsch F, Ward D. Analysis of the population dynamics of Acacia trees in the Negev desert, Israel with a spatially-explicit computer simulation model. Ecol Model 1999;117:203–24.

Please cite this article in press as: Petrovskii S, et al. Multiscale approach to pest insect monitoring: Random walks, pattern formation, synchronization, and networks. Phys Life Rev (2014), http://dx.doi.org/10.1016/j.plrev.2014.02.001

[178] Williams DW, Liebhold AM. Influence of weather on the synchrony of gypsy moth (Lepidoptera: Lymantriidae) outbreaks in New England. Environ Entomol 1995;24:987–95.

[179] Yamanaka T, Tatsuki S, Shimada M. An individual-based model for sex-pheromone-oriented flight patterns of male moths in a local area. Ecol Model 2003;161:35–51.

Please cite this article in press as: Petrovskii S, et al. Multiscale approach to pest insect monitoring: Random walks, pattern formation, synchronization, and networks. Phys Life Rev (2014), http://dx.doi.org/10.1016/j.plrev.2014.02.001